DEVELOPMENT AND VERIFICATION OF A BRUSH MODEL FOR ACTIVE DEBRIS REMOVAL

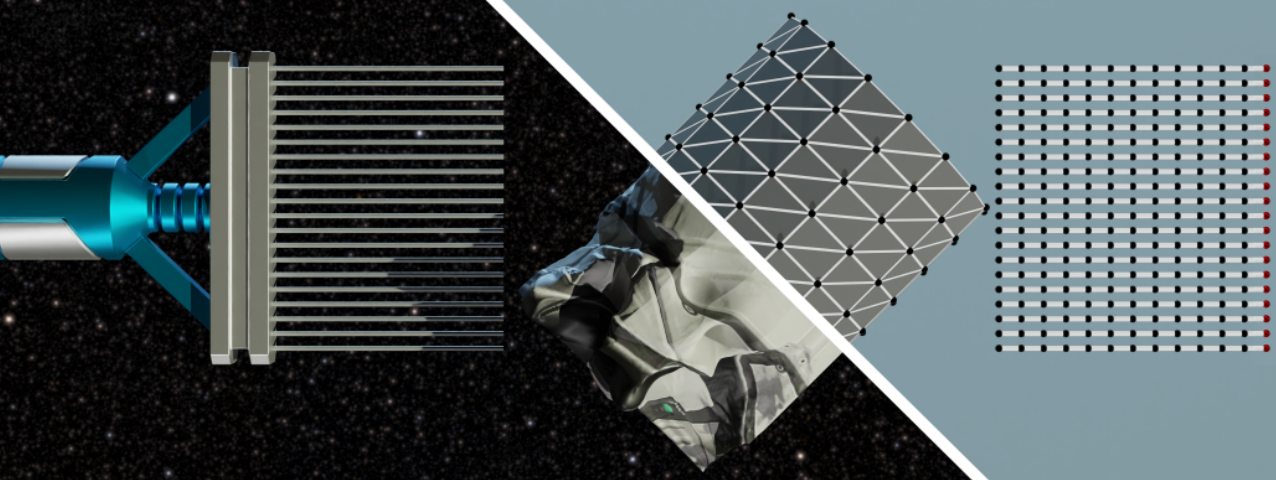

DEVELOPMENT AND VERIFICATION OF A BRUSH MODEL FOR ACTIVE DEBRIS REMOVAL

Master Thesis

Rohit KADUNGAMPARAMBIL JOHN

Faculty of Aerospace Engineering
Technische Universiteit Delft, Delft, The Netherlands,

This thesis has been approved by

Supervisor: Prof. Dr. Jian Guo

Defence committee members:

Chair	
Prof. Dr. Jian Guo	Technische Universiteit Delft
Independent Examiners:	
Prof. Dr. Sergio Turteltaub	Technische Universiteit Delft
Dr. Ines Uriol Balbin	Technische Universiteit Delft

Keywords: Brush, Discrete Element Method, YADE, Active Debris Removal

"Apurvah kopi koshoyam vidyate tava Bharati;
Vyayato vrudhim aayaati kshayam aayati sanchayat."
Knowledge is unique among all treasures;
It grows when it is spent, and it whithers when it is hidden.

A Sanskrit verse

CONTENTS

SUMMARY

This project aimed to develop and verify a numerical model of a brush. This model is meant to aid the study and design of brushes in Active Space Debris Capture. The model is based on the Discrete Element Method and uses the YADE software package to construct the brush model. This model simulates the dynamics of a bristle, their collisions among themselves and other bodies. The behaviour of the brush predicted by the DEM model was compared to observations recorded from three different experiments. The first test compared the dynamic behaviour of bristle, the second focused on the brush's static behaviour, and the final test studied its dynamic behaviour. The experiment observations fall within the behaviour predicted by the model, within the limits of the experiment.

1

INTRODUCTION

On February 10, 2009, two satellites collided in the low Earth orbit [1]. One of them was an active communication satellite and the other an inactive derelict satellite. This incident could have been avoided had the inactive satellite, space debris, been removed from LEO.

Space debris is formally defined as "All man-made objects including fragments and elements thereof, in Earth orbit or re-entering the atmosphere, that are non-functional" [2]. Its number has been steadily increasing ever since space flight was made possible, and this increase is bound to become a threat to space assets. The damage caused by space debris could vary from micro impacts to catastrophic collisions. The threat of damage to space assets supports the need to reduce the number of space debris currently in orbit and the generation of new debris. If left unchecked, the space debris population could grow beyond control. It could even reach a point when even halting all new launches to space would not stop the increase in space debris population. This phenomenon is called Kessler's syndrome [3]. This phenomenon will significantly affect the operation of space agencies, so space debris management should be among their chief concerns.

1.1. AN OVERVIEW OF SPACE DEBRIS MANAGEMENT

The main idea behind space debris management is to reduce the risk of damage caused by debris to space assets. The methods used for minimising this risk depend on multiple factors, which include, but are not limited to, the characteristics of the asset, space debris environment and management policy. After assessing these factors, avoid the debris, remove the debris, or do nothing. Apart from removing current debris, it is also worth mentioning how newer satellites can reduce space debris using post-mission disposal measures. The International Academy of Astronautics (IAA) Situation Report on Space Debris [2] recommends rocket stages be put in a path that ensures that they re-enter the atmosphere. It also recommends that the orbital lifetime of a satellite should be limited

to 25 years after the end of its mission.

Many research groups have focussed their attention on developing concepts for managing and removing space debris. Active Debris Removal (ADR) is a term used to describe missions whose objective is to remove space debris.

Among contact-based ADR concepts, the concept of soft-touch plays a significant role in their success. A collision on a hard surface could send the debris flying in space. Moreover, hard end effectors require features on debris to grab them [4]. A brush end-effector is a possible solution to the problems; it provides soft contact and can conform to the shape of its target. Conformity allows contacting a featureless surface for detumbling, and multiple brushes may be used to capture debris.

Other tools exhibit soft contact. They, however, have certain disadvantages. The soft cushion and soft electrostatic adhesion pads are other concepts coming under this category. Matunaga et al. [5] proposed a gas-filled bladder to mediate the soft contact. Their study revealed that it could reduce angular momentum magnitude; however, they also observed the cushion redistributed part of the target's angular momentum to other axes. This concept has a serious flaw. The gas bladder can be punctured if it contacts a sharp edge on the debris.

Branz et al. [6] proposed a concept that uses electrostatic attraction to connect to the target firmly. The flexible nature of the pad allows it to contact and adhere to an irregular surface. However, it requires very accurate sensors and a control system to follow the motion of the target to adhere to its surface smoothly.

We propose using a brush as it has the advantage of both these concepts and lacks their disadvantage. The electrostatic pad requires a very accurate estimation of the target's state to contact the target, whereas the gas bladder does not. Its flexibility can accommodate any error in its positioning. So does the brush. Additionally, any damage to the brush will not result in its failure, unlike the bladder.

1.2. BRUSH DETUMBLING SYSTEM

The brush detumbling system uses a brush to contact the tumbling target. This system allows the chaser to contact the target softly and distribute the contact force across a large surface such that the damage is minimal.

The idea of using a brush is relatively new, and only a few research groups have worked on this concept. Nishida et al. [7, 8] introduced the joint virtual depth control for controlling this system. They used the spring-mass-damper model to capture the behaviour of the brush. Cheng et al. studied brush detumbling in two steps. The first study focused on a fixed brush interacting with a target rotating about a fixed axis [9]. In the second study, the model consisted of a brush attached to a chaser satellite interacting with a moving target. Both the satellite and target were simulated to move along an orbit [10]. These studies developed excellent control systems for handling a brush.

On the other hand, none of the models used to model a brush for ADR uses a model which uniquely identifies a brush. These models could very well be replaced with other entities which behave similarly. For example, Cheng et al. [11] used the Euler-Bernoulli model of a cantilever to model a brush. Replacing a brush with a cantilever may not change the outcomes of this research. Nishida et al. [8, 12] used a very generic spring-mass-damper to model a brush. Developing a model specific to a brush would be a more

accurate representation of a system that uses a brush and can shine a light on behaviour unique to a brush.

1.3. MODELLING A BRUSH

Brushes find use in many applications and are the subject of many research projects. Researchers have used several methods to study them, and these models can be classified as shown in Figure 1.1. This section will present a brief discussion of these models.

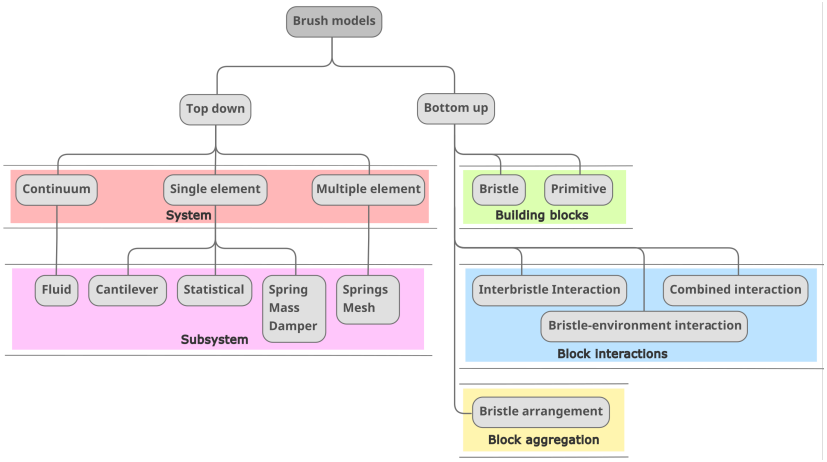

Figure 1.1: Classification of brush models

1.3.1. TOP-DOWN APPROACH

The top-down approach focuses on breaking down the individual functions of the system and assigning subsystems to handle them. In the case of modelling a brush, researchers have considered the brush as a system with various characteristics and assigned simpler mathematical entities to capture each property. The top-down approach models can be classified into three groups depending on the system's mechanics: single element system, multiple element system, and continuum system. Here, the degrees of freedom define the number of elements.

Three models use the single element concept (Figure 1.1). In the cantilever model, the brush is modelled as an elastic rod fixed at one end and a transverse load applied at the other end. This model's advantage is that the bending stiffness can be calculated from the material properties using the Euler–Bernoulli beam theory. Rawls et al. [13] used the cantilever model to predict the force needed to deform a toothbrush. Wenjie et al. [11] used it to model the behaviour of a brush contacting debris in space. However, their experiments pointed out that this model must be augmented to include non-linear phenomena. Wang et al. [14] gathered data on the behaviour of the brush and used statistical analysis to get a mathematical model. They simulated brushes with different dimensions and under different conditions using Finite Element Analysis (FEA). This data was then used to make a regression model relating the force to the deformation. The

final approach uses the spring-mass-damper system to model a brush. Nishida et al. [7] used this approach to model a brush end effector for a robotic space debris detumbling system.

The second model that comes under the top-down approach is the one that uses multiple deforming elements. This approach allows the system to have many degrees of freedom, letting it deform in several directions. Baxter et al. [15] used this method to model the deformation of a paintbrush contacting a canvas. Their model consisted of two parts: the skeleton and the surface. The skeleton is made of multiple spring-mass systems, which let the brush deform in multiple directions and return to its original shape. A subdivision mesh envelops this skeleton. The researchers focused on producing a computationally quick model that can produce accurate painting strokes. This focus on speed and its end use came at the cost of its physical fidelity.

The third model under the Top-down approach describes the system as a continuous field. Magnenat-Thalmann et al. [16] drew an analogy between the flow of a fluid around an object and the structure of hair on a person's head. In this model, the shape of an individual hair strand is that of a streamline in a fluid. This way, the model inherently possesses conformity, the ability to conform to the object's shape it contacts. Conformity is a trait lacking in other models under the top-down approach. Hair can be considered very similar to the bristle on a brush, so the models used to describe it can also be adapted to model a brush. This model, however, can only model the structure of hair when it is stationary and cannot simulate hair dynamics.

1.3.2. BOTTOM-UP APPROACH

The Bottom-Up Approach models the basic building blocks of a brush and their interactions. Then, the properties of the brush emerge from this collection and interaction of these building blocks. The bottom-up branch in Figure 1.1 shows three distinct levels: the building blocks, the block interactions and the block aggregation.

The building block is the smallest independent entity in a bottom-up model. Most brush models in the literature use a bristle as a building block, while others use a collection of bristles called a primitive [17]. However, primitives have not been researched as extensively as bristles. Xu et al. [17] modelled the behaviour of the hairy brush used in Chinese calligraphy using primitives. The authors performed multiple experiments to develop a physical model to account for ink flow, inertia and elasticity of the primitive.

In contrast to a primitive, there are many ways to model the behaviour of a bristle. Venegas et al. [18] reviewed the methods used in cleaning applications and manufacturing technology. They highlighted four methods that captured the behaviour of a brush: large deflection theory, small deflection theory, Discrete Element Method (DEM) and Finite Element Analysis (FEA). Large deflection theory is used when the bristles are expected to experience large deformations [19]. Small deflection theory is a particular case of large deformation theory when the deflection of the beam is known to be small [20]. DEM is a method that models the dynamic behaviour of a large collection of rigid bodies interacting. DEM can be used to model a bristle as a collection of cylinders chained together with a torsion spring at each joint. FEA is a method used to solve differential

equations. FEA is used to find the stress and the displacement of a bristle when forces act on it [21].

Forces mediate the interaction among the bristles and the target. These forces are calculated from deformations which are in turn calculated using geometry [19]. However, this requires calculating all interactions, which can be enormous. Hadap et al. [22] developed an alternative to this tedious method. They developed a fluid dynamics based model to capture these interactions and used it to model hair dynamics for computer animation. However, this model may not be physically valid as they focussed on making the hair simulation look visually appealing.

The final part of the bottom-up approach is how the bristles are arranged to form a brush. Not much literature was found discussing the features of different bristle arrangements.

1.4. GAPS IN LITERATURE AND RESEARCH QUESTIONS

The literature offered extensive and insightful research focussed on brushes. These studies showed different ways to approaches to thinking and modelling a brush. The different applications of the brush also shone a light on the brush's behaviour. Many of these ideas can be adapted for studying a brush's role in ADR. However, there are still some gaps and unanswered questions. This section aims to discuss these gaps and formulate a research question, including a set of sub-questions, to fill these gaps in the context of ADR.

1.4.1. GAPS IN BRUSH MODELS FROM ADR

As mentioned earlier, a noticeable gap in studies into applying a brush for ADR is the fidelity of the brush models they use. These studies use models which do not uniquely identify a brush. These models could very well be replaced with other entities which behave similarly. Developing a model specific to a brush would indeed be a more accurate representation of a system that uses a brush.

A significant downside of these models is that they have only a single degree of freedom. In other words, brushes in these models are restricted to deform only one way. A brush in real life can deform in multiple ways, so these models have minimal scope.

Apart from accuracy, these models also suffer from another disadvantage: they do not provide or propose a tedious method to translate the physical properties to the parameters of a brush. For example, a brush is made of several bristles having a specific arrangement, material properties and radius. The brush model is also defined by a similar set of parameters, but not the same. For instance, the Euler-Bernoulli model used by Cheng et al. [9, 10] is characterised by cross-section area and material properties. They do not specify the parameters of a given brush is translated to their models. Wenjie et al. [11] suggest performing experiments to calculate these parameters for each brush design. So implementing these models is difficult.

A possible reason for these shortcomings could be that these studies were meant to be pioneering studies. We speculate that the primary goal of these studies would be to expose the community to a new option for ADR. They showed us that a brush could play

the vital role of detumbling a tumbling target. These studies could motivate and pave the way for more focussed studies to expand the community's knowledge on using the brush. With this in mind, one may ask, "what about brush models from fields?"

1.4.2. GAPS IN OTHER BRUSH APPLICATIONS

In other fields, research on brush focuses only on how it interacts with other objects. However, none of them seems to ask what makes a brush special. We speculate this is a consequence of focusing solely on the brush's application. Since the brush is a ubiquitous tool, its features and properties may be implicitly understood, allowing us to find applications for it based on intuition. Once an application is found, the next step would be improving its performance, and these studies fall under this category.

Explicitly exposing these properties and understanding how they manifest may give valuable insight into brush behaviour and why it could be helpful for active debris removal. For example, balancing a bike while we ride it is something we understand and process implicitly. Focussing on its applications, such as a mountain bike or a road bike, help manufacturers design bikes capable of handling these terrains. Understanding its properties and dynamic phenomena allows us to go beyond a simple bike and develop autonomous bikes and two-wheeled robots.

The model used by these studies suffers from a few deficiencies too. Chief among them is that these models are very limited in their scope. These studies have identified symmetries and equilibria in the system to simplify the model.

For one, these studies developed models which interact with flat or smoothly curved surfaces often assumed to be larger than the brush. The simple geometry of the contacting surface helps simplify the brush model. However, the objects in space encountered during the ADR mission are rarely from or smooth; they have rough surfaces and complicated geometry.

The brushes themselves are designed to be symmetric. Figure 1.2 different brush designs focused in these studies. Notice that these designs possess translational symmetry, rotational symmetry or even both. Such symmetries can help simplify the brush model. These designs were developed through years of experience in their application and justify the specificity of these models. For example, the circular brush finds extensive use in manufacturing applications. On the other hand, ADR is a fairly new use case of a brush, and no specialised brush design has been developed for it. A model that can simulate any brush design can reduce the need for trial and error.

Most of these models were designed to predict the static behaviour of the brush. While few other studies did feature a moving brush, those models considered a quasi dynamic case. These models were developed to study a brush in continuous and smooth contact with a surface. In essence, the quasi dynamic is similar to the steady-state motion of a simple harmonic oscillator. Such a case dramatically simplifies the system's behaviour, making it easy to develop a model. ADR, on the other hand, would involve a very dynamic behaviour. In addition to continuous contact, debris handling would involve impacts and separation from the contacting body. So, the models developed in these studies lack the dynamic features necessary for studying ADR.

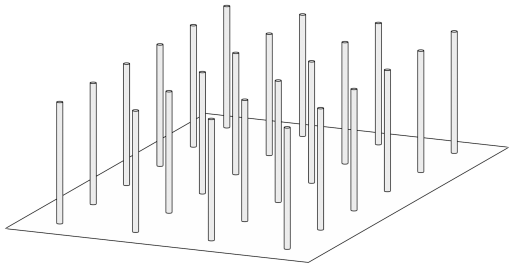

(a) *Linear array*

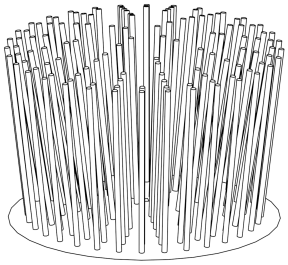

(b) *Rotary*

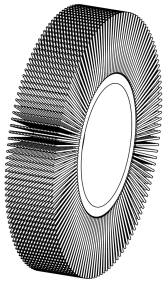

(c) *Circular*

Figure 1.2: *Three different symmetric brush designs. Notice the different spatial symmetries of these designs. The linear array has translational symmetry, the rotary brush has rotational symmetry and the circular brush has both*

The brush models also seem to ignore the interaction between bristles. This assumption simplifies the brush model. It also reduces the computational cost of the simulations. Such a reduction can be calculated as follows. Consider one collision check as one operation; for a brush with n bristles, there will be ${}^{n}C_2$ collision checks. These operations scale as $\mathcal{O}(n^2)$ and can blow up very quickly. However, this simplification is not without consequences. It eliminates the possibility of the model displaying two properties of brush (see 2.1) which could be vital to ADR.

The deficiencies discussed above make these brush models unsuitable for use in ADR. This motivates us to develop a new brush model and verify its accuracy.

1.4.3. RESEARCH QUESTIONS

The previous research in applying a brush in ADR provided grounds for its feasibility. This research aims to expand beyond that and answer the question "How does a given brush interact with tumbling debris?". This question forces us to think in general, as the brush and debris could have any arbitrary form. The answer could involve quantitative and qualitative methods to describe how this system behaves. A qualitative answer involves focusing on the properties of the brush and how they work together to make the brush detumble the debris effectively. At the same time, a mathematical model of this system that exhibits these properties could constitute a quantitative answer.

The steps taken to answer this question involves focussing on further sub-questions

and their answers. The answer to these subquestions will come together to answer the main research question. These sub-questions are given below:

- How does a brush behave?
- What makes the brush useful in ADR?
- How to implement brush behaviour into a model?
- How to test this brush model?

The first two questions mainly involve understanding a brush, its properties and what makes it a unique tool. The first question asks us to think about the different properties of a brush and deconstruct the brush into simple ideas. We can answer the second question by discussing how these brush properties work together towards making them suitable for ADR purposes. Observing brushes in experiments and simulations can shed light on the different properties of the brush. These studies on brush focussed on its application rather than its nature. The answers to these questions seek to fill this gap.

As highlighted before, there is a need for a brush model that captures all the brush's properties. Not just developing this model, it should be verified so that users can trust its quantitative and qualitative predictions.

2

BRUSH BEHAVIOUR

THE brush is one of the most ubiquitous tools in the world. It finds use in applications ranging from cleaning and art to manufacturing. Its simplest form consists of a collection of bristles affixed to a fixture. The end of the bristles at the fixture is called the root, while the other is called a tip. This is illustrated in Figure 2.1.

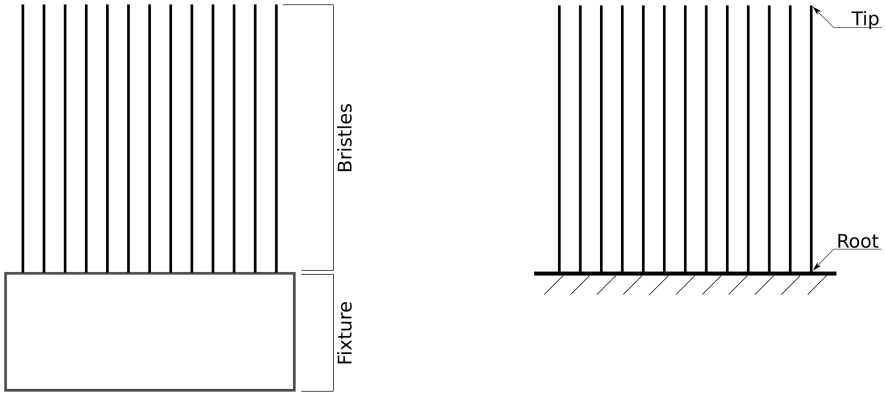

(a) (b)

Figure 2.1: *The two main components of a brush are the bristle and fixture. They are shows in 2.1a. The two ends of a bristle are named root and tip. The root is affixed to the fixture while the tip is free to move. From this point, figures of a brush would be drawn are 2.1b for the sake of simplicity.*

The literature study concluded that it could be used for Active Debris Removal. Before asking how missions can use it, we should ask makes it is a suitable tool for ADR. The first step to answer this question is to identify the properties of a brush. Identifying properties beneficial for ADR would help us understand why it is a tool suitable for ADR.

2.1. PROPERTIES OF A BRUSH

Throughout this project, we have identified a set of six properties of the brush. This set may not be exhaustive, and more properties could be found. It is believed these properties uniquely identify a brush as no other entity was found featuring this set. These properties are stiffness, dissipation, conformity, granularity, porosity, and momentum transport. This set of properties makes a brush very unique tool. By working together, these properties can enhance the capabilities of a brush. This synergy between the properties allows the brush to play a unique role in space engineering, especially ADR.

2.1.1. STIFFNESS

Stiffness is how an object resists deformation to an applied force. A brush inherits this from its constituent bristles. The collection of bristles deform together and respond with a reaction force. This reaction force resists the applied deformation. It is this reaction force that is the manifestation of stiffness. Removing the external force returns the brush to its original form.

The stiffness from the bristles is not the only source of stiffness in the brush. The fact that the bristle roots are fixed onto the brush fixture lends an additional layer of stiffness to the brush. Consider the following case. Imagine a brush is a collection of bristles, all arranged as they would be in a brush except they are not rooted to the fixture. Even though these bristles are stiff, this brush as a whole is not. Applying a force along the side of this brush would squish the bristles together. However, removing the force will not return the brush to its original shape. So, both the bristles' stiffness and the fixture play a role in making the brush stiff.

2.1.2. DISSIPATION

Dissipation is the property of an entity to disperse any local concentration throughout its entirety. In the case of a brush, any concentration of velocity tends to disperse all over the brush. Put differently, the brush tends to a state where local velocity tends to the average velocity of the brush. This process converts kinetic energy into heat, and it is an irreversible process.

Two mechanisms bring forth dissipation into a brush. The first is the dissipation inherent in the bristles. A bristle material, like any other, dampens any relative motion, such as bending, within it. The kinetic energy from the motion is converted into heat energy. The brush inherits this. Any relative movement within the brush is translated as a movement of the bristles. Since the bristles are rooted at the fixture, a bristle can only move by bending. This bending leads to dissipation.

The second mode of dissipation comes from the interaction between the bristles. In a brush that interacts with other objects, the bristles constantly collide. Contact forces mediate these collisions. These forces have two components: a perpendicular component to the contact plane and one tangential. Friction is this tangential force, and it tries to minimise any relative tangential motion between the bristles. The normal force from an inelastic collision at the contact point can also reduce the relative velocity. These two mechanisms lead to the dissipation of energy. This form of dissipation is seen in particle dampers used to dampen vibrations [23, 24]. The presence of fluid in a brush can also give rise to a source of dissipation due to drag. However, this is a not source produced by

the brush alone.

2.1.3. GRANULARITY

Granularity is the property of a physical entity for which its mechanical behaviour is greatly influenced by the size, shape and properties of its constituent grains [25]. It is often associated with granular material. Andreotti et al. define a granular material as " a collection of rigid, macroscopic particles, whose particle size is bigger than 100 μm" [24]. These particles are also called grains. We extend it to include flexible particles, in our case, the bristles. In other granular materials, the grain motion is not constrained. The brush is a collection of these bristles. For a brush, however, the bristles mainly move by deformation.

A remarkable property of granular materials is their ability to divide and join without detectable changes in their behaviour. Sand, for example, is a granular material. Dividing one cup of sand into two and mixing it back together will not show any visible difference. Consequently, granular material will not sustain any permanent damage when torn or pierced. As long as the grains remain undamaged, the granular material will not show any change.

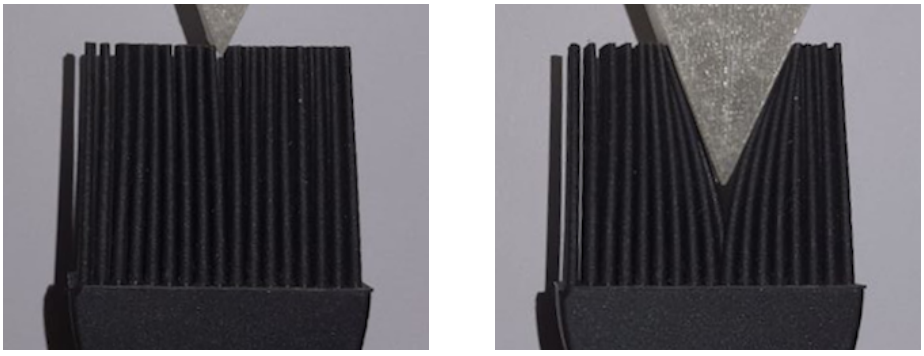

(a) *Brush before deformation* (b) *Brush after deformation*

Figure 2.2: *A brush conforming to the shape of an irregular object. Also, note that the bristles are parting to make way for the object. Removing the objects returns the brush to its original state. This demonstrates the granularity.*

2.1.4. CONFORMITY

Conformity is associated with the idea of an entity adopting certain qualities of its neighbours. It may also quantify the extent to which these qualities are adopted. For a brush, conformity is its ability to adapt the shape of an object deforming it. Doing so allows the brush to accommodate an arbitrarily shaped object into its volume. This is shown in Figure 2.2. One can imagine water flowing around an object dipped in it. Although not as pronounced as water, the bristles of brush move around the object, each contacting the object at small regions. These regions or their envelopes form a shape very similar to the object.

The ability of the brush to sustain local deformation gives rise to conformity. How-

ever, one may ask, do not all materials support local deformation? Yes, it is ubiquitous property, but brushes are unique because the bristles can undergo considerable deformation before they fail or get damaged. Consider a scenario where a solid metal block is penetrated by the object shown in Figure 2.2. With considerable force, the object can be forced into the metal block. However, it will sustain permanent damage, whereas a brush will not. Additionally, the granular nature of the brush allows it to "tear" itself into two pieces to allow objects to penetrate it.

2.1.5. MOMENTUM TRANSPORT

As the name suggests, Momentum transport allows the brush to transport momentum from one part to another without moving the whole brush. When a body impacts a brush, depending on the spacing between bristles and impact velocity, it can be observed that momentum absorbed by the brush moves away from the region of impact. Figure 2.3 shows this phenomenon. This phenomenon is similar to ripples on a water surface moving away from a stone dropped in it.

Unlike momentum transfer in fluids, momentum is not convected in a brush. It is more similar to conduction. The bristles are rooted in the fixture, preventing them from moving beyond a certain distance. The mechanism for transporting momentum in a brush is similar to that seen in sound waves. In a sound wave, adjacent particles collide, transferring their momentum to the next particle. Similarly, the bristles collide with their neighbours and transfer their momentum to their neighbouring bristles.

2.1.6. POROSITY

Porosity is the measure of space in a material. A highly porous brush will contain fewer bristles in a given cross-section than a lesser porous one. This property directly affects the stiffness and dissipation in a brush. A brush with many bristles is stiffer compared to one with fewer bristles. Many bristles in a smaller area lead to frequent bristle-bristle interactions. Just like a particle damper, an increase in interactions increase dissipation associated with friction and inelastic collision [23, 24]. It can also be argued that momentum transport occurs faster in highly dense (low porosity) brushes. In these brushes, the distance between neighbouring bristles is small. So, the distance travelled by the bristles is smaller. By assuming the bristle velocity constant, smaller bristle spacing leads to a shorter duration for the momentum to be transported across the brush.

We should note that porosity, by itself, is relevant only interactions occur at the size scale of the spaces. For example, there are large voids in the scale of atoms and subatomic particles. Nevertheless, one does not consider all matter porous just because of this fact. In a brush, these interactions could occur in the scale of the bristle diameter. For example, the spaces in a brush could trap debris of such a similar scale.

2.2. A BRUSH IN SPACE

To introduce a brush in space, we need to discuss its interactions with this system. This will be discussed in two parts. One, how does a brush would interact with its target. The properties of the brush discussed earlier would be called up to help explain this interaction. Two, how the space environment affects the brush. Factors such as radiation,

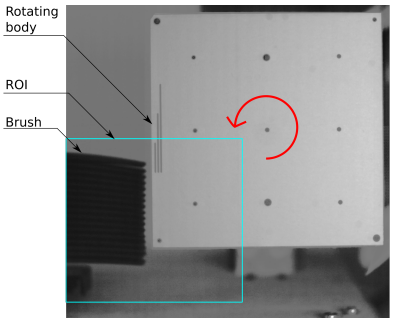

(a) *Labelled Setup*

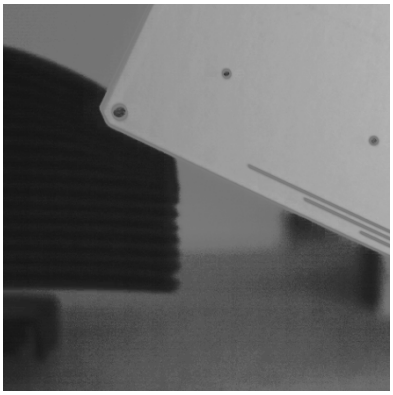

(b) *Body contacts the brush*

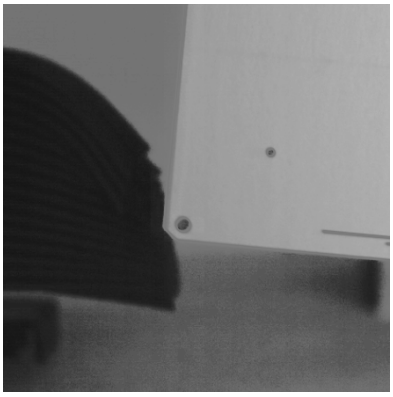

(c) *Body seprates from the brush*

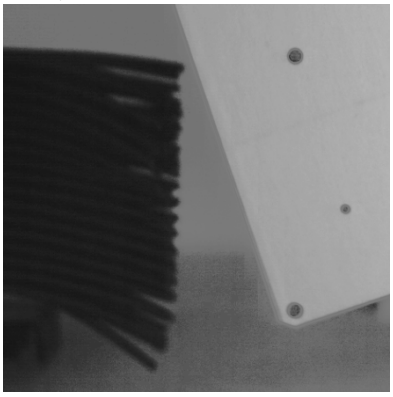

(d) *Momentum transported to bottom bristles*

Figure 2.3: *An experiment highlighting momentum transfer. The first picture shows the setup. The direction of rotation of the body is shown by the red arrow. All other pictures zoom into the region of interest (ROI). Notice that the body makes contact with a few bristles on the top half of the brush. The bristles then transport the momentum to the bottom bristles. This is shown by the bottom bristle being bending and its tip separating from the brush. The tip must carry momentum or else it will not separate cluster of bristle tips*

significant thermal fluctuation and others can greatly affect the brush's performance, and it will be briefly discussed.

2.2.1. A BRUSH FOR ADR

The previous studies showed that a brush could be used for ADR. They produce simple brush models and use them to study various use cases. They have focussed on control algorithms [7], its interaction with a tumbling object [9] or its response to deformation [11]. A question that remains unanswered is what makes it a suitable tool for ADR. This section aims to answer this question using the set of properties of a brush. It presents the relevance of each property and how these properties work together to make the brush an appealing tool.

Stiffness is the primary way for the chaser spacecraft to interact with the debris. It manifests as a reaction force brought forth by deformation. By monitoring brush deformation and controlling it through brush position, the chaser can apply controlled forces to the debris. It also allows the missions to reuse a brush after one operation.

Stiffness, by definition, is the tendency to return to an object's original shape. This property allows the brush to retain its shape and properties after multiple uses. In real life, though, there would be wear in the brush, so it will not last forever.

A brush's inertia allows it to absorb momentum from a body colliding with it. Its stiffness, however, could return it to the incident object. In ADR, this is not favourable. Dissipation can tackle this problem. It converts this kinetic energy into heat and ensures the momentum does not return to the object.

Additionally, momentum transport transports the momentum away from the impact region to other parts of the brush. Momentum transport in conjunction with dissipation makes the brush very effective at shaving away the motion of the impacting object. In the absence of momentum transfer, dissipation would occur only in the isolated impact region, which is very ineffective. With momentum transfer, the motion is transported through the bulk of the brush, allowing it to be dissipated effectively over a large area. Since the momentum carried by the bristles at the region of impact is transported away from it, there will be minimal momentum transferred back to the object. This makes it less likely to bounce off the brush.

Since contact mediates the interaction between the brush and debris, it helps to have more of it. Conformity helps the brush achieve this. It lets the brush adopt the shape of the debris. The contact force now acts over a large area, preventing any regions of enormous stress. For ADR, this is useful because it prevents damage to the debris, which could otherwise break the debris into more debris. This way, the brush can safely exert large forces to detumble the debris. Additionally, a gripper with brush contact surfaces could conform to the shape of a featureless object and grasp it. This task would be pretty challenging to achieve with a standard gripper which requires some features to grab.

Granularity allows the brush to be pierced or parted without permanent damage. This property and large deformation capabilities of the bristles allow the brush to conform to any shape easily. The stiffness would later return the brush to its original unpierced, unparted state. It also allows the brush to be easily repaired. If a section of the brush is damaged, it can be replaced with an identical set of bristles without altering the performance of the whole brush. Other soft material can completely fail if it is damaged or torn. Cracks and tears could propagate through the material rendering it ineffective.

Porosity can play essential roles in the design phase and in capturing debris. While designing, porosity can be used to fine-tune the brush's stiffness. Low porosity would lead to higher stiffness and vice versa. For ADR, the voids or spaces in the brush could potentially host small debris. These spaces could trap dust particles in them, and this could be augmented using adhesives or an electrostatic charge to hold the trapped particles in place.

Apart from the properties, a brush offers a large number of designs. Mission designers could take inspiration from different areas where a brush is used. With the bristle shape and arrangement, we can produce many designs with varying characteristics.

2.2.2. SPACE ENVIRONMENT'S EFFECT ON A BRUSH

The space environment presents many challenges to any asset in space, including the brush. Different hazards could affect its performance and must be considered before deploying this tool. In the following section, we present a brief discussion on this topic. This is a brief discussion, and further studies on this topic are strongly recommended.

The space environment can significantly affect the material properties of the brush. Radiation and vacuum are the chief causes of this effect. Rubber and plastics are materials commonly used to make brushes. Radiation can either harden rubber which eventually leads to cracking, or it can soften it into a viscous matter [26]. The low-pressure environment can lead to outgassing in both rubber and plastics, especially when these materials include volatile additives. Outgassing can affect the polymer chains making up these materials and affect their material properties.

Large temperature fluctuations can also affect the properties of the brush. Firstly, these fluctuations cause the bristles to expand or contract. Uneven expansion may damage it. Second, if the temperature soars to large values, it can melt the brush, permanently damaging it. Even when temperatures do not reach such heights, thermal cycling can harden plastics and rubber, eventually leading to cracks forming in them [26].

Additionally, the small size of the bristles means that they have a small thermal mass. As a body gets smaller, its surface area to volume ratio increases. Consequently, its capacity to emit and absorb radiation, a surface area dependent phenomenon, dominates over its heat-storing capacity, a volume-dependent phenomenon. This exacerbates the problem of thermal fluctuations in bristles.

Like any assets in space, the environment is hazardous and poses a challenge to deploying new tools. So choosing the suitable material capable of handling these dangers over its lifetime is crucial. The physics of the brush and the chemistry of its material must also be studied before deploying. We recommended further studies on this topic.

2.3. CHAPTER SUMMARY

The research studying the use of a brush in ADR had implicitly identified a few of the properties. They incorporated some of these properties into the models of a brush. However, without incorporating all of the properties of a brush, the resultant entity was not uniquely a brush. We have identified six properties: stiffness, damping, conformity, granularity, momentum transfer and porosity. This set of properties separates a brush from other physical objects. It will help us better model the brush's behaviour and help designers decide whether it is suitable for a specific application. Qualitatively, these properties have the potential to be useful for ADR too. The next step is quantifying the utility of the brush. Developing a brush model incorporating all of its properties would help us achieve this.

3

MODELLING A BRUSH

THE brush properties have allowed us the conclusion that it has the potential to be an effective tool for ADR. Developing a numerical model would help studies, such as brush design and control, focus on implementing it for ADR. This section aims to describe a model of a brush.

To do so, we propose using the technique called Discrete Element Method (DEM) to model. It is a technique frequently employed to study granular media. DEM can handle the dynamics of a large number of bodies efficiently.

Previous studies [27, 28] have employed techniques similar to this and managed to capture some of the brush's properties. These studies produced a quasi-static model that could not simulate the full dynamics. Additionally, these models were limited to specific brush designs and a brush contacting flat or curved surfaces; they could not handle any arbitrary shapes or brush design. More importantly, these studies ignored bristle-bristle interactions.

We speculate these models were developed for particular brush applications, such as manufacturing. Rather than exploring new brush designs, these studies aimed to improve the current design. We aim to develop a model which addresses the shortcomings and add additional features.

Developing our own DEM software is time-consuming and tedious. It also distracts us from the main aim of developing and verifying a brush model. So DEM will be implemented using YADE (Yet Another Dynamic Engine). It is a free and open-source software specialising in DEM.

This chapter has the following structure. First, it discusses the theoretical formulation of DEM. Second, it discusses how an ADR scene can be simulated using DEM. Finally, it presents a brief discussion on YADE.

3.1. DEM THEORY

This section presents how the Discrete Element Method works, mainly its theory and formulation. The two main components of DEM are the bodies and the operations performed on these bodies for each timestep. The bodies represent the granular material, while the operations capture the physics of the granular material. DEM can handle a large number of bodies by using simplified body geometries and efficient algorithms for the operation. In simple terms, a DEM simulation starts by initialising all objects' states, then calculating all interactions between these objects and finally numerically integrating their motion. This section will first discuss the bodies and then discuss the operations performed on them. For more details please refer [29]

3.1.1. BODIES

A body in DEM is defined by shape, material and state. The shape is the body's geometry; the material is defined by properties such as Young's modulus and Poisson's ratio, and the state defines the physical state such as position and velocity, among others. The shape and material properties do not change during the simulation, whereas a body's state does. Additionally, the object's degrees of freedom (DOF are stored in the state. Modifying the DOF allows users to constrain the motion of a body.

DEM treats all bodies in the simulation as rigid. So one might assume it is not possible to simulate flexible bodies. This is not true, however. Flexible structures can be simulated by treating them as a collection of rigid bodies and enforcing additional interaction between them. This method allows us to simulate the flexible bristles in DEM.

In this section, we shall discuss first the sphere. Following this, we shall discuss the formulation of flexible structures in DEM. Finally, we will introduce the concept of an aggregate, a method used to model rigid bodies with complex shapes in DEM.

SPHERE

A sphere is an elementary shape. Its shape is defined only by its radius. It is also the most common shape used in DEM, and its simple geometry allows collisions to be detected easily. Additionally, its symmetry simplifies Euler's rotation equations allowing them to be solved easily.

FLEXIBLE STRUCTURES

A flexible structure such as a filament or a rubber ball can be modelled using DEM as a collection of bodies called nodes. They are spheres that have additional interactions with each other. The inclusion of flexible structures extends the scope of DEM as granular material often finds itself interacting with flexible structures. For example, soil is a granular material and studying its interaction with plant roots is an important topic. Geologists could use this information to study how plant roots help soil from falling apart. Such a study is presented Bourrier et al [30]. In our case, we aim to study the interaction between bristles and tumbling debris.

The two main parts of modelling a flexible structure in DEM are its dynamic behaviour and interaction with other bodies. The dynamic behaviour captures the reaction of the flexible structure to external and internal forces. The internal interactions are

defined among the nodes in terms of Constitutive equations. These equations relate the generalised force between two nodes to their relative displacements. The generalised forces, namely, normal force $\mathbf{F}_n$, shear force increment $d\mathbf{F}_s$, bending moment $\mathbf{M}_b$ and twisting moment $\mathbf{M}_t$ are related to six relative displacements also called kinematic variables $\mathbf{u}$.

The constitutive equations used in DEM is designed in such a way to emulate beam-like behaviour [30, 31] and is given by the following set of equations.

$$\begin{aligned} \boldsymbol{F}_n &= \frac{E_n A}{L}\boldsymbol{u}_n \\ d\boldsymbol{F}_s &= \frac{12E_b I_b}{L^3}\dot{\boldsymbol{u}}_s dt \\ \boldsymbol{M}_b &= \frac{E_b I_b}{L}\boldsymbol{u}_b \\ \boldsymbol{M}_t &= \frac{G_t I_t}{L}\boldsymbol{u}_t \end{aligned} \tag{3.1}$$

The coefficients of the kinematic variables are their corresponding stiffnesses. Here E_n is the tensile modulus, E_b is the bending modulus, G_t is the shear modulus, I_b is the bending moment of inertia, I_t is the polar moment of inertia, and L is the distance between the nodes.

Nodes alone cannot simulate the flexible structure's interaction with its surroundings. There are empty spaces between the nodes. A connecting geometry occupies these empty spaces. In the case of a filament or a beam, cylinders connect the nodes. Along with the nodes, these cylinders interact with the other bodies in the simulation. The nodes behave as spheres when interacting with other bodies. The cylinder inserts a fictitious sphere at the point of contact and uses the sphere contact model to calculate force [30].

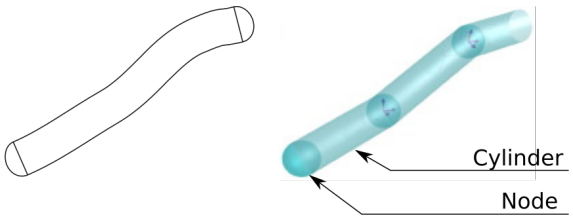

(a) *A flexible rod* (b) *DEM model of a flexible rod*

Figure 3.1: *The geometry of a flexible rod and its model in DEM*

The cylinders themselves do not have any mass; their masses are distributed among the nodes. Similarly, the contact forces experienced by the cylinders are also distributed among the nodes. This way, the dynamic behaviour of the flexible structure is described solely by the nodes, while both the cylinders and the nodes describe the contact behaviour.

DEM extends the concept of a flexible beam to model flexible surfaces. Surface tri-

angulation turns the required surface into a set of triangles, and the nodes are placed at the vertices of this geometry. Again the spaces between the nodes must be filled. Two geometries fill these spaces: cylinders form the edges, and triangular prisms form of faces of the triangulated geometry. The triangular prisms are called particle facets or pfacets [31]. Forces between the nodes are defined by eq 3.1. Like the cylinders, the contact forces at the pfacets surface are calculated by inserting a fictitious sphere. Like the cylinders, the mass of the pfacets and the forces they experience are distributed among the nodes.

This modelling of flexible structures is based on the assumption that these bodies' local deformation or strain is small. This lets DEM use a linear model to calculate force because the stress will be within the elastic limit when the strains are minor. Small strains do not mean that the overall deformation of the structure is small. It can be significant as long as the small-strain condition is valid. This method allows DEM to capture large deformations without assumptions to simplify or linearise geometric non-linearities.

AGGREGATES

As the name suggests, aggregates are composed of bodies clumped together to behave like a single body. These are used to model rigid bodies with complicated geometry. Some of its physical property is the sum of its individual. For example, the mass of the clump is the sum of the mass of all its components. The collision and interaction calculation is carried out for each element, and the resulting forces and torques are summed up and applied to the clump. Any internal forces and torques cancel due to Newton's third law of motion, so interaction among the bodies in a clump is ignored.

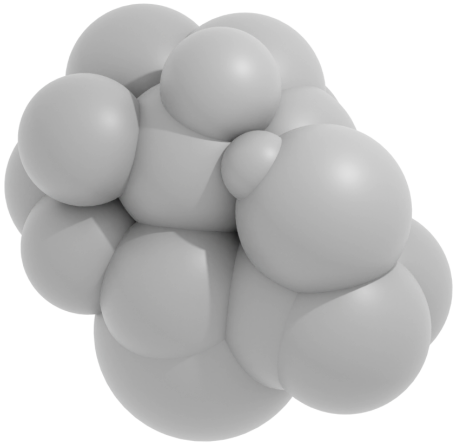

Figure 3.2: An aggregates object compoosed of a set of spheres. Notice that the sphere overlap, but they do not fly apart because the interaction among these bodies are ignored

3.1.2. OPERATIONS

Operations drive the simulation in DEM. They capture the physical behaviour of the system and allow us to predict its evolution in time. It solves Newton's second law and Euler's rotation equation for all bodies using an explicit time-stepping algorithm. The primary operations involved in a DEM simulation are detecting collisions, creating interactions and solving the motion [29]. This section aims to discuss the formulation of these operations in the order they are performed for a time step.

DETECTING COLLISIONS

Finding the overlap between two bodies or detecting collision is computationally expensive. So, collision detection is broken down into two steps to make it more efficient. These steps are approximate collision detection and exact collision detection.

The approximate collision detection is fast and works by defining a simple bounding shape $\tilde{P}_i$ that contains the i^{th} body P_i. The simulation then checks for collisions between these bounding shapes of the two bodies. If a collision is not found between the bounding shapes, one can be sure that the two corresponding bodies are not colliding. The bounding shapes are usually elementary, a box, for example, allowing fast collision detection. Once the simulation detects an approximate collision between two bodies P_i and P_j, it proceeds to calculate the exact collision geometry.

Mathematically this step can be expressed as follows

$$\forall \mathbf{x} \in \mathbb{R}^3 : x \in P_i \Rightarrow x \in \tilde{P}_i \tag{3.2}$$

When two bodies P_i and P_j collide, then $\left(P_i \cap P_j\right) \neq \emptyset \Rightarrow \left(\tilde{P}_i \cap \tilde{P}_j\right) \neq \emptyset$, where $\emptyset$ means a null set. From this one can imply the following

$$\left(\tilde{P}_i \cap \tilde{P}_j\right) = \emptyset \Rightarrow \left(P_i \cap P_j\right) = \emptyset \tag{3.3}$$

So, if approximate collision detection does not detect any collision, there is no collision between the bodies.

The sweep-and-prune algorithm is a popular algorithm used for speedy approximate collision detection. This algorithm uses Axis Aligned Bounding Boxes (AABB) as the bounding shape. Two points define them, the lower and upper corners $\in R^3$. The simulation finds the approximate collision by checking the overlap of these two AABBs along all axis. Mathematically one can find the approximate collision using the following equation. In the following, $\tilde{P}_i^{w0}$ and $\tilde{P}_i^{w1}$ represents the minimum and maximum coordinate of $\tilde{P}_i$ along the w^{th} axis.

$$\left(\tilde{P}_i \cap \tilde{P}_j\right) \neq \emptyset \Leftrightarrow \bigwedge_{w \in \{x,y,z\}} \left[\left(\left(\tilde{P}_i^{w0}, \tilde{P}_i^{w1}\right) \cap \left(\tilde{P}_j^{w0}, \tilde{P}_j^{w1}\right)\right) \neq \emptyset\right] \tag{3.4}$$

The bounding boxes of spheres are shown in figure 3.3. In the figure, all DEM detects two approximate collisions: $\tilde{P}_1$-$\tilde{P}_2$ and $\tilde{P}_2$-$\tilde{P}_3$. It does not detect a collision $\tilde{P}_1$ and $\tilde{P}_3$; this ensures the bodies P_1 and P_3 do not collide. However, one can observe the bodies P_1 and P_2 do not collide whereas P_2 and P_3 do. This will be resolved in the next step, exact collision detection.

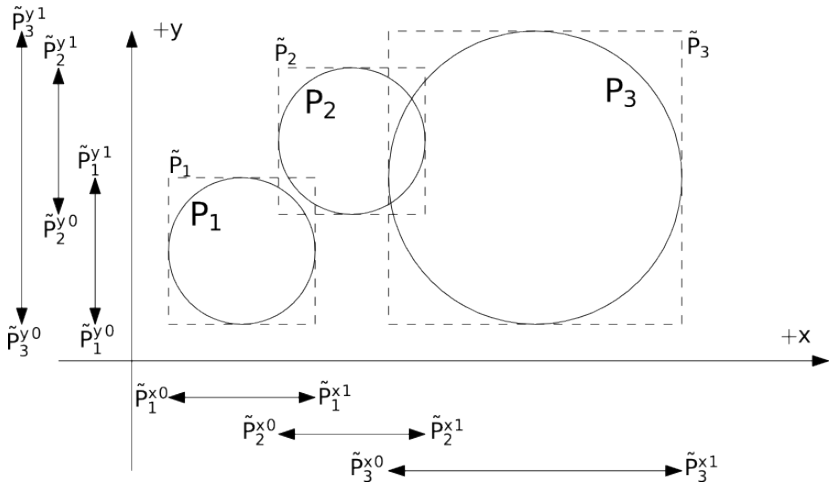

Figure 3.3: Approximate collision detection. The AABB corresponding to P_1 and P_3 do not intersect, implying that P_1 and P_3 have not collided. Taken from [29]

Unlike the previous step, the exact collision detection is slow and computationally expensive. The exact collision detection operates on the two bodies P_i and P_j; its formulation will depend on the shape of the two bodies. For example, the algorithm for detecting a sphere-sphere collision will differ from that of a sphere-cylinder collision. The general idea of this step will be discussed in this section.

Exact collision detection calculates the collision's extent and results in kinematic variables that define the geometry of the collision. These kinematic variables define the mutual configuration of the two colliding particles. Six variables define the mutual configuration of the two bodies. Figure 3.4 shows these six kinematic variables. Normal straining defines the strain along the line, **n**, joining the two centres of the spheres, whereas shearing represents the strain perpendicular to this line. This shearing comes from the component of the relative linear velocity and $\omega_1 + \omega_2$ perpendicular to **n**, where ω_1 is the angular velocity of body 1 and ω_2 is the angular velocity of body 2. Bending comes from the component of $\omega_1 - \omega_2$ perpendicular to **n**, whereas twisting comes from its component parallel to **n**.

CREATING INTERACTIONS

Interaction creation involves calculating the force acting between the two colliding bodies. Three aspects dictate this step: collision geometry, material parameters and the contact model. The exact collision algorithm produce kinematic variables (see section 3.1.2). The material parameters from the two bodies are used to calculate stiffnesses. The contact model accepts the kinematic variables and stiffnesses to calculate the forces and torques acting on the two bodies.

There are four stiffnesses, each corresponding to the four types of kinematic variables (normal straining, shearing, bending and twisting). Some interactions will only make use of the normal and shear stiffnesses. The normal stiffness of the interaction, K_N, is related to the fictitious Young's modulus of the bodies. The shear stiffness, K_T, is

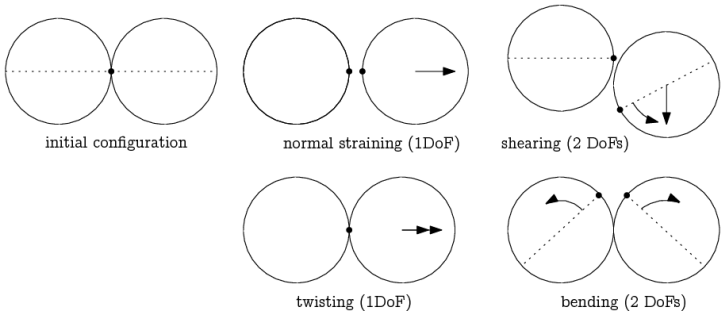

Figure 3.4: The six kinematic variables: one normal strain, two shear strain, two bending strain and one twisting strain. Taken from [29]

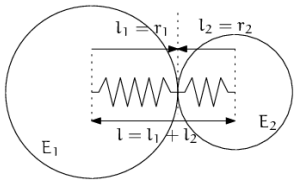

Figure 3.5: Two springs in series represent the stiffness between the two interacting spheres. Taken from [29]

a fraction of K_N. The ratio K_N/K_T represents the Poisson's ratio of the interaction. The macroscopic Young's modulus E is a function of K_N and K_N/K_T.

A commonly used method to calculate K_N is given below. K_N is calculated using two springs of length corresponding to the radii of the two interacting spheres. Let l_1 and l_2 represent the distance between the contact point and the centres of the corresponding spheres. So $l = l_1 + l_2$ represents the distance between the sphere centres, Figure 3.5. Δl represents the change in the total distance, and it is the sum of the Δl_1 and Δl_2. It is also the extent to which the two spheres overlap that represents the deformation. The forces F_1 and F_2 cause this deformation. By Newton's third law, these forces are equal in magnitude, and they are related to the corresponding deformations by $F_i = K_i \Delta l_i$.

$$\begin{aligned} K_N \Delta l = F = F_1 = F_2 \\ K_N (\Delta l_1 + \Delta l_2) = F \\ K_N \left(\frac{F}{K_1} + \frac{F}{K_2} \right) = F \\ K_1^{-1} + K_2^{-1} = K_N^{-1} \\ K_N = \frac{K_1 K_2}{K_1 + K_2} \end{aligned} \tag{3.5}$$

Here, K_i is related to the sphere's Young's modulus E_i and characteristic length $\tilde{l}_i$. The characteristic lenght is proportional to r_i.

$$K_i = E_i \tilde{l}_i$$
$$K_N = \frac{E_1 \tilde{l}_1 E_2 \tilde{l}_2}{E_1 \tilde{l}_1 + E_2 \tilde{l}_2} \tag{3.6}$$

One can observe that the steps described above in 3.6 results in an equation independent of the shape parameters (radius in this case). This step takes the material properties of the two bodies and returns the stiffness, whereas the deformation Δl represents the collision geometry, and the collision detection step calculates this value.

The step of creating interaction ends by calculating the contact force between the two bodies. The collision geometry and the stiffnesses along with the constitutive laws are used to calculate the contact force. A very popular are common constitutive law, originally proposed by Cundall [32], is shown presented here.

$$\boldsymbol{F}_N = K_N \boldsymbol{u}_N \boldsymbol{n}$$
$$\boldsymbol{F}_T^t = K_T \boldsymbol{u}_T \tag{3.7}$$

At each step, the normal displacement, $\boldsymbol{u}_N$, and shear displacement, $\boldsymbol{u}_T$, are used to calculate the forces. Note that the interaction is deleted if $\boldsymbol{u}_N > 0$. These equations result in the normal force $\boldsymbol{F}_N$ and a trial shear force $\boldsymbol{F}_T^t$. Friction mediates the shear force, so it must be checked if its value is below the limiting static friction.

$$\boldsymbol{F}_T = \begin{cases} \boldsymbol{F}_T^t \frac{|\boldsymbol{F}_N| \tan\varphi}{|\boldsymbol{F}_T^t|} & \text{if } \left|\boldsymbol{F}_T^t\right| > |\boldsymbol{F}_N| \tan\varphi \\ \boldsymbol{F}_T^t & \text{otherwise} \end{cases} \tag{3.8}$$

Here, φ is the friction angle. The final force acting on the two particles is the sum of the two forces. These forces act at the point where two spheres contact. Since the spheres may have different radii, the torques must be calculated independently. The following equations express the final force and torque acting on the two bodies.

$$\begin{aligned} \boldsymbol{F}_1 &= \boldsymbol{F} & \boldsymbol{F}_2 &= -\boldsymbol{F} \\ \boldsymbol{T}_1 &= d_1(-\boldsymbol{n}) \times \boldsymbol{F} & \boldsymbol{T}_2 &= d_2 \boldsymbol{n} \times \boldsymbol{F} \end{aligned} \tag{3.9}$$

SOLVING THE MOTION

At each timestep, a body accumulates generalised forces (forces and torques) from its interactions with other bodies. The simulation solves Newton's second law and Euler's rotation equations using the generalised forces to predict the behaviour of all bodies in the system. It uses an explicit time-stepping algorithm for solving these equations.

The leapfrog scheme is a popular scheme used to solve these equations numerically and will be discussed below. The leapfrog scheme stores even derivatives at on-step points and the odd derivatives at mid-step points. This section shows how the leapfrog scheme is implemented to calculate linear motion.

Let a be a variable representing the state of the body. The following represents its value at different timesteps.

- a^{-1} Previous timestep

- a^0 Current timestep
- a^{+1} Next timestep
- $a^{-1/2}$ Previous mid step
- $a^{+1/2}$ Next mid step

u denotes the position of a body, and it is calculated from the acceleration, which is denoted by $\ddot{\boldsymbol{u}}$. Acceleration, at the current timestep, is calculated from forces accumulated on the particle given by

$$\ddot{\boldsymbol{u}}^0 = \boldsymbol{F}/m \tag{3.10}$$

The position at the next timestep u^{+1} is calculated from the acceleration at the current timestep using the second-order finite difference equation.

$$\begin{aligned} \boldsymbol{u}^{+1} &= 2\boldsymbol{u}^0 - \boldsymbol{u}^{-1} + \ddot{\boldsymbol{u}}^0 \Delta t^2 = \\ &= \boldsymbol{u}^0 + \Delta t \left(\frac{\boldsymbol{u}^0 - \boldsymbol{u}^{-1}}{\Delta t} + \ddot{\boldsymbol{u}}^0 \Delta t \right) \end{aligned} \tag{3.11}$$

The above equation is incomplete because $\boldsymbol{u}^{-1}$ is not known in the current timestep. This information can be derived from the velocity from the previous half step (denoted by $\dot{\boldsymbol{u}}^{-1/2}$)

$$\begin{aligned} \dot{\boldsymbol{u}}^{-1/2} &\simeq \frac{\boldsymbol{u}^0 - \boldsymbol{u}^{-1}}{\Delta t} \\ \boldsymbol{u}^{+1} &= \boldsymbol{u}^0 + \Delta t \left(\dot{\boldsymbol{u}}^{-1/2} + \ddot{\boldsymbol{u}}^0 \Delta t \right) \end{aligned} \tag{3.12}$$

Note that the expression in parenthesis in equation 3.12 is, in fact, the velocity at the next half step.

$$\dot{\boldsymbol{u}}^{+1/2} \simeq \dot{\boldsymbol{u}}^{-1/2} + \ddot{\boldsymbol{u}}^0 \Delta t \tag{3.13}$$

Combining all of the equations presented above, we can summarise that the position integration is done in two steps. First is calculating velocity at the following half timestep, and later by calculating the position at the following time step.

$$\begin{aligned} \dot{\boldsymbol{u}}^{+1/2} &= \dot{\boldsymbol{u}}^{-1/2} + \ddot{\boldsymbol{u}}^0 \Delta t \\ \boldsymbol{u}^{+1} &= \boldsymbol{u}^0 + \dot{\boldsymbol{u}}^{+1/2} \Delta t \end{aligned} \tag{3.14}$$

3.2. CONSTRUCTING AN ADR SCENE IN DEM

In a contact-based ADR mission, the primary interaction occurs between the tool and the debris. These tools could be tentacles, end effectors or, in our case, a brush. In our simulations, the bodies that we will focus on are the brush and the debris.

The brush would be simulated as an array of bristles. These bristles are slender rods and will be simulated using a set of nodes and cylinders. Figure 3.6 shows how nodes

and cylinders build a bristle. It also shows how a bristle with a non-uniform radius is constructed. The roots of the bristles are fixed by constraining all the degrees of freedom of the root nodes. Aggregating all the root nodes also achieves a similar effect.

(a) *A simple bristle* (b) *A tapered bristle*

Figure 3.6: *Bristles constructed with nodes (circle) and cylinders (rectangles). A simple bristle has the same radius across its length, while the radius of a tapered bristle changes along its length. Changing the dimensions of the cylinders and nodes achieves this geometry*

The debris geometry is constructed using pfacets, cylinders and nodes. For brevity, this set of bodies would be referred to as pfacets unless stated otherwise. Pfacets form a set of solid triangular facets which can approximately recreate the geometry of any arbitrarily shaped body. The geometry of a body can be modelled in any 3D modelling software and imported into the DEM simulation.

This body made of pfacets is not rigid and can deform. Assigning a large young's modulus to this body to simulate rigidity can be unfavourable as the simulation would require very fine timesteps to remain stable. Alternatively, a rigid geometry using pfacets can be achieved by adding all its constituent bodies to an aggregate, rendering it completely rigid. Additionally, this aggregate's mass and inertia properties can be edited to match the debris's.

3.3. YADE

This section aims to present the features in YADE that will be used to construct the brush model and ADR scenarios. YADE is an extensible open-source framework for discrete numerical models, focusing on the Discrete Element Method. It stands for Yet Another Dynamic Engine. It offers a user-friendly and concise scene setup, simulation control, debugging and post-processing interface using Python. Additional information on YADE is available in [29].

3.3.1. WHY YADE

Coding our own DEM framework can be time-consuming and takes our attention away from the scientific aspect of this project. Apart from the core DEM algorithms, the framework requires other features such as input/output of files, visualisation of results, and generating the system's initial state. When developing DEM software, optimising the code and reducing its resource usage is another major task as DEM is very computationally expensive. All of these tasks distract us from actually studying the behaviour of a brush.

Using an existing framework is an obvious solution. Commercial software suites like ABAQUS, ANSYS and others are expensive and can be restrictive. Extending these softwares to include additional features is difficult as we are at the mercy of their existing interfaces. On the other hand, free and open-source frameworks do away with this restriction by allowing one to modify the software's source code. It lets us develop the code and include additional features specific to the research without worrying about cost or

developing a DEM framework. YADE is a very popular DEM package. It is documented extensively and has a very active community developing it.

3.3.2. FEATURES OF YADE

The YADE back-end is written in C++, and it uses concepts in Object-Oriented Programming extensively. C++ allows YADE to be computationally very efficient. The primary benefit of using OOP is that the code reflects the system we want to simulate. For example, the whole system would be contained in a system class; each body is an instance of the body class while the different operations belong to operation classes. The interfaces defined in each class allow them to communicate with each other. OOP makes the code very modular.

It also allows YADE to be readily extended by inheriting features when implementing new algorithms. The primary interfaces used to interact with the different components are implemented in template classes, freeing the users from worrying about integrating their code into YADE. We need only translate our algorithms into C++ code and inherit the appropriate class. The following example illustrates this process. Operations in YADE are called engines, and they are implemented as classes in C++. The forceEngine is one such class used to apply a user-defined force on all bodies in the simulation. It has access to the state of all bodies so users can implement models which require it.

For example, the dynamics of a body in orbit can be simulated by implementing the Clohessy–Wiltshire equations in a class inherited from the forceEngine class. The forceEngine class supplies the necessary information about a body's state and applies these forces to all the bodies. The Clohessy–Wiltshire class need only calculate the force from the body's state.

In YADE, the DEM model of a system is created using Python. All C++ components of YADE is wrapped within a Python wrapper, allowing them to be used in a Python script. Python allows quick and concise model development because of its simple syntax. Its extensive package library allows us to use different packages to add more features to a simulation. For example, the JSON (JavaScript Object Notation) package allows us to output the simulation results into a human-readable file.

3.3.3. YADE SIMULATIONS

A YADE simulation starts by creating the bodies in the simulation and defining their initial state. Bodies are created using helper functions in Python, which calls the appropriate body constructor. Spheres are created using the sphere function; nodes are created using the grid-node function, cylinders with the grid-connection function and particle facets using the pfacet function. Bodies can be aggregated together by passing the list of bodies to the clump function.

Operations in YADE are called engines. Engines act on all bodies by changing their state. They drive the simulation, calculating the time evolution of the system. The simulation loop in YADE consists of successively calling these engines to modify the system's state. A typical simulation loop in YADE is shown in Figure 3.7

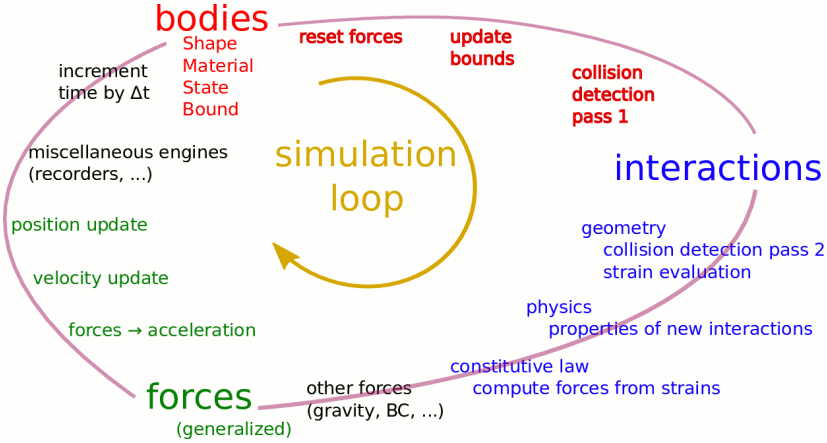

Figure 3.7: A simulation loop in YADE. It starts by resetting the force on all bodies, followed by calculating the interaction, the generalised force and finally updating the state of all bodies. Addtional steps such as data recording can be inserted at the end of the loop. Taken from [29]

3.4. CHAPTER SUMMARY

This chapter presented the Discrete Element Method. We use it to model a brush and the debris. It presented the theoretical background of DEM and discussed the models and algorithms used in a simulation. Next, it discussed how DEM is employed to model a brush and tumbling debris. Finally, it presented YADE, a free and open-source software implementation of DEM and discussed its features, relevance and workings.

4

VERIFICATION

THE previous chapter presented the brush model, and this chapter will present the methods used to verify this model. Experiments were used to verify the brush model. This chapter will discuss the details of the experiment its results and then compare these results with the predictions given by the brush model.

Alternate methods were considered for verifying the brush model. The literature study pointed to experiments conducted on brushes, and we considered using that data to verify the brush model. However, these experiments, for example, Shia et al. [28], made use of brushes with 1000s to 10,000s of bristles. Simulating such an experiment would require substantial computing resources, so they were excluded. Multibody simulations using FEM for deformation was another candidate. However, the software was not accessible. So, it was concluded to perform experiments with a brush that could be simulated with the available computing resource.

Although using an alternative numerical method to simulate a brush is difficult, it was impossible to do the same for a bristle. The brush is expected to undergo considerable deformation, so does a bristle. The cosserat rod model can efficiently predict the behaviour of a slender rod, or in our case, a bristle, undergoing large deformation. Comparing the results from DEM and a verified cosserat rod model would support the validity of the DEM bristle model.

The brush model was verified using two experiments—the first test studied the static deformation of the brush and its reaction to this deformation. The second involved the brush interacting with a rotating body. This experiment corresponds to the dynamic behaviour of a brush.

In this chapter, the experiments or alternate models and the DEM simulations are grouped under test cases. These sections will also present the results and discuss the accuracy of the DEM model. Three tests correspond to the three methods used to verify the model. The first test will focus on the dynamics of a bristle. Rather than an experiment, the DEM results would be compared to the data from a verified cosserat rod

model. The second and third tests will discuss an experiment involving the brush's static and dynamic behaviour, respectively, the corresponding DEM model.

4.1. BRISTLE DYNAMICS TESTS

As described in the previous chapter, a bristle is simulated using DEM as a slender rod. This slender rod comprises multiple spheres called nodes chained together using cylinders. The interactions between the nodes are modelled to behave like a flexible rod. The original paper [30] verified this model in the static sense: the rod was subjected to a deforming force, and its reaction force was measured. This result was then compared against the analytical solution of a rod undergoing large deformation. This section aims to check the validity of this model in the dynamic sense: the motion of the rod when subjected to external forces.

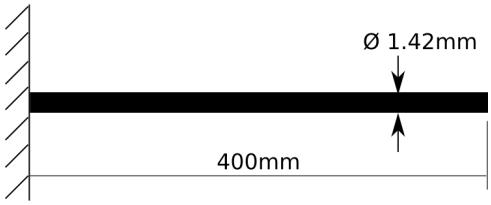

Figure 4.1: *Dimenions of the rod used in the simulations*

The rod used for verification has the following properties.

Property	Value	Unit
Young's modulus	200×10^9	N/m^2
Poisson's ratio	0.3	
Density	7640	kg/m^3
Length	0.4	m
Diameter	1.42×10^{-3}	m

Table 4.1: Physical properties of the bristle

The motion of the rod, in our case the bristle, predicted by DEM, will be compared against the predictions of another rod model called the Cosserat rod model. Like the DEM model, it captures the geometrical nonlinearities of deformations of rods. Till et al. [33] used this to develop a numerical model of a flexible robot. This model used a linear elastic material model to calculate the reaction forces. They verified this model using experiments involving a vibrating rod. Since the experimental data is not available, we shall use their numerical model to simulate their experiments, and its results will be compared against the predictions of the DEM bristle model.

The simulation consisted of a slender horizontal rod fixed at one end. Figure 4.1 shows the rod, its fixture and its dimensions. There were three test cases, each having a different way of exciting the rod's motion. In all the following cases, the rod will undergo

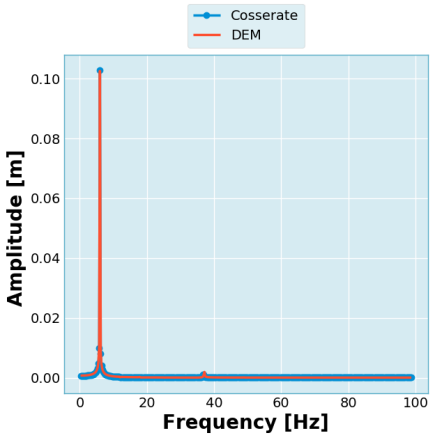

Figure 4.2: *Weight release test power spectrum. Comparison of the DEM and the cosserat rod models simulation results. The position of the free end of the rod is tracked. And this data is used to calculate this power spectrum*

vibration, and the validity of the DEM bristle model is based on the extent to which its prediction matches the cosserat rod model's prediction.

4.1.1. WEIGTH RELEASE TEST

In the weight release test, the free end of the rod was subjected to a transverse deformation and released. A 20g weight attached to the free end of the rod caused this deformation. Releasing the weight causes the rod to oscillate, allowing it to do so for 4.5s. The power spectrum, Figure 4.2, of the vibrating rod reveals that low-frequency vibration dominates the motion. Both DEM and cosserat rod model predictions agree on the lower exciting frequency and predict the insignificant higher frequency oscillations. The following cases will, however, excite the higher frequency more.

4.1.2. IMPULSE LOAD TEST AT FREE END

The rod was subjected to an impulse load at the tip for the second case. This impulse load was modelled using a piecewise function, and its graphical representation is shown in Figure 4.3. In the figure, M denotes the maximum value of the force, and d denotes the duration of the impulse.

As seen in the previous test case, both DEM and the cosserat rod model predict the same frequency of the low-frequency vibration. We observe two additional details: the high-frequency vibration is more prominent than the previous scenario, and both DEM and the cosserat rod model agree on its frequency with slight deviations.

4.1.3. FIXED END IMPULSE LOAD TEST

This test is similar to the previous case. It uses the same impulse load function, but the force is applied to a point close to the root. The load is applied at a point located at 0.0458m from the root. There are no nodes at this location for the vibrational modes of

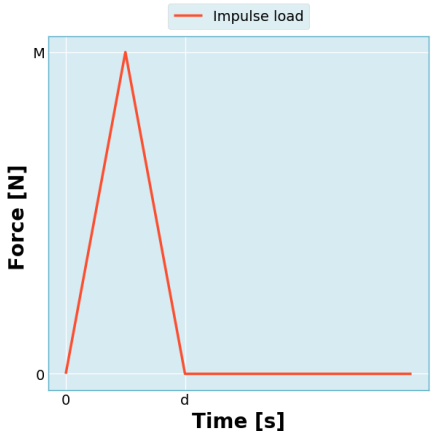

Figure 4.3: *The function used to a model the impulse load acting on the rods*

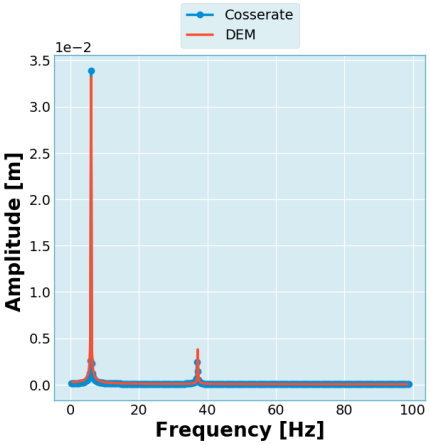

(a) *Full range*

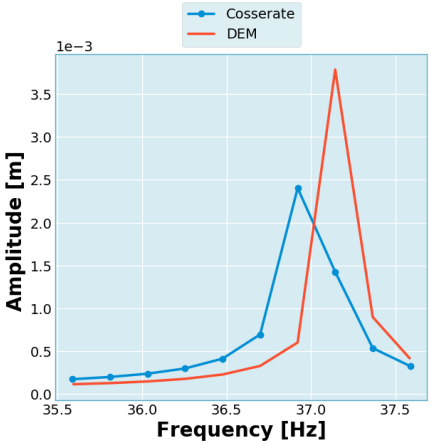

(b) *High frequency region*

Figure 4.4: *Free end impulse load test power spectrum. Comparison of the DEM and the cosserat rod model simulation results. The vibrations are observed at the free end of the rod. The first subfigure shows the entire power spectrum and while the second focuses on the high-frequency region of the power spectrum.*

the bristle in the frequency range we study. This test hopes to provide more excitation to the higher frequency vibrations. This test is called so since the load is applied close to the fixed end.

We see that both DEM and the cosserat rod model predict the same vibration frequency at the low-frequency range. However, at the higher frequency region, they predict slightly different frequencies.

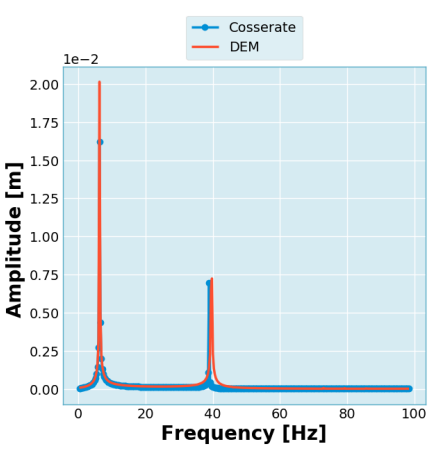

(a) *Full range*

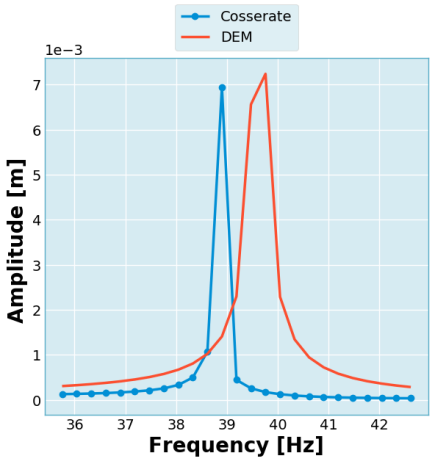

(b) *High frequency region*

Figure 4.5: *Fixed end impulse load test power spectrum. Comparison of the DEM and the cosserat rod model simulation results. The vibrations are observed at the free end of the rod. The two subfigures show the entire power spectrum and the high-frequency region of the power spectrum.*

4.1.4. DISCUSSION

The bristle modelled using DEM can correctly predict the dynamics of a bristle at lower frequencies. However, there is a slight deviation in its prediction at higher frequencies compared to the cosserat rod model. This deviation becomes an issue only if energy is somehow injected into the higher frequency region. However, it can be argued that this higher frequency component will play a lesser role in a brush. The dissipative nature of the brush prevents any excitation of high-frequency vibrations, as these vibrations would be damped quickly.

A brush is composed of bristles that interact with each other through contact forces. Friction is part of this interaction and its damps vibration. This phenomenon is made clear in the frequency response of a vibrating rod moving under the influence of friction. Using DEM to study this phenomenon, a simulation of the same bristle was set up. The bristle was excited by an oscillating load to vibrate at different frequencies. The bristle was made to rest on a surface that exerted friction force. One bristle end was fixed while an oscillating force was applied to the other, the free end. The response of the bristle to a particular frequency was obtained by setting the applied oscillating load to vibrate at that frequency.

The results, in Figure 4.6, show that the bristle responds readily to low-frequency dynamics while friction damps higher frequency dynamics. Even the peak in the high-frequency region is less than one-eighth of the corresponding low-frequency peak. This result supports the argument that friction in a brush dissipates high-frequency oscillations.

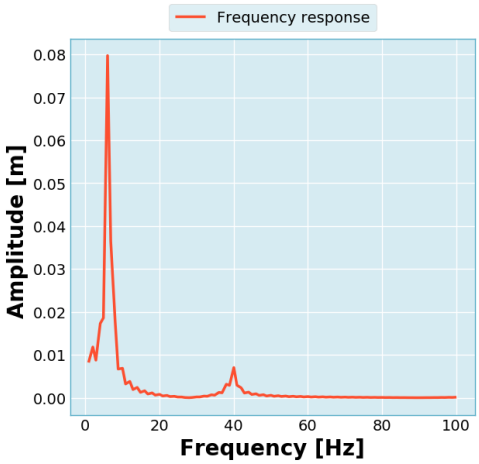

Figure 4.6: *The frequency response of a flexible rod damped by friction to an oscillating force acting on its tip.*

4.2. BRUSH STATIC TEST

The static test is the first step in verifying the DEM model of a brush. By comparing the behaviour predicted by the model and the behaviour of a brush observed in an experiment, we can conclude the extent to which the DEM model captures the brush's behaviour.

Doing a static test eliminates a significant influencer of brush behaviour: motion. Although our final aim is to develop a brush model suitable for use in managing moving space debris, the static test allows us to focus on other brush properties, which influences the fidelity of the brush model. Specifically, properties such as stiffness, dissipation, conformity and granularity of the brush are highlighted in this test.

To study these properties of the brush, first, the working of the test must be understood. The first part of this section explains the test setup and the rationale behind its design. The second part discusses the DEM model and its predictions. The third part presents the experiment setup and behaviour observed in the experiments. The final part compares the simulation results, and the experiment concludes this test.

4.2.1. DESIGN

This test aims to study how damping, stiffness and conformity manifest in the brush's behaviour. Stiffness manifests as a reaction force upon deformation, friction arises as a reaction force parallel to the contact surfaces, and finally, conformity is the ability to react to an object's shape and apply a distributed force over the surface penetrating the brush. So the requirements for this test are as follows: the brush behaviour must be observed at different states of deformation; a contact force must drive this deformation, and a part of this force must be parallel to the contact; the contact surface must penetrate the bounding surface of the brush, parting the bristles.

It was decided to use a wedge to penetrate the brush along the bristle length for the static test. This is illustrated in Figure 4.7. The three requirements stated above are sat-

isfied in the test. Since the deformation is directed along the vertical, there would be a reaction force in this direction. The contact surface between the brush and the wedge is angled away from the vertical. Consequently, a component of the tangential friction force would be directed along the vertical. Moreover, the bristles deform in such a way to accommodate the shape of the wedge. Additionally, using wedges with different angles would allow us to observe how their shape affects the brush's response.

The vertical force quantifies the reaction force generated by friction and stiffness. The conformity of the brush can be studied by changing the wedge angle and observing how the reaction force changes.

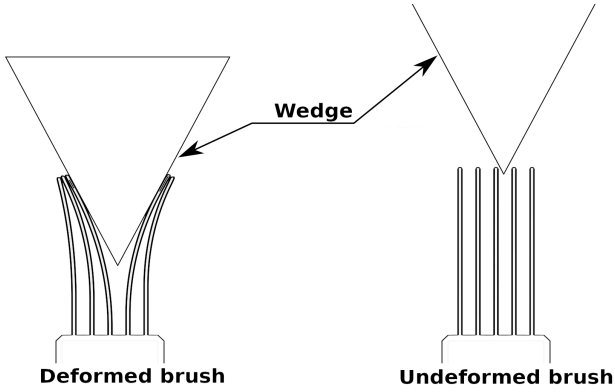

Figure 4.7: *Static test design illustration. The bristles are aligned vertically, and a wedge deforms the brush by penetrating the brush volume along the vertical direction. The wedge will be supported to not fall due to gravity. This support is not shown in the diagram.*

Additionally, more information into the physics of the test can be gleaned from the free-body diagram shown in Figure 4.8. This system has three main contact forces: wedge-bristle contact force, bristle-brush support contact force, and wedge-wedge support contact force. Since this is a static test, the system will be at equilibrium. If the brush is considered isolated, the force applied on the bristles must equal the force applied by the brush support.

Similarly, if the wedge is isolated, all the force applied by the bristles must be equal to the force applied by the wedge support. This situation presents two options to measure the reaction force generated from penetration. Their values differ because the brush and the wedge weigh different; their change is the same because the deformation of the brush causes it. This can be seen in equations. So measuring the change in force at either position would be no different.

$$\text{Total force on bristle} = \vec{F}_n + \vec{F}_t + \vec{F}_{b,y} + \vec{F}_{b,x} - m_b g \hat{j} = 0 \tag{4.1}$$

Force along the y axis/vertical axis

$$\begin{aligned} F_y &= F_n \sin(\theta/2) + F_t \cos(\theta/2) + F_{b,y} - m_b g = 0 \\ \Delta F_y &= \Delta F_n \sin(\theta/2) + \Delta F_t \cos(\theta/2) + \Delta F_{b,y} = 0 \\ \Delta F_{b,y} &= -(\Delta F_n \sin(\theta/2) + \Delta F_t \cos(\theta/2)) \end{aligned} \tag{4.2}$$

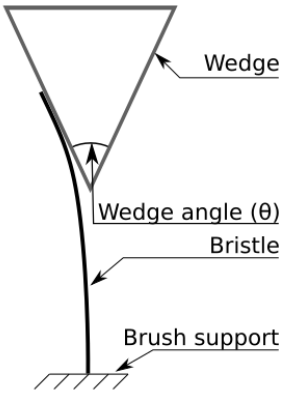

(a) *Bristle interacting with wedge*

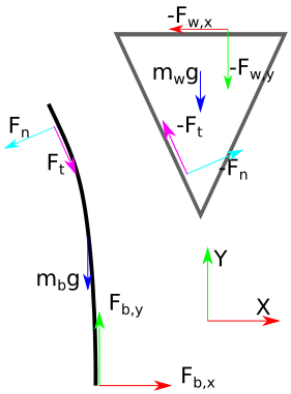

(b) *Free body diagram of the bristle and wedge*

Figure 4.8: *The two figures show how a bristle is being deformed. The first figure shows how the penetration of the wedge into the brush deforms the bristle. The second figure shows all the forces acting on the bristle and the wedge. F_n is the normal force, and F_t is the tangential force applied on the bristle by the wedge. $F_{b,x}$, $F_{b,y}$ are the x and y components, respectively, of the force applied by the brush support on the bristle. $-F_n$ and $-F_t$ are the normal and tangential forces, respectively, applied on the wedge by the bristle. $-F_{w,x}$ and $-F_{w,y}$ are the x and y components, respectively, of the force applied on the wedge by its support. X and Y represent the positive directions of the X and Y axes.*

A significant part of the test design was selecting a brush that could be simulated. The main constraint posed by the simulations is in the number of bodies. In the case of a brush, many bristles require considerable computational resources. So a brush with bristle numbering in the 100s is more favourable than one numbering in 1000s or more. Another constrain is the radius of the bristles relative to the length the wedge penetrates. Even though this is a static experiment, some movement must be present to bring about the deformation. If the radius is small, then the time step must be correspondingly small so that bodies do not pass through one another without detecting collision in one step. Finally, a brush with randomly arranged bristles is undesirable because recreating the bristle in DEM would be very difficult. A brush that meets the constraints posed by the simulation was found online, and it is shown in Figure 4.9

This brush was made of silicone rubber. The bristles had a length of 33 mm and were arranged in a 17x5 grid. The manufacturer did not mention the type of silicone rubber, so physical properties such as Young's modulus, density, et cetera had to be found elsewhere [34]. This source provides the following ranges of values for physical properties: Young's modulus = 0.001 - 0.05 GPa; density = 1100 - 2300 kg/m^3; Poisson ratio = 0.47-0.49. The range of value for Young's modulus is too large for this experiment, so its value was found experimentally. Its value was found to be $2.7 \pm 1.1 GPa$, and this experiment is detailed in appendix B. The friction coefficient was another property that had to be found experimentally. The procedure used to find this is explained in appendix C. These uncertainties would be taken into account in the simulations.

(a) *Front view* (b) *Side view* (c) *Top view*

Figure 4.9: *The brush seen from different angles. Notice that the bristles are arranged in a 17x5 grid. Recreating this arrangement in DEM would be easier than one with a random arrangement.*

4.2.2. SIMULATIONS

With the test design complete, the next step is to make a theoretical prediction of the phenomena we would observe in the experiment. The test would be simulated using DEM in YADE. This section describes this process, including the YADE model, its result and general features of this result.

SIMULATION SETUP

The simulation was set up as follows. Initially, the wedge was placed right above the bristles' tip, as shown in Figure 4.7. The nodes of the bristle at the root end were fixed by constraining their degrees of freedom. Even though their motion was restricted, they still experienced force. They do not move because YADE sets their acceleration to zero for all iterations. The force experienced by these nodes will equal the sum of the bristle weight and the reaction force. The wedge was modelled as a clump of pfacet, whereas the brush was modelled using grid-nodes and grid-connections. This is illustrated in Figure 4.10.

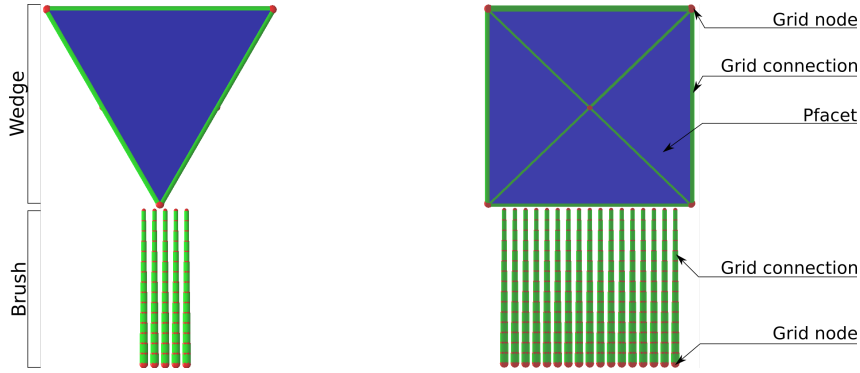

(a) *Front view* (b) *Side view*

Figure 4.10: *The bodies modelled in YADE. The colours indicate the different objects that make up the brush and wedge. Grid-nodes are coloured red; the grid-connections are coloured green, and pfacets are coloured blue. Note that the sizes of the objects have been exaggerated for the sake of clarity.*

In the simulations, the wedge moved into the brush in steps of 1mm and reached a maximum depth of 33 mm before retracting. The first part of the simulation is called loading, while the second is called unloading. The bristle's length for the chosen brush is 33 mm, and it would not be possible to go beyond that length. The speed of the wedge motion followed a parabolic function of time, gradually increasing, reaching its peak, and reducing to zero. Such a profile avoided large accelerations. This function had two parameters: maximum acceleration (a_m) and penetration (s), the step size.

$$
\begin{aligned}
v(t) &= -k(t(t-t_d)) \\
&\text{where} \\
k &= a_m / t_d \\
t_d &= \sqrt{(6s/a_m)} \\
v(t) &\Rightarrow \text{Velocity as a function of time } t \\
a_m &\Rightarrow \text{Maximum acceleration} \\
t_d &\Rightarrow \text{Duration of one step} \\
s &\Rightarrow \text{Penetration step size} = 1mm
\end{aligned}
\tag{4.3}
$$

The simulation loop had three steps: move the wedge and stop, wait till equilibrium and record the force. The simulation initialises by creating the brush and the wedge objects. The wedge occupied a space right above the brush without touching it. Next, the simulation script moves the wedge down one step. Moving the wedge into the brush will set the bristles into motion. The simulation waits for the bristles to reach equilibrium to measure the static response of the brush. The script runs a predefined number of iterations and calculates the standard deviation of the total force measured at the fixed end of the brush in that duration. This process is continued until the standard deviation is within a threshold, signifying the brush has reached equilibrium. At equilibrium, the total force at the bristle roots is recorded. The simulation repeats this moving, waiting, and recording cycle until the wedge reaches the maximum penetration depth. At this point, the wedge starts retracting from the brush by changing the direction of the motion. The simulation stops once the wedge moves out of the brush volume. Figure 4.11 shows a flow chart representing the simulation script. These steps were repeated for wedges with different angles.

SIMULATION PREDICTION AND DICUSSION

This section will briefly discuss these results, including some peculiar features. The main observations of the force response were its non-linear nature, hysteresis and increasing magnitude with larger wedge angles. This set of observations and the magnitude of the force response constitutes the simulation prediction.

The reaction force is a non-linear function of penetration. Two factors contribute to this nonlinearity. Firstly, the bristles bend to accommodate the wedge into the brush. Bending in itself is a non-linear phenomenon. The brush inherits this nonlinearity, and it manifests in this experiment. Secondly, more bristles deform when the wedge reaches further into the brush. The wedge bends only one or two bristles for shallow depths.

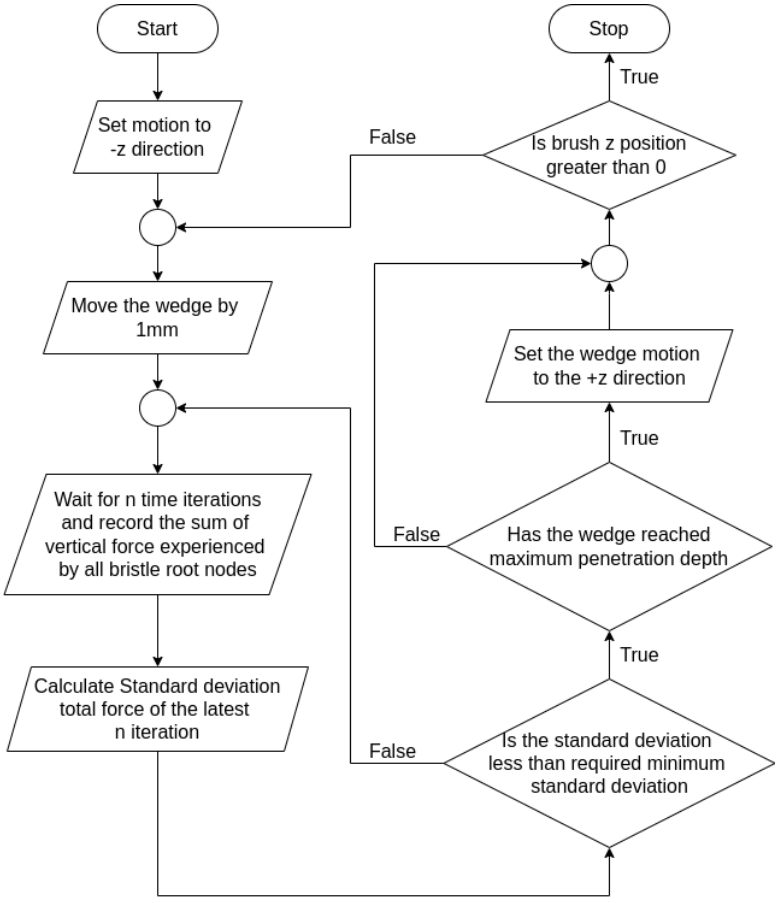

Figure 4.11: *Static test simulation logic*

However, as it penetrates deeper into the brush, these two bristles touch their neighbours, bending them, and further penetration forces these neighbours to touch their neighbours. This cascade of bristle bending leads to nonlinearity as a group of many bristle bending has a higher stiffness than a few. Thus, these two factors work together to make the reaction force a non-linear function of penetration.

An interesting feature observed in the graph is that the retraction curve does not coincide with the penetration curve. This phenomenon results from the friction acting between the bristles and the wedge. Friction points to a direction against the motion. When the wedge penetrates the brush, friction has a component pointing upwards against the penetration. The reaction force due to stiffness of the bristles also has a component pointing upwards, resulting in a large vertical force. When the wedge is retracted, the friction has a component pointing downward against the retraction. The reaction force due to stiffness, however, still points upwards. The resultant vertical force would

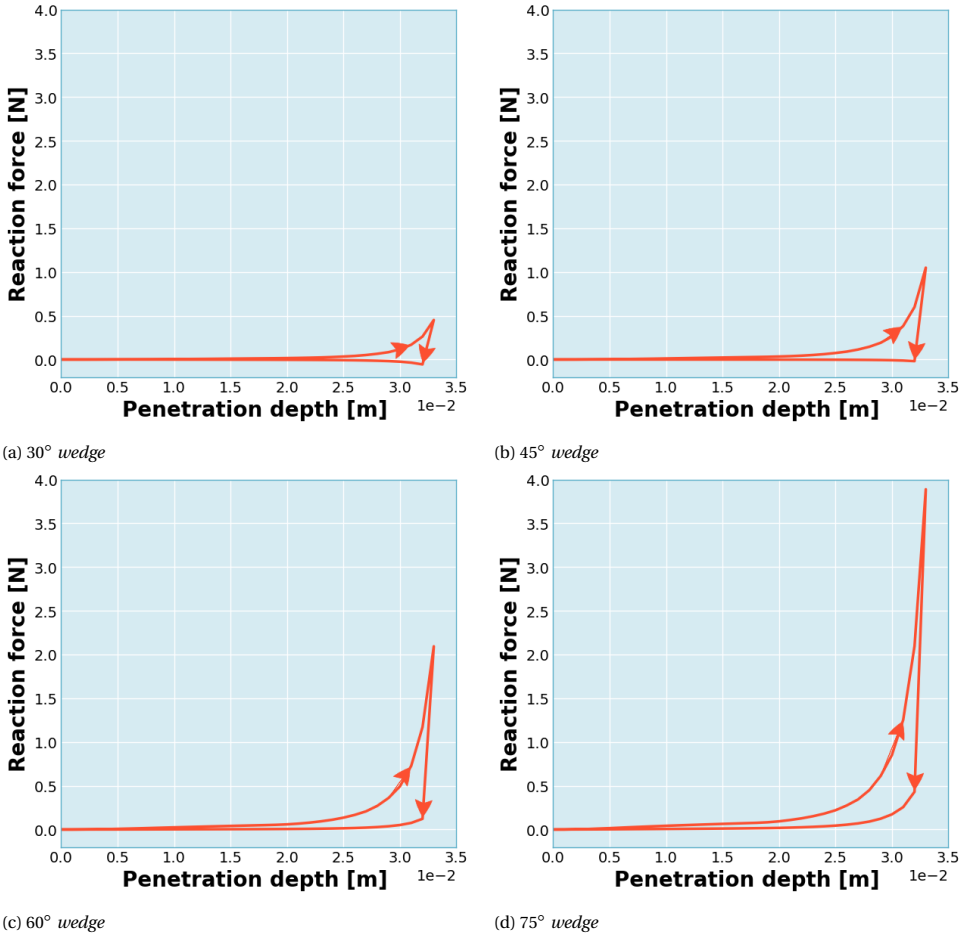

(a) 30° *wedge*

(b) 45° *wedge*

(c) 60° *wedge*

(d) 75° *wedge*

Figure 4.12: *DEM prediction of the response of the brush to four wedges with different angle. The arrows show the direction of deformation. When the wedge penetrates, the depth increases, shown by the arrow pointing to the right on the top curve. When it retracts, the depth decreases and this is shown by the arrow pointing to the left on the bottom curve.*

be lower. This mismatch manifests as two separate curves in Figure 4.12

Another observation is that the retraction curve jumps almost immediately to zero when the wedge angle is 30° while it approaches zero at a slower rate for higher angles. This, again, can be attributed to friction. At lower angles, friction contributes more to the vertical force, dominating its behaviour. On the other hand, the vertical force has a lower influence of friction at higher angles. Alternatively, we can use eq. 4.2 to explain this behaviour. In the equation friction or F_t has a coefficient $cos(\theta/2)$. So this term loses significance at high values of θ.

Finally, higher wedge angles equated to higher bristle bending, resulting in higher

reaction force. This phenomenon is shown in Figure 4.12. Notice that as the wedge angles increase, the maximum reaction force increases. This phenomenon is explained by the bristle bending more when deformed by a wedge with a higher angle. An increase in bending increases the reaction force generated by the brush.

ERRORS IN PARAMETERS

The simulations depended on certain parameters whose values were uncertain. These could influence the predictions and had to be handled. There were four main parameters whose values were uncertain: the radius of the bristles, Young's modulus of the bristle, coefficients of friction in the bristle-wedge and bristle-bristle interaction.

A sensitivity study was conducted on how variations in these parameters could potentially influence the simulation. This study was done for all four wedges. Figure 4.13 shows the result for the 30° wedge and appendix D contains the remaining graphs. The sensitivity to each parameter was tested across each value's error range. Note that the bristles have a conical shape, so they do not have a fixed radius. The sensitivity study uses error in radius instead of absolute radius.

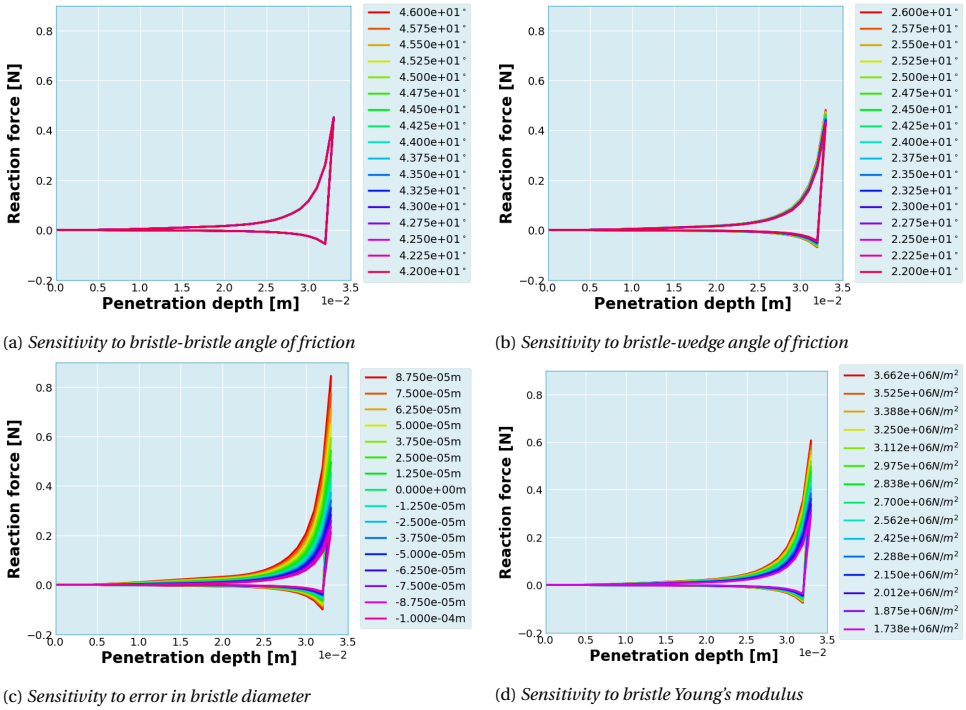

(a) *Sensitivity to bristle-bristle angle of friction*

(b) *Sensitivity to bristle-wedge angle of friction*

(c) *Sensitivity to error in bristle diameter*

(d) *Sensitivity to bristle Young's modulus*

Figure 4.13: *The sensitivity of the static test to different parameters. These are the results from the sensitivity study with a* 30° *wedge.*

The sensitivity study shows that the static test is most sensitive to error in bristle radius, and it is least sensitive to bristle-bristle friction coefficient. The first can be explained by the fact that the reaction force generated by the brush is a function of its

stiffness, also known as flexure rigidity. Consider the bristle to be a slender rod with a circular cross-section. Then the stiffness is a product of Young's modulus, E, and the area moment of inertia (I) of its cross-section. The following equation gives this property.

$$I_{x,\text{circle}} = \frac{\pi}{2} r^4 \tag{4.4}$$

The Young's modulus had a close error of 40.74%, whereas the radius had an average error of 13.3%. However, Young's modulus is linearly proportional to stiffness, while the stiffness is related to the fourth power of the radius. This difference explains why the static test was more sensitive to the radius. The bristle-wedge friction angle has a lesser effect because of a lower error, around 9%. Finally, we see two reasons why the bristle-bristle friction angle had virtually zero influence on the static test. Firstly, there was no tangential deformation between the bristle; in simpler terms, the bristles were pushing each other and not sliding against each other. Friction, as a result, is not experienced between the bristles. So the angle of friction has no influence. Secondly, the static friction between the bristles could be below the maximum allowable friction, also known as limiting static friction. The static friction angle gives this maximum value of static friction. If the friction developed between two surfaces is below the maximum value, changes in the static friction angle will not affect the friction value. Additional experiments are required to test which one of these hypotheses is correct. This, however, is beyond the scope of this project.

The sensitivity analysis shows how each parameter influences the force response. In the experiment, it is possibly more than one would have a value different from the mean. To capture this possibility, we performed a Monte Carlo simulation. Values of the parameters would be chosen at random within their uncertainty range, and a system with these values would be simulated using DEM. This was repeated 100 times, using a script, for each wedge angle. The mean value and the standard of force at each penetration step were calculated from the results. The results from this simulation would later be compared with experimental results in section 4.2.4.

4.2.3. EXPERIMENT

Armed with the theoretical prediction, the next step to construct and perform the experiment can be carried out. This section first discusses the apparatus used in the experiment, followed by the experiment procedure and finally, the results from the experiment.

APPARATUS

Apart from the test design, the experiment design was mainly influenced by the availability of the experiment apparatus. The first was the brush. As mentioned before, it had to have the right features so that it could be simulated. See section 4.2.1 for more information. Figure 4.9 shows a few pictures of this brush.

The next important apparatus in the experiment was the force sensor used to measure the vertical force. A weighing scale was found online, and it had a maximum measuring capability of 500g and an error of 0.13g. (See appendix A for more information). Placing the brush on the weighing balance ensures that no forces other than gravity, the

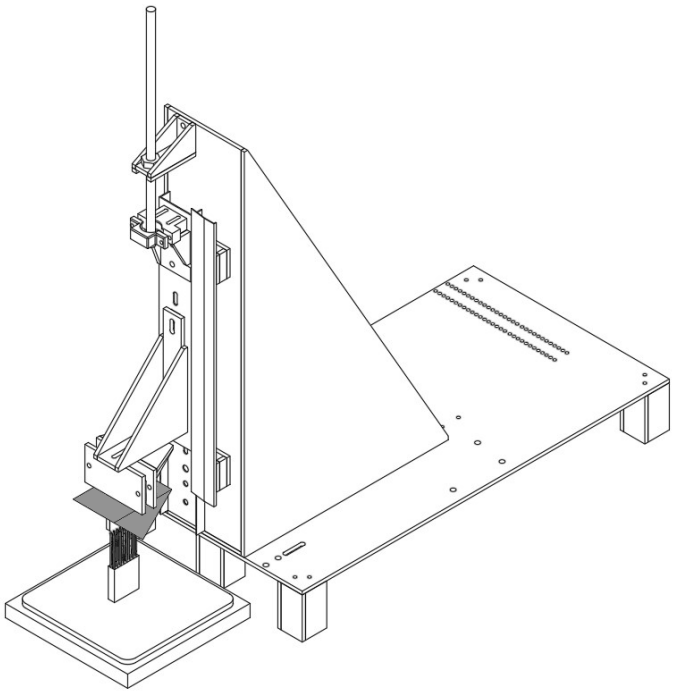

Figure 4.14: *Drawing showing the static test experiment setup assembled*

brush-wedge contact force, and the brush-weighing balance act on the brush. The force measured by the scale certainly comes from the brush-wedge interaction and gravity.

The wedge was manufactured using FDM 3D printing. It is a quick and cost-effective method to make parts with complicated geometry. Four wedges were made in total, each with different angles. These angles were 30°, 45°, 60° and 75°.

The wedge needs to be supported and provided with a provision to move vertically. A vertical motion guide achieves this role. A ruler placed parallel to the motion allows us to track the vertical position of the wedge. The assembly is shown in Figure 4.14 and Figure 4.15 shows its labelled and exploded view. The clamp connects the wedge to the assembly. The linear slider supports the clamp and restricts its motion to the vertical direction. The position is controlled by a threaded rod that connects the slider to the frame. Twisting the threaded rod moves the slider and allows very fine-tuned control of its vertical position.

PROCEDURE

The experiment procedure is relatively straightforward and similar to the simulation. The experiment setup is shown in Figure 4.16. The brush was rested on the weighing scale under the wedge. The wedge was lowered by twisting the threaded rod until it barely touched the brush. This marked the reference position of the wedge, and all positions are measured relative to this. The value shown on the scale indicated the zero load

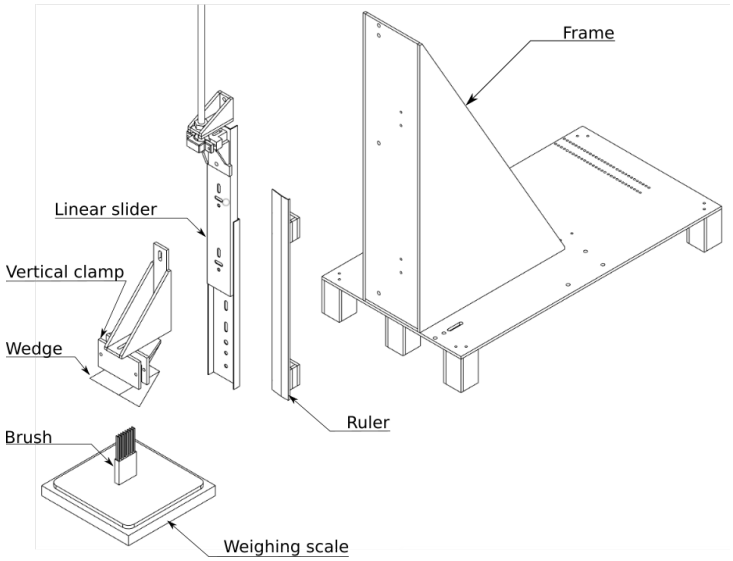

Figure 4.15: *Exploded view static test experiment setup assembled*

force, which is the weight of the brush. Similar to the position, this reading is a reference, and all later readings are relative to this value.

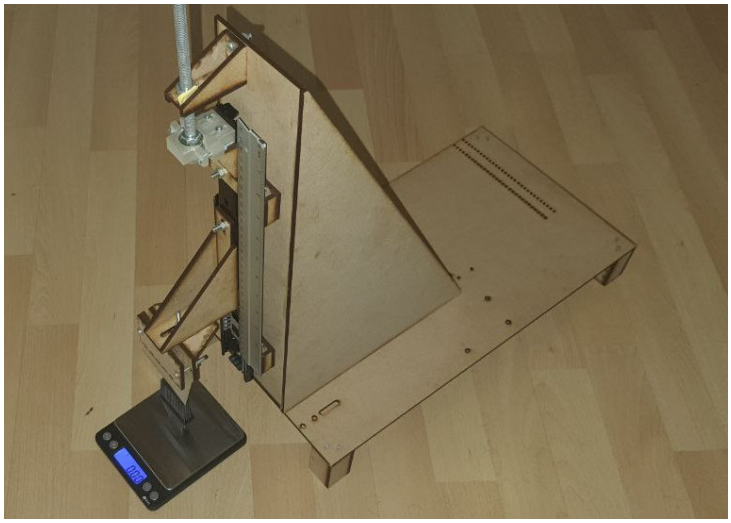

Figure 4.16: *Brush static test: Hardware experiment setup*

Once the reference values are noted, the wedge is moved 1mm into the brush, deforming it. The weighing scale displayed fluctuating values, so it was given time to settle. The force displayed on the scale was noted. The steps, move, wait, and measure, were

repeated until the wedge reached a penetration of 33mm. This depth is the length of the bristles, and it would not be possible to penetrate beyond this value. Beyond this, the reaction force had a value higher than what could be measured by the weighing scale. Now the wedge was withdrawn from the brush by raising it in steps of 1mm. This, again, was followed by a waiting period, and the force value was measured. These steps were repeated until the wedge was withdrawn entirely from the brush. This experiment was carried out for different values of wedge angles.

RESULT

A glance shows that the experiment results have features similar to the theoretical prediction. The response is non-linear, and loading and unloading curves are separate. The results are visualised as a force response curve, and it is shown in Figure 4.17

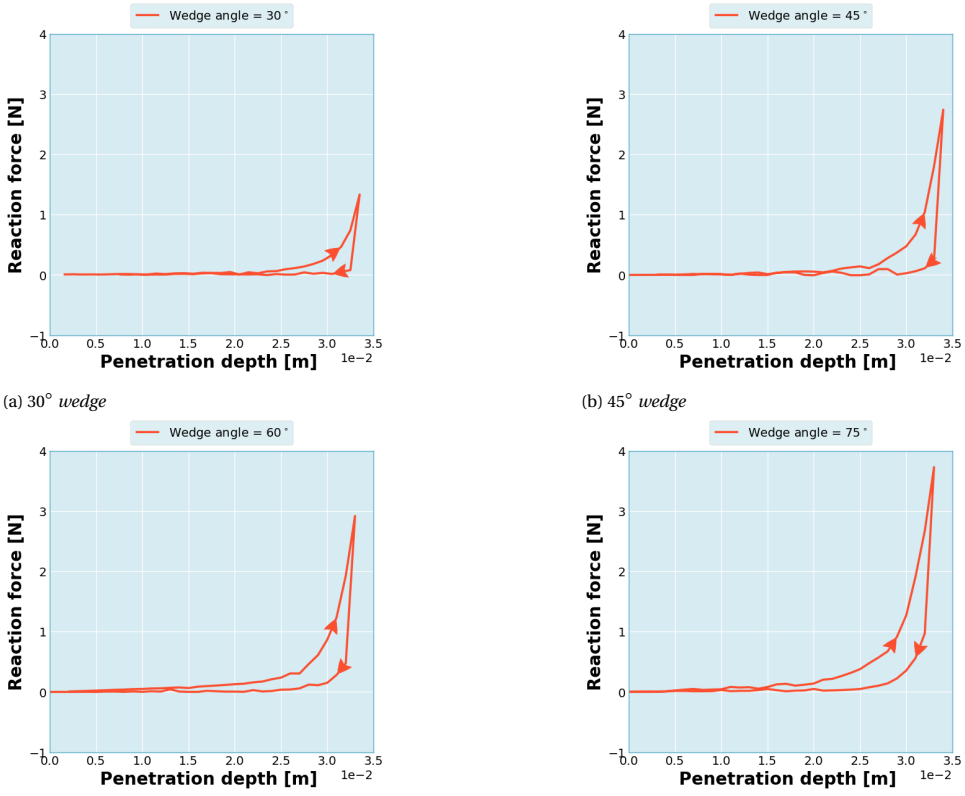

(a) 30° *wedge*

(b) 45° *wedge*

(c) 60° *wedge*

(d) 75° *wedge*

Figure 4.17: *Reaction force vs penetration depth observed in the static test experiment for different wedges. The arrows indicate the direction in which the wedge is moved. When the arrow points to the right, it indicates the wedge penetrating the brush, and the one pointing to the left-hand side indicates the wedge being retracted from the brush.*

4.2.4. COMPARING EXPERIMENT AND SIMULATIONS RESULTS

The uncertainty in the physical parameters implies that we cannot directly compare the simulations with the experiment. Moreover, the sensitivity study only considered varying one parameter. The Monte Carlo simulations, described in section 4.2.2, was a way to handle this. The result from this simulation will be compared with the experiment results in this section.

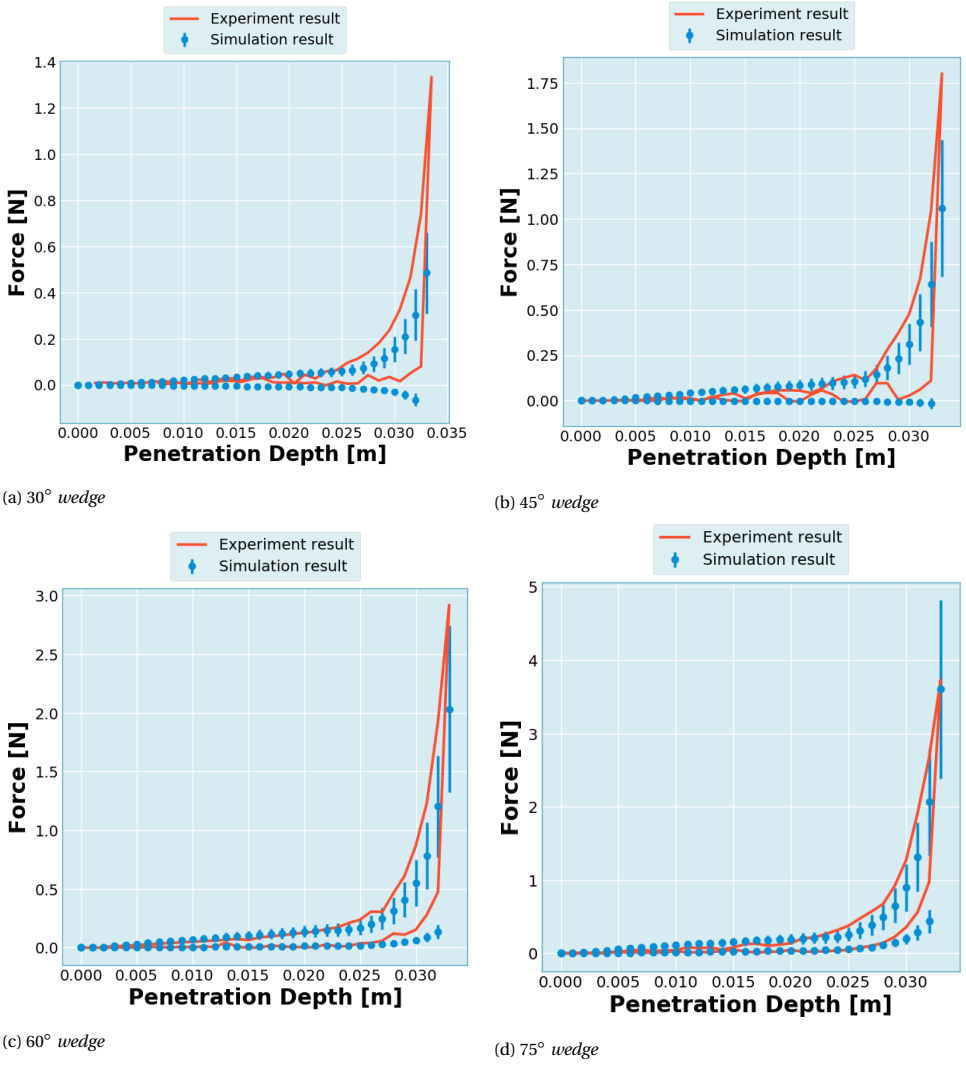

(a) 30° *wedge*

(b) 45° *wedge*

(c) 60° *wedge*

(d) 75° *wedge*

Figure 4.18: *Results from the Monte Carlo simulations for four wedge angles. Four parameters were randomly varied for each simulation, and the results show the mean and standard deviation from all the simulations. The experiment results are shown in solid lines. The mean value from the Monte Carlo simulations are shown as circles, and the error bars represent the standard deviation.*

Figure 4.18 shows that for a wedge angle of 30° experiment results have a considerable deviation from the simulation, whereas, for 60° and 75° wedges, the experiment results falls within one standard deviation of the Monte Carlo simulation result. Studying the differences between these cases could reveal why we observe this deviation.

The difference in the wedge angle affects two phenomena: the amount of deformation and the magnitude of the friction component. At lower wedge angles, The brush experiences lower deformation, and the vertical force is more substantially influenced by friction and vice versa. To test whether the model fails at lower deformation, we observed brush's response at small penetration values for 60° and 75° wedges. We find that even at the initial stages of penetration, the experiment results fall within one standard deviation of the Monte Carlo simulations (See Figure 4.19). Thus we can rule out the model failing at small deformation. So, friction must have a different influence than expected.

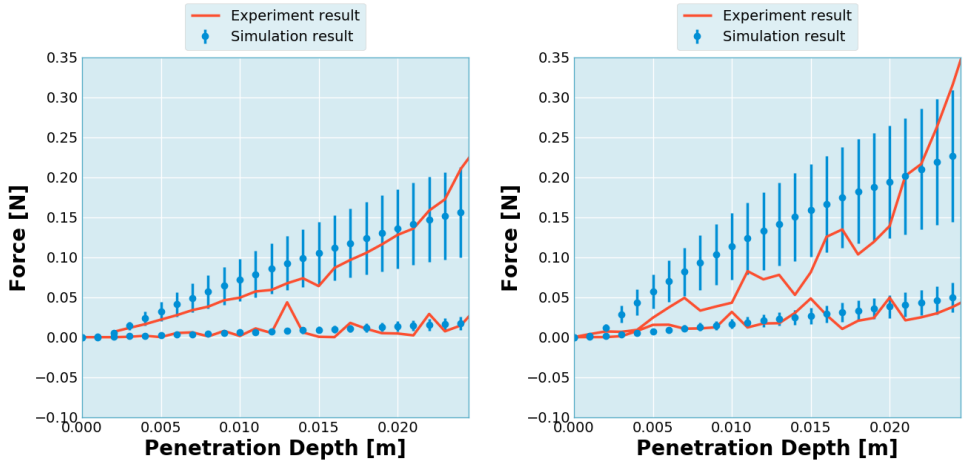

(a) 60° *wedge* (b) 75° *wedge*

Figure 4.19: *The static test experiment and Monte Carlo simulations at small deformations. Note that even at this range of small deformation, the experiment follows the DEM model's prediction.*

This unexpected effect of friction may be explained as follows. The wedge was manufactured using a 3D printing technique called Fused Deposition Modeling (FDM). This method has the benefit of making complicated parts cost-effective. However, it produces a very directional and rough surface finish. Consequently, the friction behaviour would be directional and could not be captured in the DEM model. Modelling this directional friction and measuring the friction coefficient is beyond this project's scope.

4.2.5. DISCUSSION

The static experiment showed that the DEM model could capture the response of a brush to deformation. There are some disparities between the results produced by the simulations and the experiment. It is speculated that this is caused by the quirk of the method used to manufacture the wedge. So it can be concluded that within the error expected

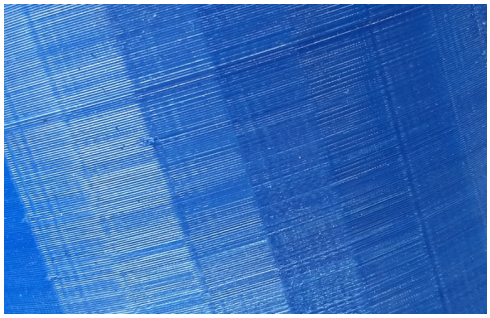

Figure 4.20: *The surface of a part manufactured using 3D printing. Notice the lines visible on the surface. These are artefacts of the FDM manufacturing process and greatly influences the behaviour of friction.*

from the experiments, the DEM model can recreate the brush's behaviour.

Moreover, this test also highlights the unique properties of a brush. Firstly this test shows the brush's ability conform to the shape of deforming object and react accordingly. This is made clear in Figure 4.21. The wedge makes contact at one point on the soft body, whereas the wedge contacts the brush along a larger region. Changing the wedge angle will not change the contact point on the soft body, while the angle will change how the brush conforms to the wedge. This change results in a different response, implying that the brush adapts to the body deforming it. This test also shows granularity. The wedge separated the bristles into two groups; they returned to their original single group after the wedge was removed. The wedge could not permanently separate the bristles into two groups. The wedge would cut other non-granular soft material into two pieces. In the model, having the wedge penetrate the brush multiple times yielded the same results. This test highlights the unique properties of the brush, and it also shows that the DEM model right captures these properties.

The previous brush models would not perform as good as the DEM model for this test. Most of the models coming under the Top-down approach (see 1.3.1) would neither show conformity nor granularity. The single element models have no provisions to simulate how the bristles could part into two to accommodate the wedge and conform to its shape. The continuous field model can simulate these two properties, but it was designed only to simulate the appearance of hair, so it is not physically accurate. The models coming under the Bottom-up approach has a better chance at simulating these properties. However, they were highly specialised to simulate contact with a flat or circular object. Additionally, these models considered only bristle-object interaction and omitted bristle-bristle interaction, which is one component of the nonlinearity.

4.3. BRUSH DYNAMIC TEST

The static test studied how a brush responds to a static deformation and the extent to which the DEM model was able to capture this phenomenon. In space, however, nothing is ever stationary. For detumbling and capturing space debris, we must predict how a brush and a moving object interact with each other. A brush interacting with a moving body forms a dynamic system. The test detailed in this section aims to study one such

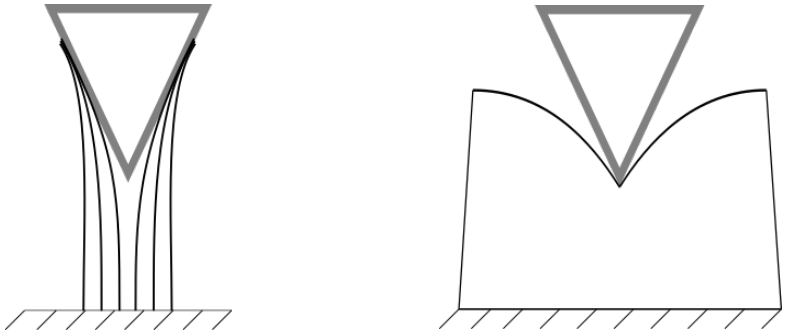

(a) *Wedge deforming a brush*

(b) *Wedge deforming a body made of soft material*

Figure 4.21: *Comparison between the response of a brush and soft body to a wedge penetrating them. Notice that the soft body contacts the wedge at a single point. Whereas the brush contacts wedge along a region, conforming to its shape.*

dynamic system and verify the predictions made by the DEM model using an experiment.

Although the brush is intended to be used in space, it is impossible to experiment in an environment similar to space with limited available resources. So, we must keep the differences between the experiment and space environments in mind while performing the experiment and simulating. The significant differences include air resistance and the lack of weightlessness. The influence of gravity may be eliminated by restricting the degree of freedom influenced by gravity, i.e. vertical motion. In contrast, air resistance is more difficult to eliminate, so its effect must be considered.

The first part of this section explains the design of this test. It explores the different options, the basic assumptions and the quantities that would be observed. The second part presents preliminary simulations. These simulations would be used to make a qualitative prediction of the experiment results. Following this, in the third part, we discuss the details of the experiment. This part includes the design of the apparatuses, the experiment procedure and the result post-processing. The fourth part presents the secondary simulations in which we use parts of the experiment data to initialise the simulation. The following section compares these results from the experiment and the simulations quantitatively. It highlights the similarities and the differences and provides reasons for the differences.

4.3.1. DESIGN

The brush alone by itself is a complicated dynamic system. It consists of multiple bristles deforming and colliding with each other. Tracking its motion is very difficult without reducing its complexity. We may use imaging techniques to track the motion of the bristles, but this process cannot track the bristle deep within the brush. We may reduce the number of bristles and limit it to a single row, but there may not be enough "brush" to conform to a body that defeats the brush's purpose.

It may not be possible to observe the dynamics of a brush directly, but it is possible to study its dynamics indirectly. By observing the dynamics of a body moving under the influence of the brush, we can analyse the dynamics of the brush. This process is similar to studying a black hole. We cannot directly observe a black hole, but we can infer its properties by observing the orbital motion of heavenly bodies moving around it.

Studying the interaction between a brush and an unconstrained body can be difficult. Gravity dominates the dynamics on the Earth's surface, so its influence must be reduced to be close to a space environment. It is possible to limit the influence of gravity by constraining the vertical motion. This constraint leaves the body with five remaining degrees of motion: three axes of rotation and two axes of translation. It is also not helpful to leave the remaining translation axes unconstrained. Two reasons support this idea. Firstly, when a body interacts with a brush, reaction forces produced by the brush will push the object away from it. Although this is how this system will behave in space, it does not allow us to continue observing the brush's influence on the body. Initially, the brush would be stationary, and the interaction with the body sets the bristles into motion. If the body moves away from the brush, it will not be possible to study the influence of the bristle in motion. So the body must remain fixed at a position to study the influence of the moving bristles.

Secondly, it is difficult to construct an experimental setup that constrains the vertical motion while freeing the other axes. One possible option would be to use an air table that supports a body above an air cushion. This lets the body move freely in the horizontal plane. However, the body would, now, be influenced by the dynamics of this air cushion and the brush. These dynamics introduces additional sources of errors. So, fixing all the translational motion of the body is more straightforward and allows us to observe the influence of moving bristles. Finally, the system is further simplified by fixing two of the three remaining rotational degrees of freedom. Again, this is due to the technical difficulty of designing and building a machine capable of supporting a body able to spin along three axes.

The system consists of a fixed brush and a body capable of spinning along one axis. The body is chosen to have a cuboid shape as this is one the most common form-factors of satellites in space. It is also a simple shape, lending itself to easy manufacture. The body would be given an initial angular velocity, after which it would contact the brush. The interaction with the brush would cause the target to slow down, which indicates the dynamics of the brush. So, the main quantities observed in this test are the body's angular velocity and time. A simple illustration of this test is shown in Figure 4.22. Changing the brush's position relative to the body allows for more variation in the experiment. This gives additional data to verify the brush model.

4.3.2. PRELIMINARY SIMULATIONS

The simulations are split into two due to some drawbacks of the experiment. It was not possible to devise a method to consistently set the initial velocity of the body in the experiment, and the body had to be moved manually. This limitation makes it impossible to know the body's initial velocity before doing the experiments. Due to this limitation, we cannot make a complete theoretical prediction before the experiment. So, the simu-

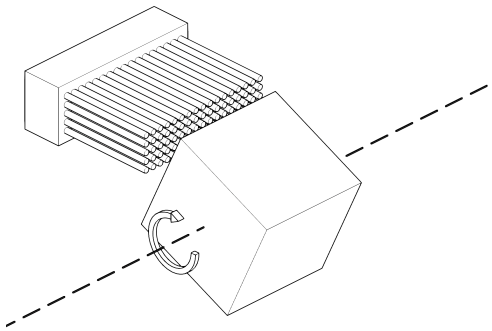

Figure 4.22: *A Diagram showing how the brush and the rotating body are arranged. The dashed line and the arrow shows the rotation of the body.*

lations were split into two. The preliminary simulations set a fixed velocity and make a qualitative prediction. The secondary simulations use experimental data to set the initial velocity, and its result is compared with the simulations qualitatively. This section presents a discussion on the simulation setup and the results of the preliminary simulations.

Due to constraints in the experiment design, it was not possible to recreate the experiment exactly in a DEM simulation. Nevertheless, that does not mean it is not possible to perform simulations to predict the general characteristics of the experiment results. This section presents a brief discussion of these simulations.

SIMULATION SETUP

The brush model remains the same since the same brush is used in both experiments. The body, however, uses a different geometry, and its rigidity plays a more significant role. A flexible body would vibrate violently and alter the dynamics of the system. As before, it is constructed using pfacets. A body composed of pfacets is highly flexible so the system would suffer from vibrations. These vibrations are eliminated by adding this set of pfacets into a clump (see section 3.1.1), essentially turning the whole set into a single object. Figure 4.23 shows the objects making up the system.

There were six configurations considered for the brush in the simulation. Each configuration is defined by the position and orientation of the brush relative to the moving body. There were two positions along the horizontal line and two positions along the vertical, which amounts to four positions when combined. To understand the positions set along the horizontal, consider Figure 4.24. The first position along the horizontal is shown in Figure 4.24a. The second position is halfway between the positions shown in Figure 4.24. Along the vertical, the brush was placed at the same level as the rotation axis and placed at the top face level. The brush was oriented horizontally in all of these positions; specifically, the rows with 17 bristles were oriented horizontally. Additionally, the experiment was performed orienting the brush vertically and changing its position along the horizontal. All of the configurations described here are shown in Figure 4.25

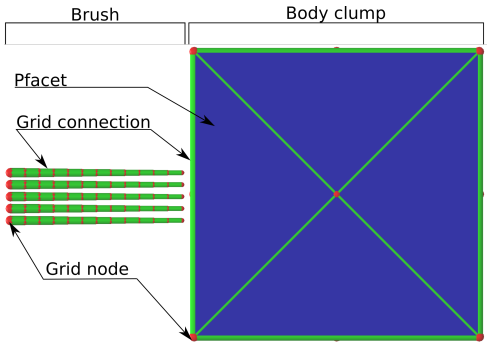

Figure 4.23: *The various objects used to model the system*

(a) *Brush touching one face*

(b) *Brush touching one edge*

Figure 4.24: *The two extreme position of the brush touching the body.*

The simulation started by giving the body an initial velocity. The angular velocity was tracked throughout the simulation. The main output of these simulations would be qualitative features seen in the result and not the actual value of the velocity. With the limited resources, it would not be easy to accurately and consistently set an initial velocity for the body in the experiments. Later in section 4.3.4, we describe a method to initialise the simulations using the initial velocity observed in the experiment.

RESULTS AND DISCUSSION

As seen in Figure 4.26, the most obvious observation is that body comes to a halt and stays there. The brush managed to soak up the angular momentum from the body. There was minimal angular momentum transferred back into the brush. This suggests that the kinetic energy is dissipated in the brush.

The sharp decrease in angular velocity marks the period when the body makes contact with the brush. Since no other moments are acting on the body, its deceleration must be brought forth by the brush. Comparing the graph with the YADE Graphical User Interface (GUI) cements this as it shows the body contacting the brush during this period.

Upon closed inspection of the graph, it is evident that the change in angular velocity is different for all collisions. Not only is the change in velocity during the collision is different for different collisions, but the profile of this change is also different. Perhaps, it is a function of velocity.

A simulation was set up with the same brush configuration but with a different angu-

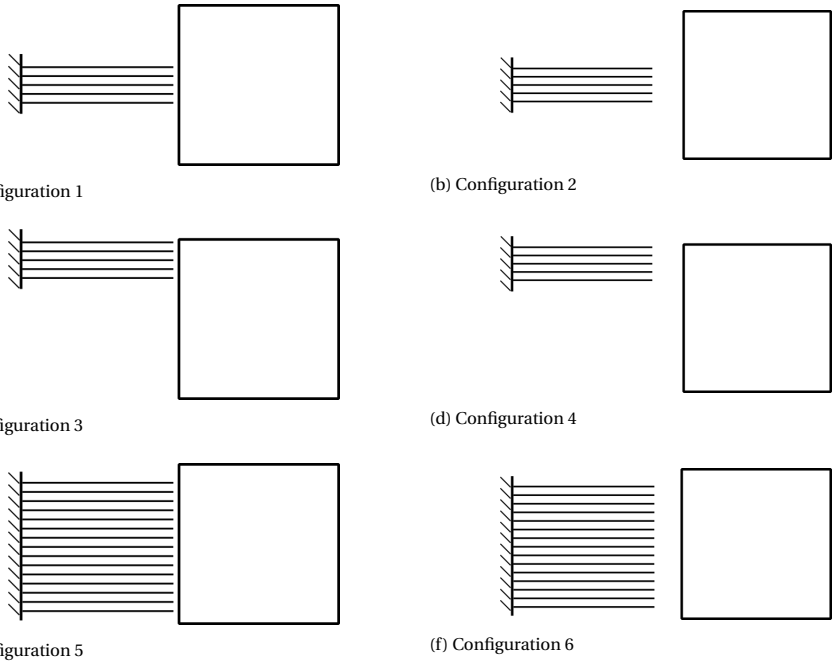

(a) Configuration 1

(b) Configuration 2

(c) Configuration 3

(d) Configuration 4

(e) Configuration 5

(f) Configuration 6

Figure 4.25: *The different positions and orientations of the brush relative to the rotating body. The axis of rotation of the body is perpendicular to the page*

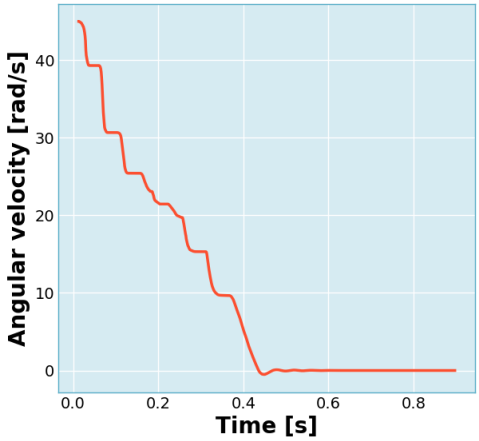

Figure 4.26: *The angular velocity of the body reducing with time from one of the preliminary simulaitons.*

lar velocity to test whether the change in angular velocity is a function of angular velocity. This value equalled the angular velocity after the first collision with the brush. The result from the simulation is shown in Figure 4.27, and it falsifies this hypothesis. Visual inspection of the brush and the body through the YADE GUI reveals that the bristles un-

dergo a complex motion. The state of the bristles is different each time the body collides with the brush and with a different initial velocity. This idea is evidenced by Figure 4.28. So the deceleration of the body depends on the whole of the system.

Inspection of the YADE GUI during the simulation showed the momentum transfer property of the brush. The phenomenon discussed in section 2.1.5 was clearly visible. The body contacted one part of the bristle, and this momentum was transported to the other ends of the brush.

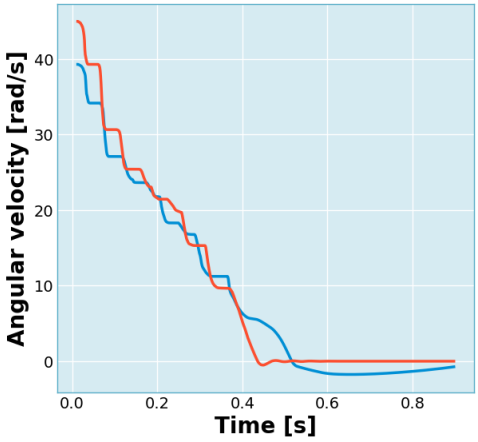

Figure 4.27: *The angular velocity of the body reducing with time from one of the preliminary simulaitons.*

(a) Before the first collision (b) Before the second collision (c) Before the third collision

Figure 4.28: *The position of the different bristles in the brush before three successive collision. Notice that the bristles have a different arrangement/state before each collision. Picture taken from the YADE GUI*

With regards to the position of the brush, we observed the following. The brush stopped faster when the brush was closer to the body when compared to a position farther away from the body. The body has a higher overlap with the brush when it is closer, suggesting it spends more time interacting with it. An increased interaction period would lead to more momentum transfer and the faster it comes to rest. On the other hand, there was no clear distinction between which one of the two orientations brought the body to rest faster. So we cannot make a concrete prediction on the differences in the response due to different orientations.

To summarise, the primary outcome of the preliminary simulations are a set of predictions. These predictions are given below. The body comes to a halt after multiple interactions with the brush. A sharp change in velocity marks each interaction. This change in angular velocity need not be the same for all interactions with the brush. The brush position with the higher overlap with the target brings it to rest faster.

4.3.3. EXPERIMENT

The test design describes what is to be done in the experiment; this section describes implementing the ideas discussed in the previous section into an experiment.

This experiment uses the same brush as before. One of the significant challenges was recording the angular velocity of the body. Two options were considered: a rotary encoder and a high-speed camera. The rotary encoder would be attached to the axle supporting the body's rotation, and it directly measures the angular velocity of the target. In contrast, the high-speed camera records video footage of the rotating body. Markers placed on the body allow us to use an image processing program to track the body's orientation, which, in turn, allows us to calculate the body's angular velocity. It was decided to use the camera because the rotary encoder would have introduced friction to the body—this friction, in addition to air resistance and friction from the axle supports, could dominate the dynamics instead of the brush. Moreover, the body's angular position is significant in this test as it determines the deformation of the brush. An encoder measures the angular velocity, and an error in its measurement would cause the calculated angular position to drift.

The experiment would also require hardware to support the body's motion and a mechanism to fix the brush at different positions relative to the body. The next part of this section presents the details of this hardware, which includes its design and manufacture. It also provides details for the setup used to record the video footage of the experiment.

APPARATUS

There are four main apparatuses in the experiment: the brush, the body, the high-speed camera and the supporting assembly. A drawing of this assembly is shown in Figure 4.29. Three bodies were made with different dimensions, but all had cuboidal shapes. The different dimensions allow studying how the brush responds to different sized objects. The body was made of a rigid foam material called NECURON. It is lightweight and hard enough to not deform under the loads exerted by the brush. It was made into cubes of the size 20mm, 40mm, and 60mm. It was manufactured at the CAMLAB in the Faculty of Architecture.

The supporting rig supports both brush and the body. It allows the brush to be fixed at different positions and supports the body while it rotates. The supporting rig can be further split into two sub-assemblies: the brush support assembly and the body support assembly.

The body support assembly consists of the following parts: an axle running through the body, ball bearings supporting the axle and bearing housings supporting the bearings. The axle was an 8mm threaded stainless steel rod. This part was chosen because it

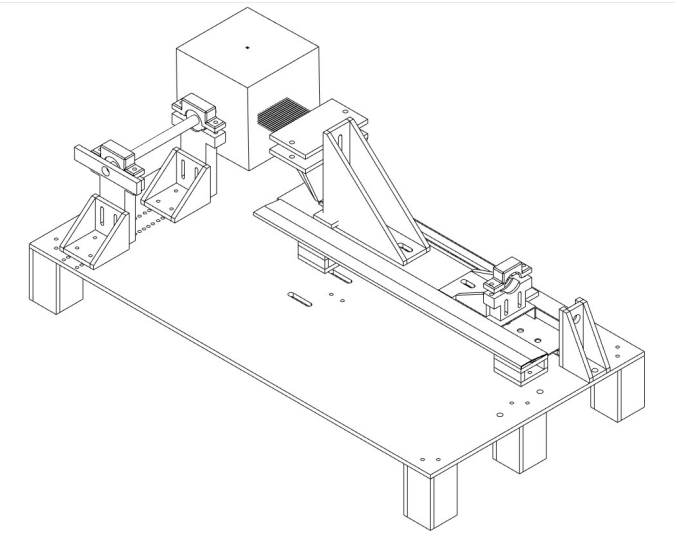

Figure 4.29: *A drawing of the brush, the body and the supporting rig assembled.*

is stiff enough not to bend under the body's weight. Moreover, the bearing used to support it, model name 608, is ubiquitous and is frequently used in applications that require minimal friction.

The brush support assembly comprises the linear slider assembly, the right-angled frame, and the brush vice. The brush is fixed to the assembly through the brush vice. The right-angled frame supports the brush vice. The brush vice can be moved into different vertical positions on the right-angled frame. Additionally, the brush can be fixed in two orientations, vertical or horizontal, on the right-angled frame. The right-angled frame is connected to the linear slide, and it allows the right-angled-frame-brush-vice assembly to move along a horizontal line. The horizontal and vertical motion allows the user to fix the brush at any point along a plane perpendicular to the rotation axis. Additional information and diagrams of this setup are presented Appendix **??**

The main requirement for the high-speed camera was its frame rate. This value must be high enough to keep up with the dynamics of the brush. When isolated, the brush's dynamics is mainly seen as oscillations of the bristles. A simulation in YADE estimated this oscillation to have a frequency close to 5Hz. For a detailed analysis, it was chosen to sample data at a rate of 100 entries for each oscillation, and this gives a frame rate of 500 frames per second (FPS).

A high-speed camera with this minimum frame rate was available at the high-speed laboratory of the aerospace engineering faculty. Prof Ferdinand Schrijer is in charge of this camera and kindly allowed us to use this camera for our experiment. The camera was a Photron FASTCAM SA1.1, and it was had capable of shooting video at 5400FPS at a resolution of 1024px x 1024px.

Along with the high-speed camera, the markers on the body forms the hardware el-

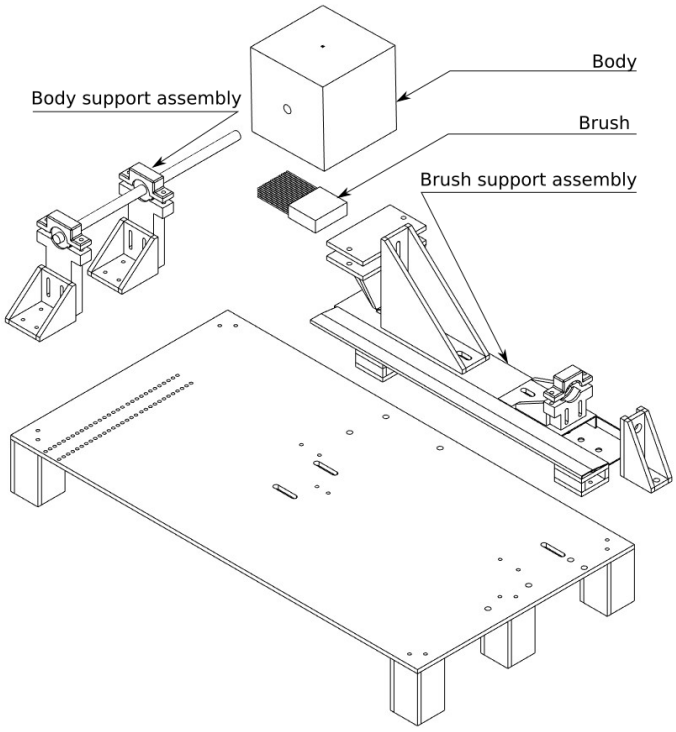

Figure 4.30: *An exploded view of the brush, the body and the supporting rig. The subassemblies of the supporting rig are shown in the figure.*

ements of the angular velocity measurement system. The markers should supply sufficient contrast for the image processing algorithm to track them. Angular position can be tracked in two dimensions with two points. So there must be at least a minimum of two markers. Thirteen black circular markers were placed on a white background to minimise error and maximise the probability of detecting the orientation. The markers are shown in Figure 4.31.

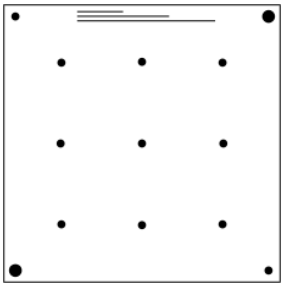

Figure 4.31: *The markers used for tracking the orientation of the body. This would be printed on paper and the square outline is used to align the cutout onto the body*

As mentioned above, the main reason to use so many markers is to minimise the risk of not tracking the body's motion. The markers cannot be tracked when there is insufficient contrast between them and the background. This happens when the markers are out of focus, their neighbourhood does not have sufficient light, or they appear smeared in the image due to motion blur. Since the tracked object is a rigid body, all parts must rotate with the same angular velocity. So, it is not necessary to track the same pair of points to calculate the body's angular position. Having trackers placed uniformly on the body ensures that a few would be in a region with good lighting and focus.

Moreover, having them at different radial positions ensures the markers move at different speeds. The markers place further away from the centre moves faster and can reveal the slightest movement. However, they are susceptible to motion blur. Hence, it is necessary to have markers placed closer to the centre.

PROCEDURE

With the apparatus ready, the next step is performing the experiment. This section presents the details of the experiment, including the setup of the apparatus and the procedure for experimenting.

Figure 4.32: *brush dynamic test: Experiment setup*

The apparatuses were placed as shown in Figure 4.32. The camera points directly at the body face pasted with the markers. Care was taken so that the whole body was placed such that it took up the majority of the camera's field of vision. Such a position ensures better resolution of the markers. Consequently, the camera's position had to be moved for the different bodies as they had different dimensions. The camera has limited internal memory, so it stops automatically when the memory is full.

Before performing the experiment with the brush, it was necessary to record the effect of the air resistance and bearing friction. This data would later be processed to model the influence of these damping sources. The body was manually made to rotate and allowed to slow down while being recorded by the camera. This process was repeated with different initial velocities.

The experiments involving the brush has a similar procedure. First, the brush was moved to the desired location. Second, the camera recording was started. Then, the body was rotated manually and released to start moving freely right before its initial collision with the brush. The body was allowed to slow down under the influence of the

brush and friction. The experiment was repeated for the different sized bodies and different brush positions. The brush positions are described in section 4.3.2

POST PROCESSING

Manually analysing the video footage from the high-speed camera is time-consuming and cumbersome. Image processing makes this process more efficient and repeatable. The image processing library OpenCV [35] and the C++ language provided the framework for processing the footage. The image processing results in the raw orientation data. This data contains noise, and it is fed into a low pass filter to remove the high-frequency noise.

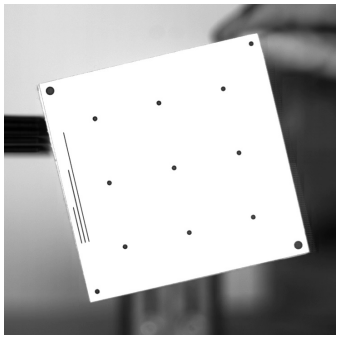

(a) Step 0: Get the frame from the video

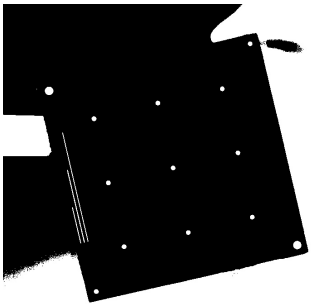

(b) Step 1: Image thresholding

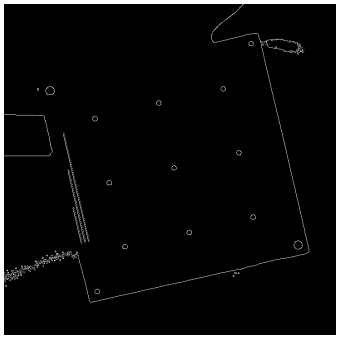

(c) Step 2: Edge detection

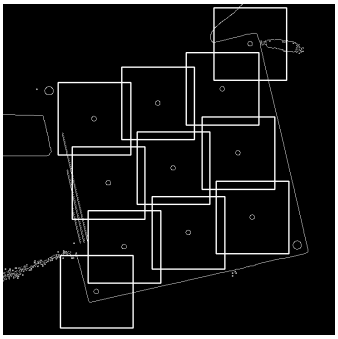

(d) Step 3: Template matching

Figure 4.33: *The steps taken to detect the trackers' position in the video footage. First, the image is converted into a binary image depending on a threshold value. Second, the edges in the binary image are detected. Finally, the circles in the edges image are matched to a template, determining its location and these are marked using an ROI. This ROI serves as the search region to find the new location of the marker in the next frame.*

The three main steps in image processing are image thresholding, edge detection and template matching. Image thresholding outputs a binary image, an image consisting of only ones and zeroes for its pixels, based on a threshold value. If the pixel value is greater than the threshold, it is assigned zero, and otherwise, it is assigned one. This is illustrated in Figure 4.33b. Since the markers are black disks on a white background, this process greatly enhances the contrast between the markers and the background. It makes the

next process, edge detection, easier by making the image very sharp, eliminating image artefacts and unwanted structures.

Edge detection, as the name suggests, is used to detect edges. It detects the outlines of objects by detecting sudden discontinuities in the image. So it is necessary to have a sharp image because image blurring can smoothen out the discontinuity of the colours, thus rendering this process ineffective. Image thresholding is a way to increase the sharpness of an image. Edge detection returns a binary image where the edges are marked with a pixel value of 1, and everything else is 0. The result of this process is shown in figure 4.33c. These two processes are carried out on both the template and source images.

Template matching is a technique used to find occurrences of a given image of an object, or its template, in the source image. Simply put, it works by sliding the template image across the source image and assigning a score at each location based on matching between the template and that location. The locations with the highest scores are said to be matched. The previous two steps improve the chances of matching the template with the markers and reduce the chance of matching it with any other objects. In Figure 4.33d, the location of the detected markers is shown by the white squares with the markers at their centres. These squares are essential for the next step.

The squares defined in the previous step form region around each marker called the region of interest (ROI). In the following video frame, these regions are used to detect the position of the markers. This detection is based on the assumption that the markers do not move substantially between consecutive frames. Each marker does not leave its ROI, and only one marker would be found in each ROI. So as the marker moves with the body, its ROI moves with it. Moreover, the assumption can be strengthened by adjusting the squares' size so that it remains valid. This approach to tracking the markers has a couple of benefits. It eliminates the need to search the whole image to find each marker. It also serves to identify each marker as it is associated with its ROI.

This sequence of processes culminates with the extraction of the position of the markers in the video footage. The results from each step is shown in Figure 4.33

The marker at the centre moves only slightly, so the chances of not detecting it are minimal. It is chosen to act as the origin of a coordinate system used to calculate the body's orientation. The body's initial orientation is defined by letting the user select a reference marker. Its angular position with respect to the origin defines the body's orientation, and all other markers use it as the reference to initialise their position. Once initialised, the position of any marker can be used to calculate the orientation of the body. Since there are twelve markers, the chances of not detecting all of them are minimal. When multiple markers are detected, then the orientation of the body is the average of the orientations calculated from each marker. Figure 4.34 provides the algorithm used to extract data from the video footage.

The raw data obtained from the image processing contains noise. This noise is not noticeable in the orientation data but becomes evident in the angular velocity data. This is high-frequency noise, so feeding the orientation data into a low pass filter removes this noise. Figure 4.35 shows the raw angular velocity data and the filtered data.

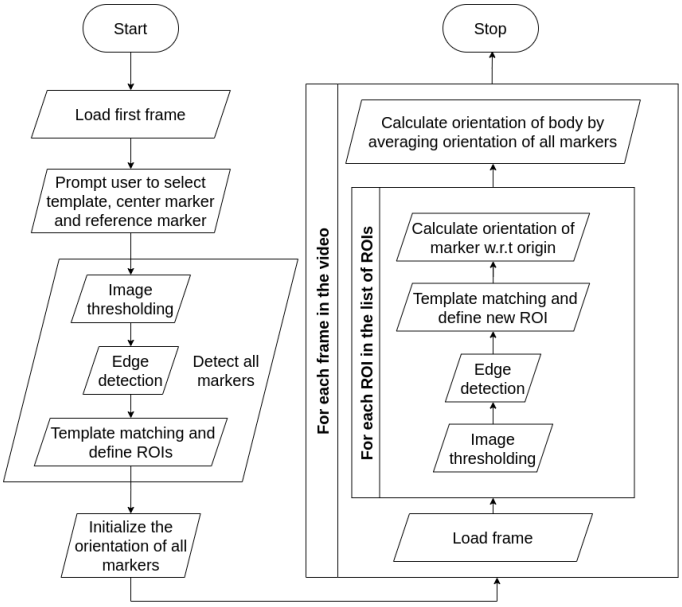

Figure 4.34: *Image processing algorithm. Note that the loops are indicated on the margins of the loop boxes.*

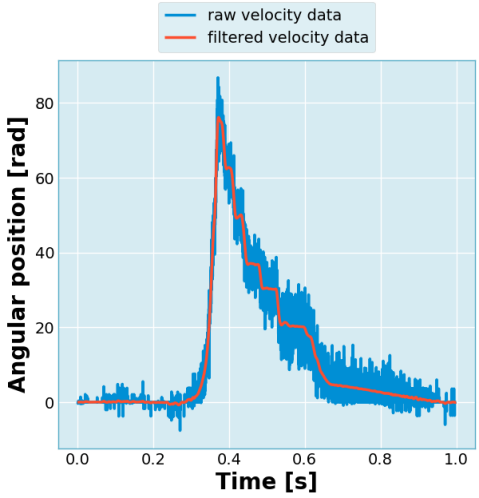

Figure 4.35: *Comparing the raw angular velocity data and its result after removing its high-frequency component. Also, note the sudden change in angular velocity and how it is not the same at different parts of the curve.*

RESULTS

The angular velocity vs time graph reveals much information regarding the system's dynamics. The sudden decrease in velocity marks the part when the brush contacts the body. Moreover, the change in velocity during each contact is different, which is visi-

ble in 4.35. This is a significant observation; it results from the dynamic variation of the brush's state.

Consider this system in the static sense, i.e. the body is moving at a snail's pace. The brush's deformation dictates the force it exerts on the body, and in this case, the deformation is a function of the body's angular position. Now, when the brush starts moving, its force depends on its deformation and the change in the brush's momentum. This difference is similar to the fact that the force exerted by a stationary pillow's deformation is much less than the contact force exerted by the impact of a moving pillow.

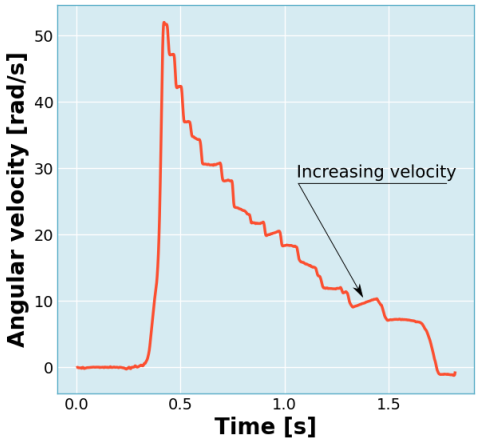

Figure 4.36: *The anomalous behaviour of the body when it increases in velocity*

The rotation axis is slightly offset from the body's centre of mass due to manufacturing errors. This error explains why the velocity increases at some points for some of the bodies. The body's angular velocity should not increase if all forces in the system work towards dampening the motion. The following argument explains why the angular velocity increases.

When the rotation axis is offset from the body's centre of mass, the body behaves like a pendulum. The pendulum gains velocity when it moves from its highest position. This effect, however, is apparent only when the velocity is small. The following equations illustrate this phenomenon. The equation shows that when v_{avg} is very large, the change is velocity $(v_1 - v_2)$, due to this phenomenon, is small. It also shows that the change in velocity is proportional to the axis offset.

Apart from the main observation discussed above, the experiment showcased momentum transport within a brush in action. Figure 2.3 shows this phenomenon. The body collides with one part of the brush. It absorbs the momentum and sets the contacting bristles in motion. Later this motion is transferred to other parts of the brush, setting those bristles in motion.

$$
\begin{aligned}
\text{Total Energy} &= \text{Kinematic energy} + \text{Potential energy} \\
T &= \frac{1}{2}mv^2 + mgh \\
\frac{1}{2}m{v_1}^2 + mgh_{min} &= \frac{1}{2}m{v_2}^2 + mgh_{max} \\
\frac{1}{2}m{v_1}^2 - \frac{1}{2}m{v_2}^2 &= mgh_{max} - mgh_{min} \\
\frac{1}{2}m(v_1 + v_2)(v_1 - v_2) &= mg(h_{max} - h_{min}) \\
v_{avg} &= \frac{1}{2}(v_2 + v_2) \\
(v_1 - v_2) &= \frac{g}{v_{avg}}(h_{max} - h_{min})
\end{aligned}
\tag{4.5}
$$

4.3.4. SECONDARY SIMULATION

In these simulations, the initial velocity captured from the experiments will be used to initialise the body. The core simulation setup is the same as the preliminary simulations with minor modifications. These, along with the results, will be discussed in this section.

SETUP

The logic for the DEM simulation is relatively straightforward. The experiment started with manually moving the body, and the also simulation started so. The body is forced to move using the angular position and velocity data, just as in the experiment. A user-defined engine forced the body to move so (see 3.1.2). Once it acquires the same initial angular velocity, the body is released from the influence of the engine. It then contacts the brush and is free is slow down to it under its influence. Figure 4.37 shows the two stages of the motion of the body. Friction and air resistance also play a role in the system's dynamics.

There are two components to friction in this system: air drag and bearing friction. However, the friction model implemented in the simulation model combines both. The underlying assumption in this model is that the force is a function of velocity alone. Since most dissipative effects are modelled using a first-order differential equation, we aim to do the same. It is a differential equation relating angular acceleration with velocity in this case. This model is shown in the following equation.

$$\alpha = \frac{d\omega}{dt} = -k_1\omega - k_2 sign(\omega) \tag{4.6}$$

The first term, $-k_1\omega$, captures the dissipative effect of air resistance and the second term, $-k_2 sign(\omega)$, models the kinetic friction in the bearing. In this model, friction acts against the motion, so the coefficients k_1 and k_2 are positive real numbers.

Recall, before performing the experiment between the brush and the rotating body, we performed an experiment in which the body was allowed to come to rest under the influence of friction. The data from this experiment would be used to construct the model.

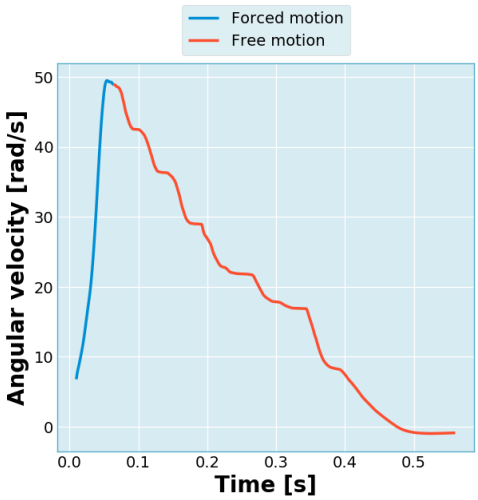

Figure 4.37: *The velocity of the body as a function of time. Notice the two parts of the motion. The first part, labelled forced, shows the motion forced to follow the part of the experiment where the body is set into motion manually. The second part, labelled free motion, shows the velocity of the body changing under the influence of the brush and friction*

The model is constructed by calculating the values of velocity and acceleration at each time instant and fitting the coefficients k_1 and k_2 from eq 4.6 to this data. As before, the raw data is highly noisy, so a low pass filter removes most of the high-frequency noise in the raw data. Figure 4.38a shows this function fitting. This model is then verified by comparing it to the experimental observation. The evolution of its velocity is calculated using the body's initial state and the damping model. This is shown in Figure 4.38b. Additional results can be seen in appendix F

ERROR HANDLING

As with the static simulations, the uncertainty in the physical properties must be incorporated into the simulations. This uncertainty has a profound influence on the simulation outcomes. Although a complicated task, small strides were taken to tackle this uncertainty. Like the static simulations, a sensitivity analysis shows how each property affects the simulation outcome and how the simulations agree with the experimental observations.

This section will present the simulation of one of the experiments and its sensitivity. The results for all other experiments can be found in appendix F. The static test showed that the reaction force was insensitive to changes in the friction angle compared to other properties. In addition to the two remaining properties studied in the static text, the dynamic test introduced additional property, bristle material density.

The results for sensitivity analysis are shown in Figure 4.39. This study used the 60mm body, and the brush was oriented vertically and touching the body's face. The results show that the dynamics are susceptible to changes in the diameter of the bristles. Its reason is similar to the results from section 4.2.2. The bristle stiffness depends on the

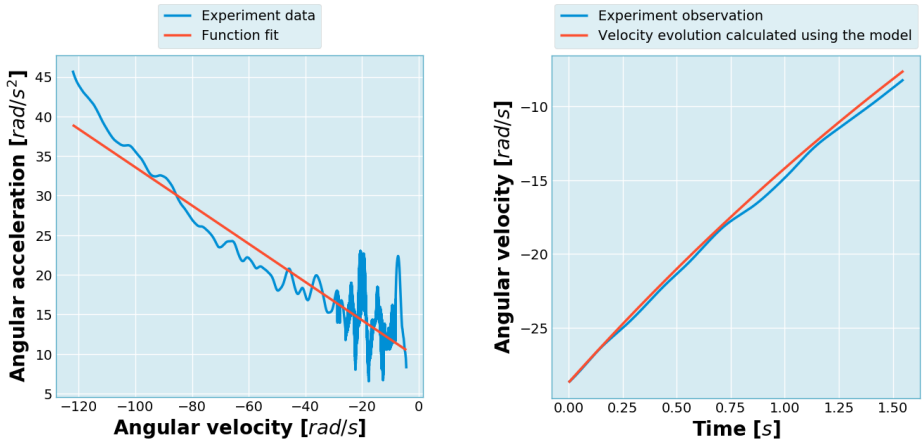

(a) *Angular acceleration vs velocity* (b) *Velocity vs time*

Figure 4.38: *The friction model. The first figure shows the acceleration as a function of velocity. The experimental data is used to construct a model. The second figure shows how the experiment observation compares with the results predicted by the model. These figures show the response of the body with dimensions 40mmx40mmx40mm.*

fourth power of diameter while it linearly depends on Young's modulus.

The following observations are made from the first collision with the brush. The result suggests that the brush stiffness can vary more effectively by varying the bristle diameter instead of changing the material. The sensitivity analysis also suggests that a heavier brush tends to be less effective at reducing the body's angular velocity in this neighbourhood of values. Meanwhile, a stiffer brush, one with higher Young's modulus or diameter, is more effective in reducing the body's angular velocity.

On the other hand, consider a very stiff brush, perhaps one that is infinitely stiff. This brush might as well be considered as a rigid body. If the body collided with this brush, it would rebound, and its angular velocity would be reversed.

So, in short, the angular velocity, after the collision, decreases for increasing stiffness in one neighbourhood of values, while it changes to its negative value in another neighbourhood. Assuming the relationship between change in angular velocity with stiffness is continuous, there must be an optimum stiffness where the angular velocity becomes very small, even zero, after the first collision.

Just with just three parameters, there is a potential for optimising the effectiveness of a brush at reducing the angular velocity or detumbling a rotating body. However, other properties such as the inertia of the tumbling body could potentially affect these dynamics too. So, rather than optimising for one body, it would be wise to optimise for a range of bodies.

4.3.5. COMPARING EXPERIMENT AND SIMULATION RESULTS

The results from the experiment and simulations can now be compared. This comparison will be made in two parts. The first part will compare the preliminary simulations with the experiments qualitatively. As mentioned previously, difficulty in setting the ini-

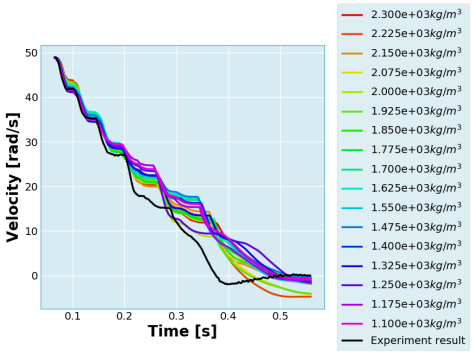

(a) Density

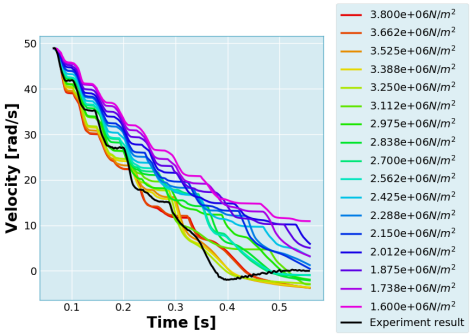

(b) Young's modulus

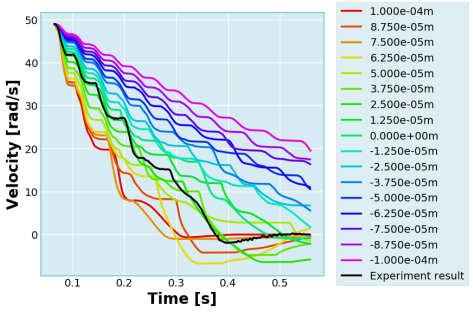

(c) Diameter

Figure 4.39: *The results from the sensitivity analysis of three physical properties. Each subfigure shows the sensitivity to one property. The bristle diameter has highest influence on the outcome of the simulation. The experiment results are also shown in these figures*

tial angular velocity in the experiment stops us from comparing it quantitatively. The second part compares the experiment with the secondary simulations. These simulations used the initial velocity data from the experiment to initialise the simulations so that we could compare them quantitatively.

PRELIMINARY SIMULATIONS AND EXPERIMENT

The first prediction made in the preliminary simulations was that the angular velocity would reduce to zero after multiple collisions with minimal angular momentum transferred back into the body. This was found to be mostly true. However, for a few experiments, the brush remained in contact with the body long enough for it to halt and rotate backwards. The velocity gained through this quickly dissipated in the following brush collision.

The second prediction was that the change in angular velocity is not the same for all interactions with the brush. The experiments also showed different angular velocity changes with no discernible trend. This is an important observation because Cheng et al. [9] predicted a linear increase with increasing contact duration. Neither the experiment

nor the preliminary simulations showed this trend. What was seen is shown in Figure 4.40

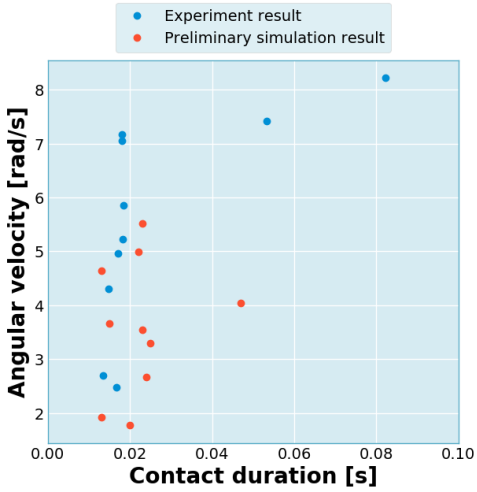

Figure 4.40: *Plotting angular velocity change during a collision with the brush vs the contact duration. Notice that this is not a linear graph as opposed to a linear trend predicted by Cheng et al [9]*

The final prediction was also observed in the experiments. The body comes to rest much more quickly when had a higher overlap with the brush during rotation. This overlap is higher when the brush is closer to the body centre. Configure 1 (Figure 4.25a) slowed down faster compared to configuration 4 (Figure 4.25d).

SECONDARY SIMULATIONS AND EXPERIMENT

The results are shown in the Figure 4.39. Although the experiment results do not follow the simulation result exactly, it lies within the range of results predicted by sensitivity analysis. The case with the 20mm body showed maximum deviation between the simulation and experiment.

This difference between the experiment and the simulations may be attributed to the uncertain physical properties of the brush. Moreover, the exact initial configuration of the brush is also unknown because the bristles are not perfectly aligned and have a small amount of randomness to their orientation because of manufacturing defects. The brush construction in the model was altered to study the effect of randomness in bristle orientation.

A bristle is constructed by specifying the position of its tip and root. The bristle tips and bristle root collection would be an evenly ordered array in a perfect brush. The bristle tips would have a random perturbation in a real brush, changing the bristle orientation. In the simulation, each bristle tip was randomly perturbed within a given variance; in this case, it was $4 \times 10^{-10} m^2$. Figure 4.41 shows the influence of this randomness on the dynamics of the system.

The sensitivity analysis only considered the variation of one parameter from its mean.

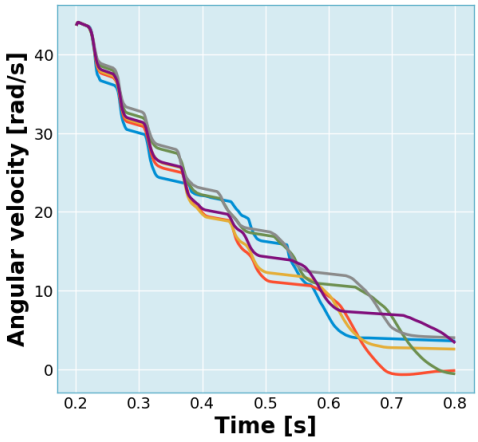

Figure 4.41: *Effect of randomness in bristle orientation on the dynamics of the system. The different curves show the dynamics of a brush given a random pertubation on the bristle orientation*

It could be the case that multiple parameters were off their mean in the experiment. Such deviation could lead to drastic variations. Some of the experiment results were entirely out of the range predicted by the sensitivity analysis. It is speculated that a combination of variations in all parameters could have caused this. Additional tests are recommended to verify this.

There is one other reason why some of the experiment results do not match the simulation results. It could be inaccuracies in the YADE simulation software. Although the core DEM framework of YADE is thoroughly tested and verified, some new features are not. For example, pFacets were introduced to model complicated geometry. It was found that there were bugs in the code for handling an aggregate of pfacets. This is illustrated with the following example.

In this simulation, two brushes face each other, and the cube is placed between them. The roots of each brush are added to a clump; this acts as the brush fixture. The cube was given the initial angular velocity, and now the angular momentum of this system was recorded. Now the per cent change in angular momentum of this system was compared against the size of the cube. This is shown in Figure H.4. The results clearly show considerable change in the system's angular momentum with the 20mm cube after the collision. Appendix H has more information regarding this. In the YADE simulation with the brush and the body, there are many such collisions with the brush. The error could accumulate and lead to the seen discrepancy. This could explain why there is a large deviation for the case with the 20mm body.

4.3.6. DISCUSSION

This test shows that DEM can capture the dynamics of the interaction between a brush and a rotating body. There were some discrepancies; these could be attributed to the uncertainty in the physical properties and error in the angular momentum integrator

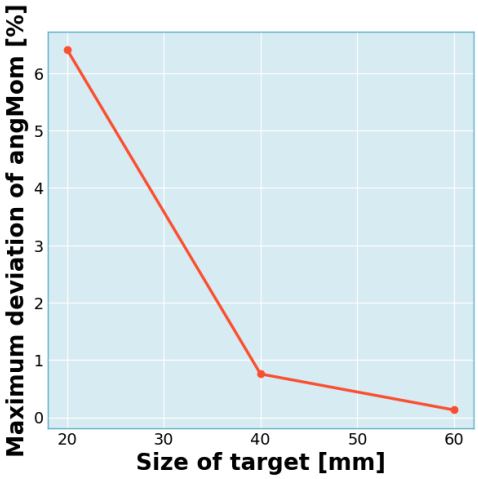

Figure 4.42: textitGraph showing error in angular momentum conservation for the case with the brush. Notice that the error is small for bigger bodies

of the YADE software. To verify the former, it is recommended to perform additional tests with more accurate measurements of those properties. As for the latter, this error was reported to the YADE community. They are a very active community, and they have fixed source code errors reported by this project in the past. So we are optimistic that they will fix the error.

4.4. CHAPTER SUMMARY AND DISCUSSION

The three tests have revealed that the DEM model is fully capable of modelling the behaviour of a brush. The single bristle dynamic test showed that the model could simulate its dynamic behaviour. The static test verified that model could predict the correct reaction force to deformed brush. It also highlighted unique features of the brush, particularly conformity and granularity. The dynamic test studied the behaviour of a system consisting of a rooted brush and a rotating body. Again, the model was capable of predicting the behaviour of the brush. It also showed momentum transfer in action in the brush.

Although these experiments have not verified the DEM model to a high degree of accuracy, they have verified that it could capture the general behaviour. The initial design stage would benefit immensely from this model as it would do away with the need to prototype every brush design at that stage. Its role in a more detailed study, in our recommendation, requires additional study.

One of the significant downsides of the tests were the uncertainties in the physical properties of the brush. These uncertainties resulted in significant variations in the results calculated by the model. Even though the experiment results were very close to the values within these variations, it would be reasonable to expect more precise experiments to quantify the capabilities of the DEM model. These could include the cases

when this model is accurate and when they are not. So, better experiments are recommended to learn more about the DEM model.

5

Conclusion and Recomendations

This project was started to study the interaction between a brush and space debris. This chapter presents the answers to the research questions posed at the beginning of this text and discusses this project's conclusions. Following this, a few recommendations on improving the results from the project are also presented.

5.1. Answering the research questions

The research question and the sub research question guided the progress of this project. The previous chapters contain the information which forms the answers to these questions. This information will be condensed and consolidated into answers to questions in this section. First, each sub research question will be discussed, followed by the main research question.

How does a brush behave? Answering this question took us on a path to study the various properties of a brush. In the general sense, it resulted in a set of properties. These properties are stiffness, dissipation, conformity, granularity, porosity, and momentum transport. This set may not be exhaustive, but these properties work together to capture the brush's behaviour. Additionally, the DEM model of the brush developed in this project can predict how a specific brush design would behave in a given scenario. The properties of a brush are discussed in detail in section 2.1.

What makes the brush useful in ADR? Previous researches such as Cheng et al. [9] and Nishida et al. [12] have suggested using a brush for ADR, those have not suggested why. The set of properties of a brush helped answer this question. Stiffness allows the brush to apply a reactive force opposing the target's motion while conformity distributes this force evenly across a large contact area. This opposition transfers the momentum into the brush. Dissipation and momentum transfer work together to keep most of this momentum from going back to the target. Granularity allows the brush to take the pun-

ishment that would damage other materials. It allows the brush to "tear" without sustaining any permanent damage. Section 2.2.1 answers this question in more detail.

How to implement brush behaviour into a model? The brush model was developed using the Discrete Element Method. The key here is that DEM captures the interactions among the brush's bristles, which was absent in other models we found in the literature. Together with the flexible nature of the bristles, these interactions managed to capture all the properties we found earlier. Moreover, the dynamics of any arbitrarily shaped rigid or flexible objects can be modelled using DEM, thus making this framework very useful for ADR studies. Chapter 3 presents the details of this model.

How to test this brush model? The three test cases used to verify the brush model forms the answer to this question. The first step involved verifying the dynamics of the bristle, the building block in this bottom-up brush model. Following this, the static behaviour of the brush was verified and finally, the dynamic behaviour. The steps and the result are discussed in chapter 4.

The answers to these research questions help us answer the main research question, which is **How does a given brush interact with tumbling debris?**. A very general answer to this question would be that the brush absorbs part of the momentum and dissipates the kinetic energy within itself. When supplied with details regarding the brush and the debris, a more specific answer can be found using the brush model developed in this project.

5.2. CONCLUSION

The main concluding point from the project can be summarized in three points. These are presented below.

Firstly, The brush is versatile, resilient, and effective for detumbling tumbling debris. Its properties let it effectively absorb and dissipate motion from a body contacting it. Its behaviour can easily be influenced by changing its design parameters such as bristle dimensions, bristle orientation and arrangement.

Secondly, DEM can be used to construct a model of any brush design. The DEM builds a brush model bristle by bristle. This method lets us copy the exact structure of any brush design we can think of into the digital realm and simulate its behaviour. Such flexibility makes it an invaluable tool during a space mission's design and prototyping stage. On the other hand, the models used in previous studies [7, 8, 10] had minimal scope.

Finally, the test cases studies in this project support the validity of the DEM brush. The first test supported the validity of the dynamics of the building block of the model. The second supported the accuracy of the force response of a brush. The final test supported the dynamics of a system with a brush calculated by the model. Additionally, we found parts of this test that can be improved.

5.3. RECOMENDATIONS

There is always room for improvements and refinements. This project is no different. It is also possible to extend the outcomes of this research into other use cases. This section presents a few ways to improve the brush model and some additional use cases for a brush in space engineering.

5.3.1. MORE INTO BRUSH FOR ADR

This project is among the first steps in using DEM for simulating a brush. It has its shortcomings and failures. Nevertheless, we have identified ways future projects could extend our research and refine the brush model. These are mentioned below.

IMPROVED EXPERIMENTS

There were significant uncertainties in the brush's physical properties we used to verify the brush model. This translated into uncertainties in the theoretical predictions. Additionally, the dynamic test case also had some shortcomings. We recommend additional experiments with better accuracy and design.

BETTER SOFTWARE

The YADE software used in this project had many useful features and some shortcomings. There was a bug in integrating the angular momentum when using a pfacet clump. This could be fixed through careful examination of its C++ source code. Moreover, the software was slow when simulating the brushed used in this project. Using a brush with more bristles was, at times, infeasible. So we recommend improving its performance for simulating a brush or maybe fork the source code and modifying it specifically for simulating a brush. This project showed that DEM is beneficial for simulating a brush, and the next step would be improving its performance.

TEST BRUSH IN MISSION SIMULATIONS

Cheng et al. [10] and Nishida et al. [7, 8] presented studies on controlling a spacecraft with a brush to detumble debris. However, they used a very simple brush model. It is recommended to perform these studies with the DEM model, so we move closer to understanding the dynamics of this system and perhaps design ADR missions that use a brush.

5.3.2. ADDITIONAL USE CASES OF A BRUSH

This project began on the premise of developing a brush model for studying its potential role in detumbling space debris. Nevertheless, other use cases have been identified, and some of them are presented in this section.

SPACE FUR

Depending on its stiffness, a brush has the property of being able to apply soft contact on bodies deforming it. It means that it takes a large deformation to apply a large force. In contrast, hard materials like solid plastics and metals apply a large reaction force for small surface deformation. Large deformations and stresses could lead to permanent shape changes in these materials and even damage. In space, this could spell disaster

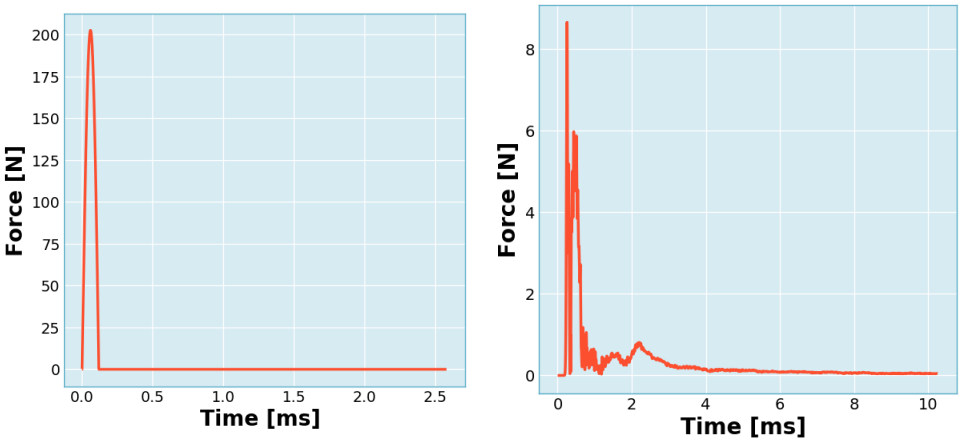

(a) *Contact force generated by a solid surface*

(b) *Contact force generated by space fur*

Figure 5.1: *Contact force plotted against time for two cases: solid surface and space fur. In these simulations, a spherical projectile incident on the surface at an angle of* 45 deg *to its normal at* $50\sqrt{2}$ *m/s. The contact force transmitted through the surface for the solid surface is orders of magnitudes larger than the force transmitted by the space fur.*

5

for spacecraft skin if debris impacts damage them. A brush could help reduce damage to spacecraft skin.

Imagine a spacecraft's outer skin covered with numerous bristles, like fur on an animal's skin. When fast-moving debris collides with such a spacecraft, it must go through this fur. As the debris penetrates the fur, its reaction force increases, and the debris loses momentum as it penetrates the fur. This slow-down happens over the bristles' length and considerable time instead of a shallow and quick contact for hard surfaces. The maximum force experienced in this system reduces, limiting any damage done to the spacecraft.

This effect could also be achieved using other soft materials. We propose that this fur is a better alternative. Why? When soft materials are subjected to large deformations or stress, they could crack or tear. Such a tear could propagate, rendering the whole soft surface damaged and susceptible to further damage. Repairing such damage would potentially require replacing the whole surface.

On the other hand, the fur owes its softness to the small radius of the bristles. The bristles could be made of tough material, resistant to tearing and damage, while the fur, as a whole, remains soft because of the small bristle radius. Moreover, fur material cannot "tear" because of its semi-granular nature. Neither can tears or cracks propagate across the fur. If the bristles are ever damaged, that part of the fur could be replaced without affecting the whole's integrity. Additionally, the softness of the fur can be controlled by varying the radii of the bristles, changing the space between the bristles or even experimenting with multiple coats of fur, making space fur more versatile.

Figure 5.1 compares the surface force experienced by a hard surface and a surface covered by fur when a spherical object impacts them. It is clear that the fur significantly

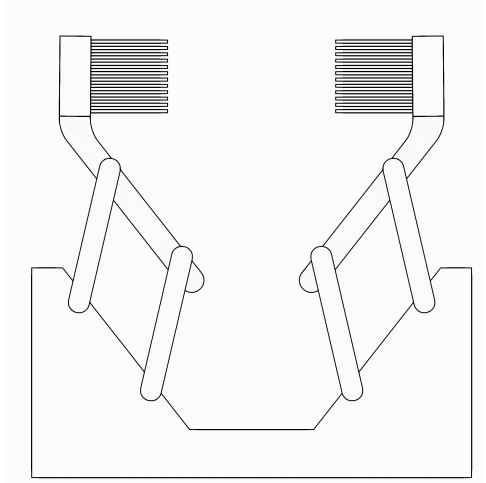

Figure 5.2: *A gripper brush. Notice the bristles covering the surfaces that would contact its intended target.*

reduces the force applied by the spherical object.

GRIPPER BRUSH

The Gripper brush is an extension of using a brush to detumble. It involves using two brushes to detumble and capture the debris. The concept is quite simple. Two or more brushes grab the tumbling debris. This concept's main advantage is that it combines detumbling and capturing into a single tool rather than relying on two different tools, which simplifies the system. Figure 5.2 shows a simple design of such a tool.

The soft contact provided by the brush makes sure the target does not get away by bouncing off a hard surface. Imagine how a ball reacts when it collides with a hard surface and loose sand. The ball tends to bounce off the former while it halts when it falls on the latter. These are two extreme behaviour, and the brush falls somewhere between them. The brush design can be tweaked to tend to either end of this spectrum.

BRUSH ASSISTED DOCKING

Docking is one of the most complicated and risky operations in space. It mainly involves hard surfaces mechanically mating. Minor deviation or misalignment could lead to failure. A soft contact could help handle these uncertainties. A hard contact would lead to a large and almost instant transfer of momentum between the two docking space assets causing them to drift apart. We recommend using a brush to interface between the two bodies. This concept is illustrated in Figure 5.3. Soft contact would soften the collision and slow down this momentum transfer, allowing more time for additional manoeuvres to correct the operation.

The brush surface would benefit from the advantages discussed for space fur. Although soft, the brush interface could be made of tough material and reduces any damage during docking. The softness can be controlled by the brush's design. Additionally,

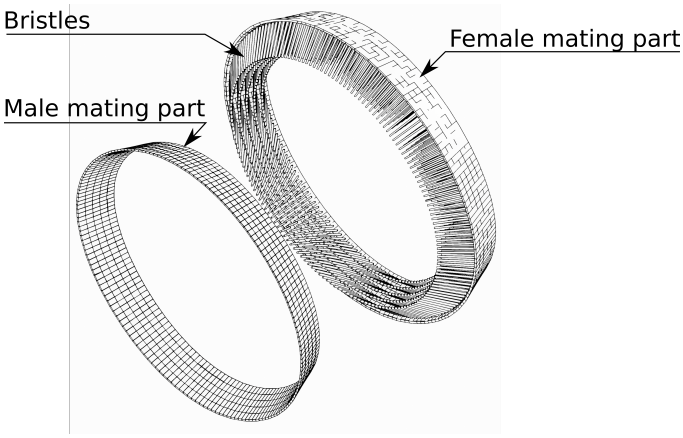

Figure 5.3: *The two mating parts used during the docking operation. The bristles interface between the two mating parts, providing the soft contact*

the friction developed in the bristles could also dampen any relative velocity between two mating bodies.

MICRO OBJECT BRUSH TRAP

Space contains many millimetre and sub-millimetre sized objects travelling at speeds. These objects may need to be sampled for scientific purposes or for capturing micro debris. However, their small size and considerable speed make catching them difficult. We propose using a surface covered in sticky bristles to solve this problem.

This concept builds on the space fur concept. The bristles would slow down these objects and perhaps trap them. The porous nature of the brush allows these particles to be trapped in its voids. Adding adhesives or an electrostatic charge could ensure that the objects stick to the bristles. This concept is similar to flypaper. Instead of a sticky surface, we propose using a sticky brush. A similar mechanism is seen in nature, employed by carnivorous plants to trap prey.

5.4. SUMMARY

This project aimed to develop and verify a numerical model of a brush. This model is meant to aid the study and design of brushes in Active Space Debris Capture. The model is based on the Discrete Element Method and uses the YADE software package to construct the brush model. This model simulates the dynamics of a bristle, their collisions among themselves and other bodies. The brush's behaviour predicted by the DEM model was compared to observations recorded from three different experiments. The first test compared the dynamic behaviour of bristle, the second focused on the brush's static behaviour, and the final test studied its dynamic behaviour. The experiment observations fall within the behaviour predicted by the model, within the limits of the experiment. This report then concludes by presenting the relevance of this project, some improvements and providing some recommendations for future research.

ACKNOWLEDGEMENTS

This project is not, by any means, the result of my effort alone. I received invaluable support from many people, and I would like to thank them. First of all, I would like to thank Professor Jian Guo for supervising this project. His advice and patient support tremendously improved the quality of my work. He told me when I should slow down when I was moving too fast with my analysis and hasten when I focussed too much on the details. He gave me the freedom to solve problems my way while setting me on the path to find the solution. I am deeply grateful for all of this.

I want to thank Dr John D. Till for helping me with the model he developed based on the Cosserate rod model. This model was essential for the verification step in this project. I want to thank Professor Saullo Giovani Pereira Castro from the Aerospace Structures and Computational Mechanics group for his advice on the dynamics of structures. I want to extend my gratitude to Prof Ferdinand Schrijer of the Aerodynamics, Wind Energy, and Propulsion group for lending us the High-speed camera. This camera was a crucial part of the hardware experiments.

The pandemic affected all of us in many ways. I want to thank my friends for helping me cope with isolation. I had stumbled and fallen, but they helped me get back up march on ahead with this project. Finally, I would like to thank my parents and my brother. They helped and supported me in all possible ways.

REFERENCES

[1] T. Kelso *et al.*, *Analysis of the iridium 33 cosmos 2251 collision,* (2009).

[2] I. O. Campaigns, *Inter-agency space debris coordination committee,* 43rd Session of UNCOPUOS S&T SC (2006).

[3] D. J. Kessler and B. G. Cour-Palais, *Collision frequency of artificial satellites: The creation of a debris belt,* Journal of Geophysical Research: Space Physics **83**, 2637 (1978).

[4] M. Shan, J. Guo, and E. Gill, *Review and comparison of active space debris capturing and removal methods,* Progress in Aerospace Sciences **80**, 18 (2016).

[5] S. Matunaga, T. Kanzawa, and Y. Ohkami, *Rotational motion-damper for the capture of an uncontrolled floating satellite,* Control Engineering Practice **9**, 199 (2001).

[6] F. Branz, L. Savoili, A. Francesconi, F. Sansone, J. Krahn, and C. Menon, *Soft-docking system for capture of irregularly shaped, uncontrolled space objects,* 6th European Conference on Space Debris, ESA/ESOC (April 22-25) (2013).

[7] S. I. Nishida and S. Kawamoto, *Strategy for capturing of a tumbling space debris,* Acta Astronautica **68**, 113 (2011).

[8] S.-I. Nishida and S. Kawamoto, *Capturing a space debris by space robot,* .

[9] W. Cheng, Z. Li, and Y. He, *Modeling and Analysis of Contact Detumbling by Using Flexible Brush,* Proceedings of the 2019 IEEE International Conference on Unmanned Systems, ICUS 2019 , 95 (2019).

[10] W. Cheng, Z. Li, and Y. He, *Strategy and Control for Robotic Detumbling of Space Debris by Using Flexible Brush,* Proceedings of 2019 3rd IEEE International Conference on Robotics and Automation Sciences, ICRAS 2019 , 41 (2019).

[11] D. Wenjie, Z. Haibo, W. Dayi, and Z. Zhibin, *Experiment-based contact dynamic modeling for detumbling a disabled satellite,* Advances in the Astronautical Sciences **165**, 2053 (2018).

[12] S.-I. Nishida and S. Kawamoto, *Strategy for capturing of a tumbling space debris,* (2009) pp. 1978–1984, cited By 1.

[13] H. R. Rawls, N. J. Mkwayi-Tulloch, and M. E. Krull, *A mathematical model for predicting toothbrush stiffness,* Dental Materials **6**, 111 (1990).

[14] C. Wang, H. Guo, Y. Zhao, Q. Sun, and L. Zhao, *Statistical Analysis of Industrial Grinding Brush Force Characteristics Based on Finite Element Approach,* Mathematical Problems in Engineering **2018** (2018), 10.1155/2018/7362705.

[15] B. Baxter, V. Scheib, M. C. Lin, and D. Manocha, *DAB: Interactive haptic painting with 3D virtual brushes,* Proceedings of the 28th Annual Conference on Computer Graphics and Interactive Techniques, SIGGRAPH 2001 , 461 (2001).

[16] N. Magnenat-Thalmann and D. Thalmann, *Handbook of virtual humans* (John Wiley & Sons, 2005).

[17] S. Xu, M. Tang, F. Lau, and Y. Pan, *A solid model based virtual hairy brush,* Computer Graphics Forum **21**, 299 (2002).

[18] L. V. Vanegas Useche, M. M. Abdel Wahab, and G. A. Parker, *Brush dynamics: Models and characteristics,* (2006).

[19] R. J. Stango, S. M. Heinrich, and C. Y. Shia, *Analysis of constrained filament deformation and stiffness properties of brushes,* Journal of Manufacturing Science and Engineering, Transactions of the ASME **111**, 238 (1989).

[20] J. W. Chew, B. L. Lapworth, and P. J. Millener, *Mathematical modeling of brush seals,* International Journal of Heat and Fluid Flow **16**, 493 (1995).

[21] M. A. Wahab, G. Parker, and C. Wang, *Modelling rotary sweeping brushes and analyzing brush characteristic using finite element method,* Finite Elements in Analysis and Design **43**, 521 (2007).

[22] S. Hadap and N. Magnenat-Thalmann, *Modeling dynamic hair as a continuum,* Computer Graphics Forum **20**, 329 (2001).

[23] Z. Lu, Z. Wang, S. F. Masri, and X. Lu, *Particle impact dampers: Past, present, and future,* Structural Control and Health Monitoring **25** (2018), 10.1002/stc.2058.

[24] B. Andreotti, Y. . Forterre, and O. T. A. T. T. Pouliquen, *Granular media : between fluid and solid*, nv - 1 onl ed. (Cambridge University Press, Cambridge, 2013).

[25] H. Sakaguchi, A. Murakami, T. Hasegawa, and A. Shirai, *Connected lattice cellular-automation particles: a model for pattern formation in vibrating granular media,* Soils and Foundations **36**, 105 (1996).

[26] *Space materials database. material selection,* .

[27] R. J. Stango and C. Y. Shia, *Analysis of filament deformation for a freely rotating cup brush,* Journal of Manufacturing Science and Engineering, Transactions of the ASME **119**, 298 (1997).

[28] C.-Y. Shia, R. J. Stango, and S. M. Heinrich, *Analysis of Contact Mechanics for a Circular Filamentary Brush/Workpart System,* Journal of Manufacturing Science and Engineering **120**, 715 (1998).

[29] V. Šmilauer *et al.*, *Yade Documentation 2nd ed* (The Yade Project, 2015) http://yade-dem.org/doc/.

[30] F. Bourrier, F. Kneib, B. Chareyre, and T. Fourcaud, *Discrete modeling of granular soils reinforcement by plant roots,* Ecological Engineering **61**, 646 (2013).

[31] A. Effeindzourou, B. Chareyre, K. Thoeni, A. Giacomini, and F. Kneib, *Modelling of deformable structures in the general framework of the discrete element method,* Geotextiles and Geomembranes **44**, 143 (2016).

[32] P. A. Cundall and O. D. Strack, *A discrete numerical model for granular assemblies,* geotechnique **29**, 47 (1979).

[33] J. Till, V. Aloi, and C. Rucker, *Real-time dynamics of soft and continuum robots based on cosserat rod models,* International Journal of Robotics Research **38**, 723 (2019).

[34] *Properties: Silicone rubber,* [Online; accessed 1-December-2021].

[35] G. Bradski, *The OpenCV Library,* Dr. Dobb's Journal of Software Tools (2000).

[36] L. Warneke, *Calibration weights classification for balances,* `https://laboratoryresource.com.au/?navaction=getitem&id=237` (2020).

[37] P. E. des classes and D. M. Légale, *Weights of classes part 1: Metrological and technical requirements partie 1: Exigences métrologiques et techniques organisation internationale,* (2004).

[38] *Friction,* (2021), [Online; accessed 1-December-2021].

A

EXPERIMENT: WEIGHING SCALE ERROR

A High Precision Digital Scale was used to measure the force exerted by the brush on the wedge in the static test. It is shown in Figure A.1. This section provides a brief discussion of measuring its precision. The manufacturer claims a precision of 0.01g; this claim must be verified.

Figure A.1: *Weigh scale*

The precision would be measured using calibration weights. These are weights manufactured in such a way to have a highly precise mass. The following masses were used for this experiment: 50g, 100g, 200g. Information about the calibrated weights was not available, so it was assumed to have the worst accuracy and belongs to class M_3 [36, 37]. This class has an accuracy of 25mg.

The calibration weights were placed on the weighing surface, and the measurement was recorded. The weights were changed in steps of 50g from 50g to 500g. This process was repeated for different positions on the weighing surface. Recording the values when the weights were placed at different locations gave an additional error source.

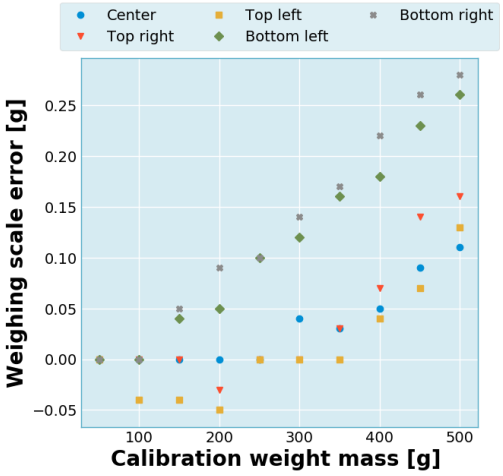

Figure A.2: *The error in measured weight*

The results obtained are shown Figure A.2. The error increases with increasing weights, and the minimum error is observed weight is measured at the centre of the weighing surface. The standard deviation of all errors is 0.13g. In conclusion, it is recommended to measure weight or force while having contact at the centre of the weighing surface.

B

EXPERIMENT: BRUSH YOUNG'S MODULUS

This experiment aims to obtain Young's modulus of the silicone material in the brush. It was found using a simple extension test. A bristle constituting the brush was extended, the extension and the reaction force was measured. Young's modulus was calculated from the results. However, the bristle in the chosen brush had a conical shape, so additional theory formulation was required.

Consider a slender cone with radii r_1 and r_2 with length L. The stress σ is equation $E\varepsilon$ where E is Young's modulus, and ε is the strain. Strain, for axial deformation, equals $\Delta L/L$ where L is the length of the body and ΔL is the axial deformation. When a body is under tension, stress equals F/A where F is the tensile force, and A is the cross-section area. The deformation can now be expressed as a function of all other parameters as follows:

$$\sigma = E\varepsilon = E\frac{\Delta L}{L} = \frac{F}{A} \Rightarrow \Delta L = \frac{F}{AE} \tag{B.1}$$

A slender conical rod under tension will have non-uniform stress because its cross-section area varies while the tension remains constant. So the equation above holds only for an infinitesimal section dl, and the total deformation ΔL can be found by integrating Eq. B.1. The following equation captures this:

$$\Delta L = \int d\delta = \frac{F}{E}\int_0^L \frac{dl}{A} \tag{B.2}$$

The radius of a slender conical rod is a linear function of axial position l. Now the area can be expressed as a function of l

$$\begin{aligned} A &= \pi r^2 \\ r &= \left(\frac{r_2 - r_1}{L}\right) l + r_1 \end{aligned} \tag{B.3}$$

B

Substituting Eq. B.3 in Eq. B.2 gives the following

$$\Delta L = \int_0^L \frac{F}{\pi E} \frac{dl}{\left[\left(\frac{r_2 - r_1}{L}\right) l + r_1\right]^2} \tag{B.4}$$

The integral in Eq. B.4 evaluates to the following:

$$\Delta L = \frac{FL}{\pi E r_1 r_2} \tag{B.5}$$

Now, by measuring the tension F in the bristle and the extension ΔL it is possible to calculate Young's modulus. Let k be the slope of the $F - \Delta L$ graph, then Young's modulus can be expressed as:

$$\begin{aligned} E &= \frac{FL}{\pi \Delta L r_1 r_2} \\ E &= \frac{kL}{\pi r_1 r_2} \end{aligned} \tag{B.6}$$

The error in Young's modulus can be found by passing the equation through a log function, removing the negative and differentiating the results leading to the following.

$$\begin{aligned} \log E &= \log\left(\frac{FL}{\pi \Delta L r_1 r_2}\right) \\ \log E &= \log F + \log L + \log \pi + \log \Delta L + \log r_1 + \log r_2 \\ d\log E &= d\log F + d\log L + d\log \pi + d\log \Delta L + d\log r_1 + d\log r_2 \\ \frac{dE}{E} &= \frac{dF}{F} + \frac{dL}{L} + \frac{d\Delta L}{\Delta L} + \frac{dr_1}{r_1} + \frac{dr_2}{r_2} \end{aligned} \tag{B.7}$$

In Eq. B.7, dE is the error of Young's modulus, dF is the error in the measure tensile force and so on.

The weighing scale described in appendix A was used to measure the force. This scale, however, was designed to measure compressive loads. So a pair of clamps had to be made to hold the bristle when it is extended. The clamps extend the bristle when they are brought together or compressed. One clamp was placed on the weighing scale, and the vertical motion guide supported the other (See appendix **??**). These clamps were 3D printed and were made out of PLA (Poly Lactic acid).

Moving the upper clamp down extends the bristle. This motion was carried out in steps of 1mm till a maximum extension and back. The force was recorded at each step. Once the extension was removed, the force was re-recorded. This value is the weight of the clamps and the bristle. It will be subtracted from the previous measurements to get the tensile force. The tensile force was plotted against the corresponding extension, and this graph is shown in Figure B.2.

The the parameters in equations B.7 and B.6 were measured and are given below:

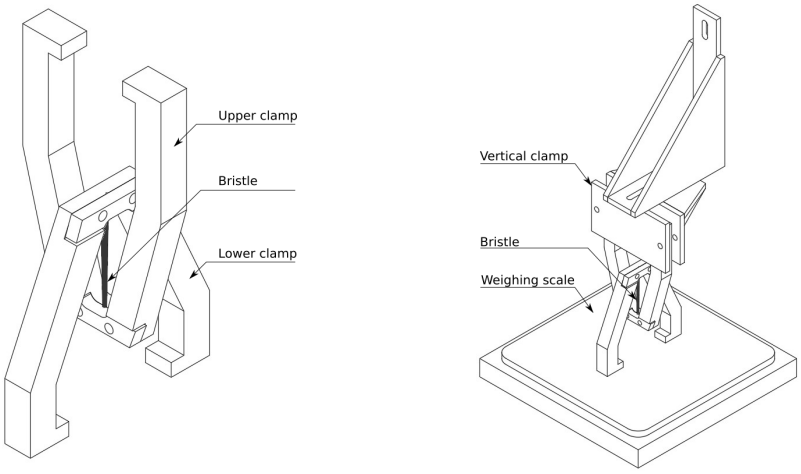

(a) *The two clamps holding the bristle*

(b) *The vertical motion assembly along with the clamp*

Figure B.1: *Hardware setup to measure bristle's Young's modulus.*

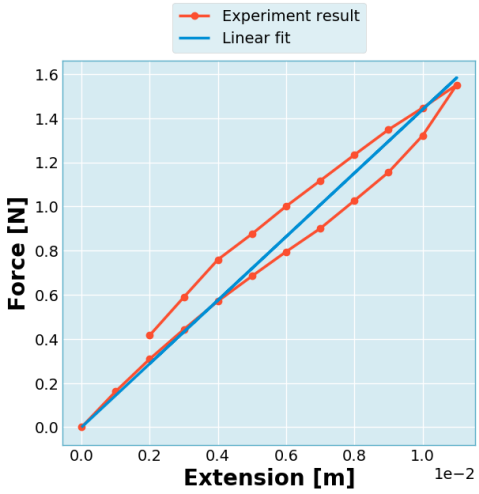

Figure B.2: *Tensile force in brislte vs axial extension of bristle. The experiment result and the linear fit is shown in this figure. It shows the loading and unloading curve. The slope can be calculated from the linear fit*

$$
\begin{aligned}
r_1 &= 1mm \\
r_1 &= 0.5mm \\
L &= 30mm \\
dF &= 2g^{1} \\
dL &= 1mm \\
dr_1 &= 0.1mm \\
dr_2 &= 0.1mm \\
d\Delta L &= 1mm
\end{aligned}
\tag{B.8}
$$

Using equations B.6 and B.7 along with the experiment data, Young's modulus was calculated. Its value is $2.7 \times 10^6 \pm 1.1 \times 10^6 N/m^2$. All components, excluding the bristle, were assumed to be rigid and did not reform. However, in reality, this is not true. There will always be a small deformation.

C

Experiment: Friction Coefficients

This experiment aims to find the coefficient of friction between the surfaces that contact in the YADE models. Silicone-silicone, silicone-3D printed PLA, and silicone-hard foam are the surface pairs whose friction coefficient would be calculated in this experiment.

In the YADE model, we use Coulomb friction to model friction. Here, the angle of friction would be used to calculate the coefficient of friction. Consider one of the two contact surfaces, body A with surface A, fixed but able to incline, and the other, body B with surface B, is resting on the first, free to move. Inclining body A would, at first, have body B remain at rest because of static friction. Then there comes a critical angle beyond which gravity overcomes friction and body B starts moving. This critical angle is the angle of friction. Figure C.1b shows the different forces acting on body B and also the surfaces in contact.

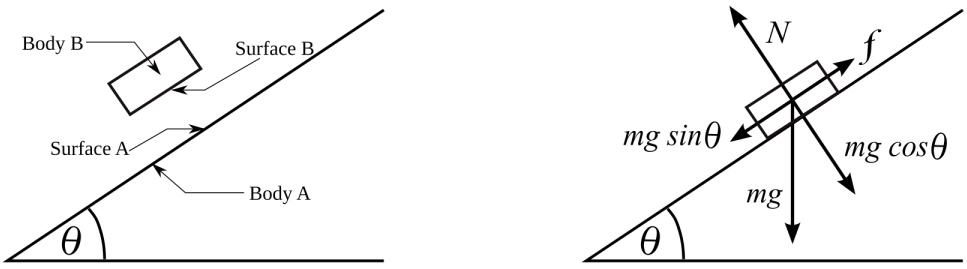

(a) *Surfaces and bodies*

(b) *Free body diagram*

Figure C.1: *The free body diagram showing the different forces acting on body B. Weight mg is split into tangential and normal components. N is the normal reaction force and f is the frictional force. Taken from [38]*

At the critical angle the following conditions are satisfied:

$$\begin{aligned} f &= mg\sin(\theta) \\ f &= \mu_s N \end{aligned} \tag{C.1}$$

To measure the angle of friction, one of the surfaces of interest was fixed to a sheet of MDF (Medium Density Fibreboard). Inclining the MDF board inclines the surface. The angle was measured using the “Level" application in an iPhone SE. It uses the internal accelerometer to measure the orientation of the iPhone against the gravity vector. The iPhone was also fixed to the MDF sheet so that the smartphone monitors its inclination. This app has a precision of 1°. A silicone sample was placed on the fixed surface, and the MDF sheet was inclined until the bristle started moving. Repeating this step 30 times yields a better estimation. The coefficient of friction in terms of angle of friction was calculated, and the results are given below.

- Silicone-silicone: $44° \pm 2°$
- Silicone-3D printed PLA: $24° \pm 2°$
- Silicone-hardfoam: $36° \pm 2°$

D

BRUSH STATIC TEST: SENSITIVITY STUDY

The values of the physical parameters of the brush and its material were not certain. This uncertainty could potentially affect the results produced by the simulations in the static test. The uncertain properties relevant to the static test were the bristle diameter, the bristle-bristle friction coefficient, bristle-wedge friction coefficient and the bristle Young's modulus. A sensitivity study was performed to test how each of these parameters affects the outcome of the static test simulation for different wedge angles. The results from this study and the hardware experiment are shown below.

The sensitivity study shows that the static test is most sensitive to error in bristle radius, and it is least sensitive to bristle-bristle friction coefficient. The first can be explained by the fact that the reaction force generated by the brush is a function of its stiffness, also known as flexure rigidity. Consider the bristle to be a slender rod with a circular cross-section. Then the stiffness is a product of Young's modulus, E, and the area moment of inertia (I) of its cross-section. The following equation gives this property.

$$I_{x,\text{circle}} = \frac{\pi}{2} r^4 \tag{D.1}$$

The Young's modulus had a close error of 40.74%, whereas the radius had an average error of 13.3%. However, Young's modulus is linearly proportional to stiffness, while the stiffness is related to the fourth power of the radius. This difference explains why the static test was more sensitive to the radius. The bristle-wedge friction angle has a lower impact because of a lower error, around 9%. Finally, we see two reasons why the bristle-bristle friction angle had virtually zero influence on the static test. Firstly, there was no tangential deformation between the bristle; in simpler terms, the bristles were pushing each other and not sliding against each other. Friction, as a result, is not experienced between the bristles. So the angle of friction has no influence. Secondly, the static friction between the bristles could be below the maximum allowable friction, also known as limiting static friction. The static friction angle gives this maximum value of static friction.

If the friction developed between two surfaces is below the maximum value, changes in the static friction angle will not affect the friction value. Additional experiments are required to test which one of these hypotheses is correct. Testing this hypothesis, however, is beyond the scope of this project.

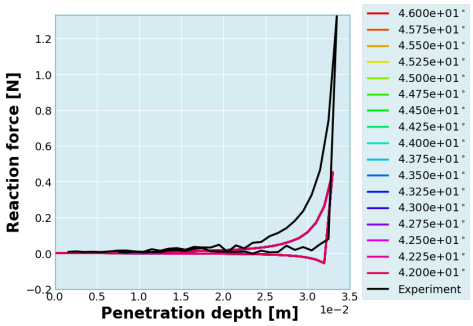

(a) *Sensitivity to bristle-bristle friction*

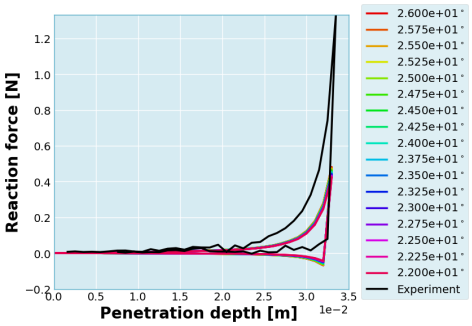

(b) *Sensitivity to bristle-wedge friction*

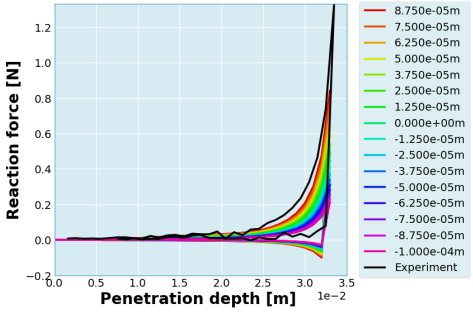

(c) *Sensitivity to error in bristle diameter*

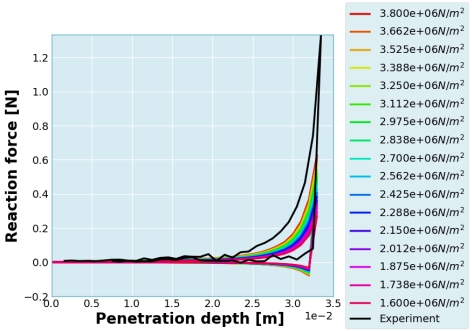

(d) *Sensitivity to bristle Young's modulus*

Figure D.1: *The sensitivity of the static test to different parameters. These are the results from the sensitivity study with a* 30° *wedge*

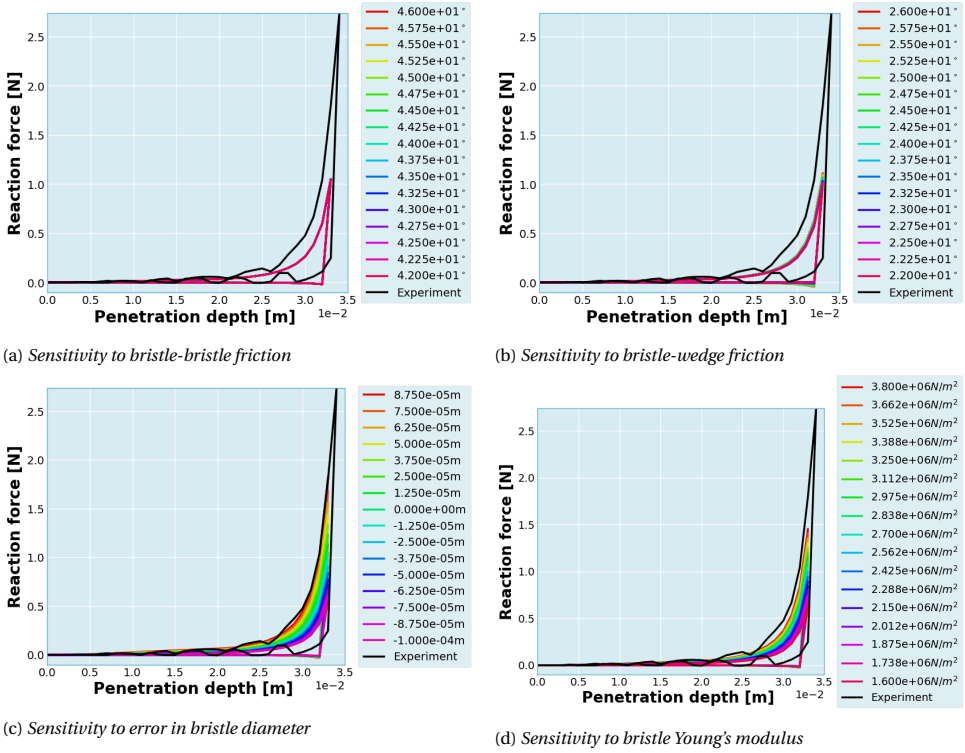

(a) *Sensitivity to bristle-bristle friction*

(b) *Sensitivity to bristle-wedge friction*

(c) *Sensitivity to error in bristle diameter*

(d) *Sensitivity to bristle Young's modulus*

Figure D.2: *The sensitivity of the static test to different parameters. These are the results from the sensitivity study with a* 45° *wedge*

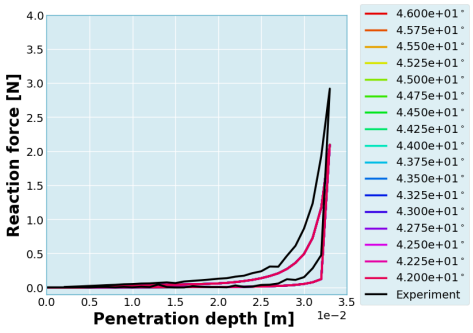

(a) *Sensitivity to bristle-bristle friction*

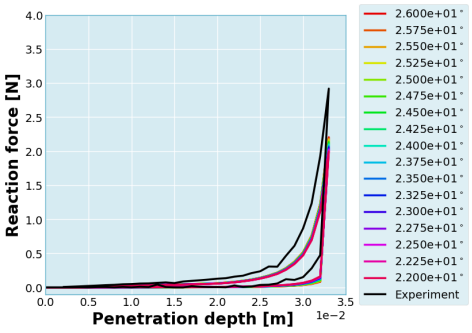

(b) *Sensitivity to bristle-wedge friction*

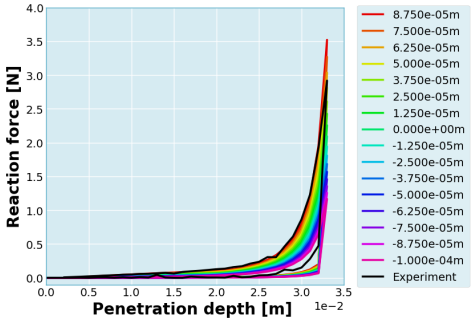

(c) *Sensitivity to error in bristle diameter*

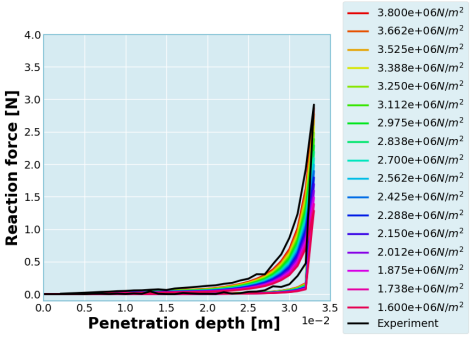

(d) *Sensitivity to bristle Young's modulus*

Figure D.3: *The sensitivity of the static test to different parameters. These are the results from the sensitivity study with a* 60° *wedge*

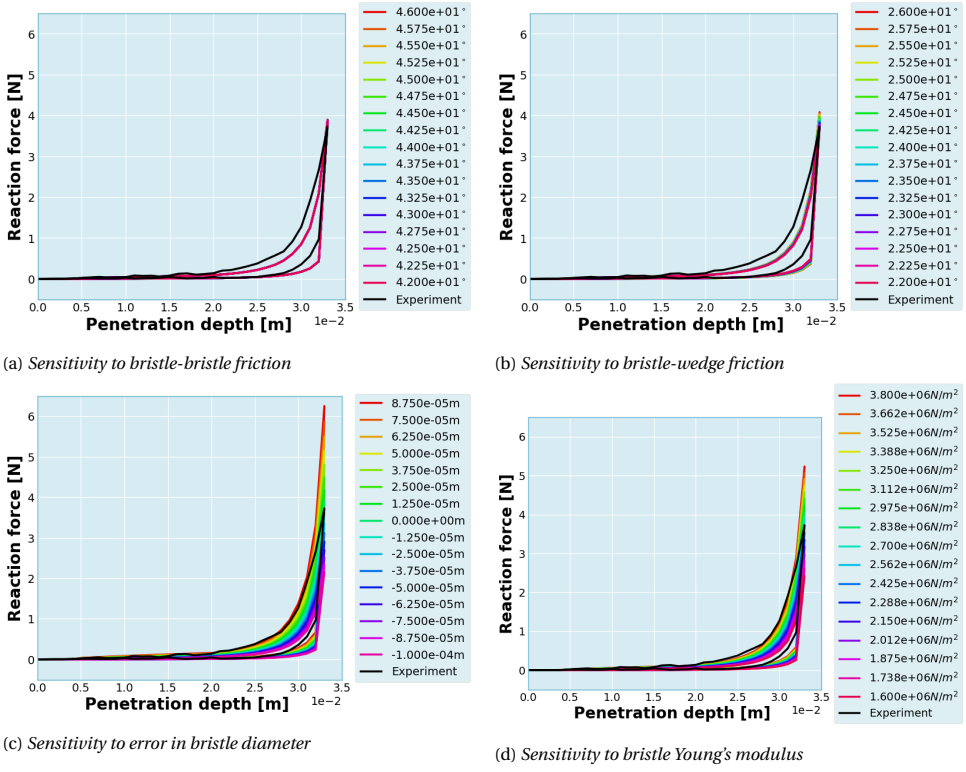

(a) *Sensitivity to bristle-bristle friction*

(b) *Sensitivity to bristle-wedge friction*

(c) *Sensitivity to error in bristle diameter*

(d) *Sensitivity to bristle Young's modulus*

Figure D.4: *The sensitivity of the static test to different parameters. These are the results from the sensitivity study with a* 75° *wedge*

E

DEM BRUSH MODEL: EFFECT OF BRISTLE REFINEMENT

The results from the simulations are also affected by one other parameter, the number of nodes in a bristle. Generally, as the number of nodes increases, the accuracy of the simulation increases. This result is shown in Figure E.2. However, we cannot arbitrarily increase the number of nodes as we see fit. There is an upper limit to this number. The grid-nodes in the bristles also behave like spheres. The grid-node-body class inherits the sphere-body class, so it has all properties of a sphere in addition to its own properties. Because of this, YADE detects a collision when two grid-nodes overlap and will cause the bristle to fall apart. So the maximum number of grid nodes a bristle can accommodate is the number that comes right before the grid-nodes overlap. This is shown in Figure E.1

(a) *Maximum number of grid nodes* (b) *Minimum number of grid nodes*

Figure E.1: *The limits to the number of grid-nodes a bristle can accomodate. This number is maximum right before the grid-nodes overlap. The lower limit is the trivial case of two end nodes.*

Figure E.2 also suggests another result. We need not use the maximum number of nodes to get a fairly accurate result. For example, in this case, any number greater than ten gives a satisfactory prediction of the brush behaviour. However, this number will not be the same for all brushes and must be found for each case. Once this number is found, it can save a substantial computing resource.

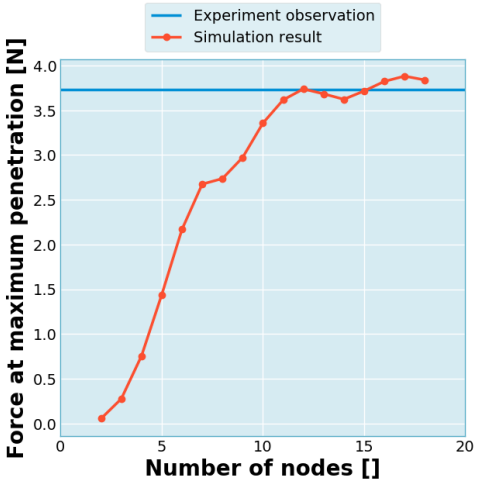

Figure E.2: *The force at maximum penetration vs the number of nodes. The results are for the wedge with a* 75° *angle. This figure shows at the YADE model approaches the experiment result as the number of nodes increases.*

F

BRUSH DYNAMIC TEST: EXTERNAL DISSIPATION MODEL

In the experiment for the brush dynamics test case, it was observed that the body slowed down, over a period of time, on its own. We speculate that friction in the bearings that support the body's rotation and air drag caused this. It becomes necessary to include this effect in the simulations model to compare the simulations with the experiment. This section explains how this model was constructed.

We do not aim to construct a very high fidelity model, but one that is simple and reasonably captures the dissipation caused by external factors. This dissipative force was assumed to be a linear function of angular velocity. This model is shown in the following equation.

$$\alpha = \frac{d\omega}{dt} = -k_1\omega - k_2 sign(\omega) \tag{F.1}$$

The first term, $-k_1\omega$, captures the dissipative effect of air resistance and the second term, $-k_2 sign(\omega)$, models the kinetic friction in the bearing. In this model, friction acts against the motion, so the coefficients k_1 and k_2 are positive real numbers.

The values for k_1 and k_2 were found using a hardware experiment. The body, supported by the setup used for the brush dynamics experiment, was spun and allowed to come to rest. The brush was kept away from the body, slowing down due to dissipative forces alone. The model is constructed by calculating the values of velocity and acceleration at each time instant and fitting the coefficients k_1 and k_2 from eq F.1 to this data. The raw data is highly noisy, so a low pass filter removes most of the high-frequency noise in the raw data. The three different bodies had different dissipation characteristics, so the construction was carried out for the three bodies. Comparing the body's motion in a simulation with the damping model and the experimental observation showed that this model could capture the damping to a reasonable extent. The function fitting and the comparison of the simulated motion and the experimental observations are shown in the following graphs.

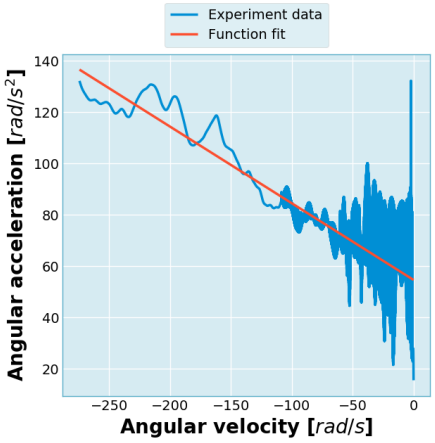

(a) *Angular acceleration vs velocity*

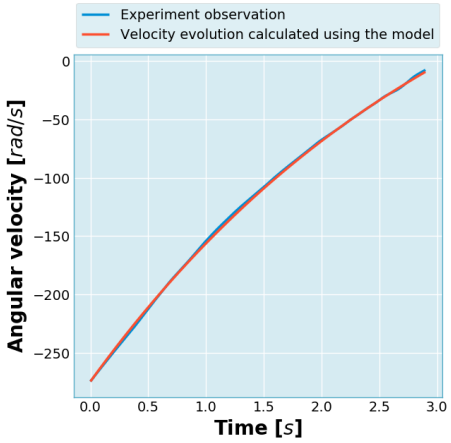

(b) *Velocity vs time*

Figure F.1: *The friction model. The first figure shows the acceleration as a function of velocity. The experimental data is used to construct a model. The second figure shows how the experiment observation compares with the results predicted by the model. These figures show the response of the body with dimension 20mmx20mmx20mm*

F

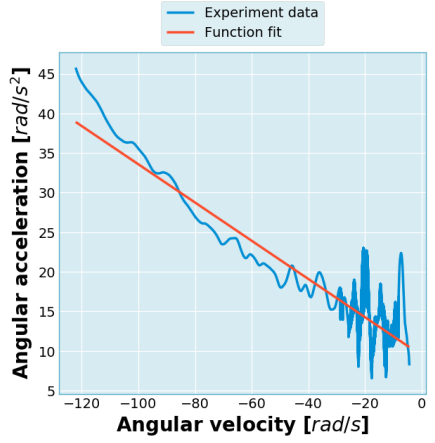

(a) *Angular acceleration vs velocity*

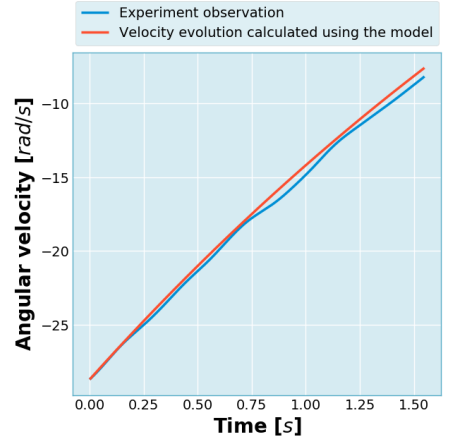

(b) *Velocity vs time*

Figure F.2: *The friction model. The first figure shows the acceleration as a function of velocity. The experimental data is used to construct a model. The second figure shows how the experiment observation compares with the results predicted by the model. These figures show the response of the body with dimension 40mmx40mmx40mm*

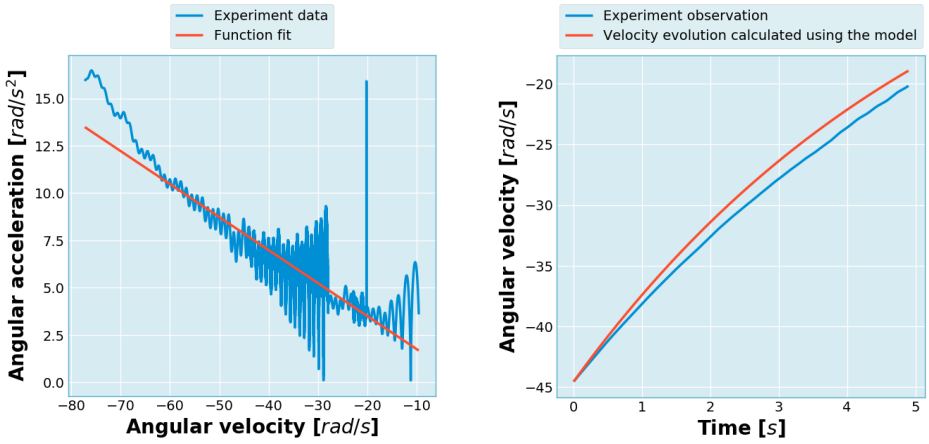

(a) *Angular acceleration vs velocity*

(b) *Velocity vs time*

Figure E.3: *The friction model. The first figure shows the acceleration as a function of velocity. The experimental data is used to construct a model. The second figure shows how the experiment observation compares with the results predicted by the model. These figures show the response of the body with dimension 60mmx60mmx60mm*

F

G

BRUSH DYNAMIC TEST: SENSITIVITY STUDY

There were uncertainties in the values of the physical parameters of the brush. These uncertainties translated into the variation in the data resulting from the brush dynamic test simulations. The uncertain properties relevant to the brush dynamic test were the bristle diameter, the bristle density and the bristle Young's modulus. A sensitivity study helped us understand how the variation of each of these parameters affected the simulation outcome and resulted in a range of behaviour that could be compared to the results from the hardware experiments. The results from the sensitivity studies are shown below. It was found that the bristle diameter had the most substantial influence on the simulations. The results from the sensitivity study and the hardware experiment are shown below.

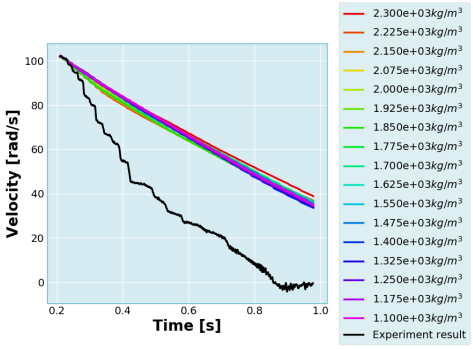

(a) Density

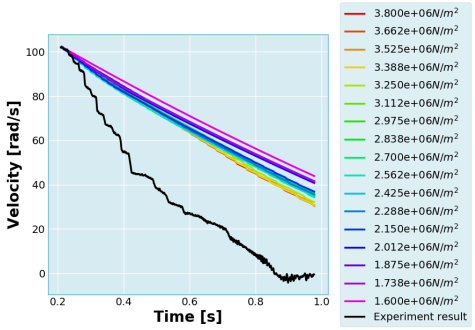

(b) Young's modulus

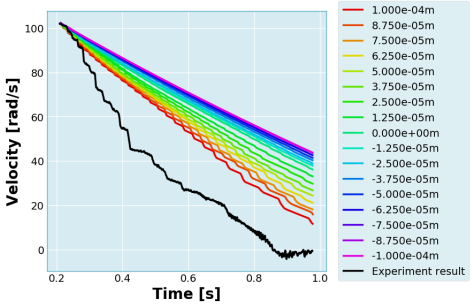

(c) Diameter

Figure G.1: *The results from the sensitivity analysis of three physical properties. Each subfigure shows the sensitivity to one property. The bristle diameter has highest influence on the outcome of the simulation. The experiment results are also shown in these figures*

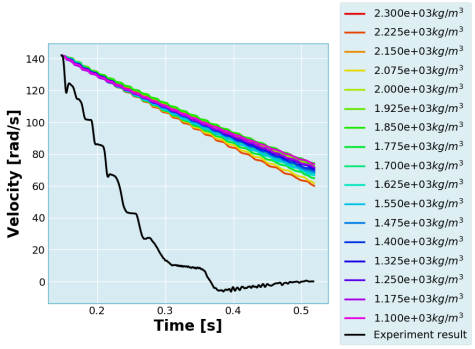

(a) Density

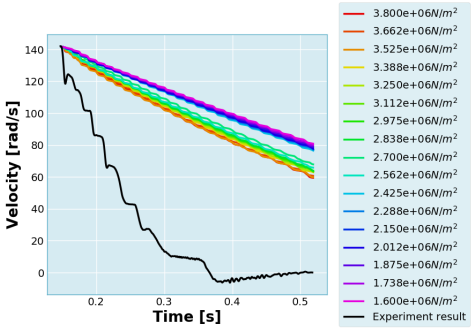

(b) Young's modulus

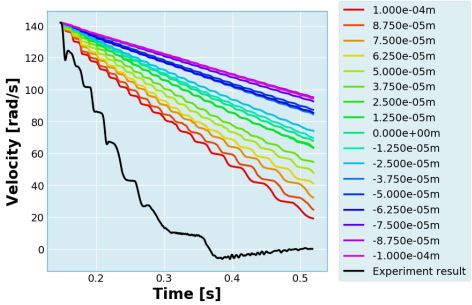

(c) Diameter

Figure G.2: *The results from the sensitivity analysis of three physical properties. Each subfigure shows the sensitivity to one property. The bristle diameter has highest influence on the outcome of the simulation. The experiment results are also shown in these figures*

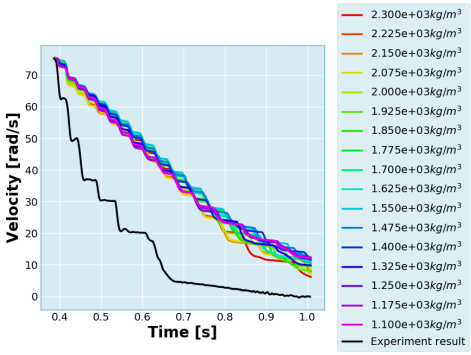

(a) Density

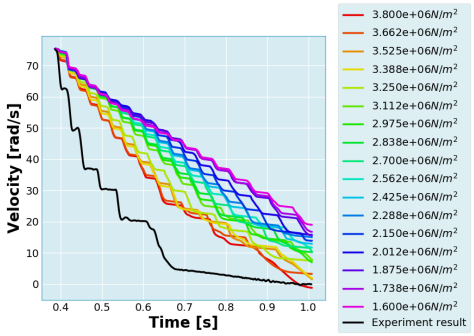

(b) Young's modulus

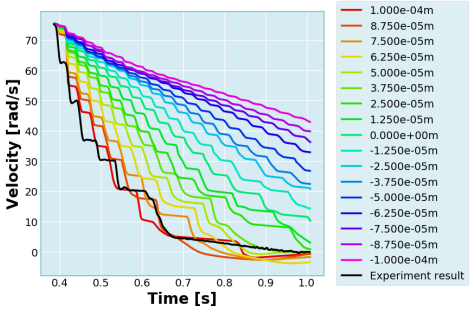

(c) Diameter

Figure G.3: *The results from the sensitivity analysis of three physical properties. Each subfigure shows the sensitivity to one property. The bristle diameter has highest influence on the outcome of the simulation. The experiment results are also shown in these figures*

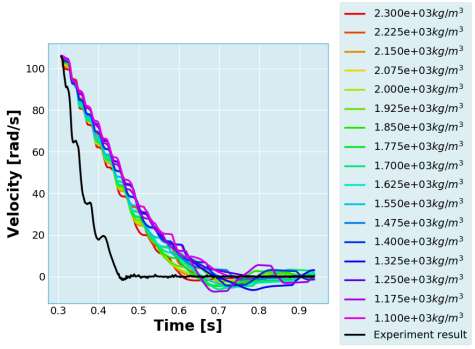

(a) Density

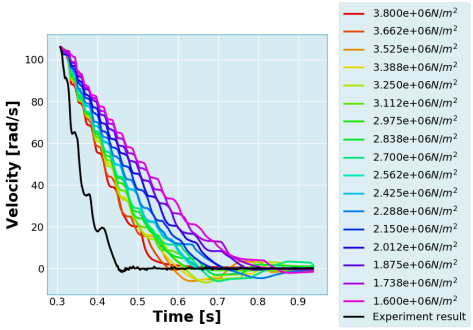

(b) Young's modulus

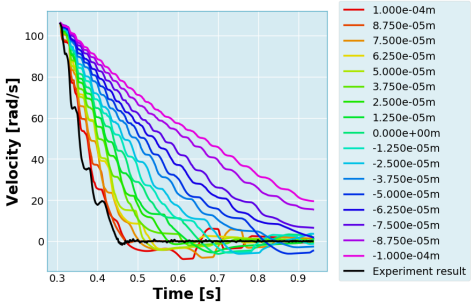

(c) Diameter

Figure G.4: *The results from the sensitivity analysis of three physical properties. Each subfigure shows the sensitivity to one property. The bristle diameter has highest influence on the outcome of the simulation. The experiment results are also shown in these figures*

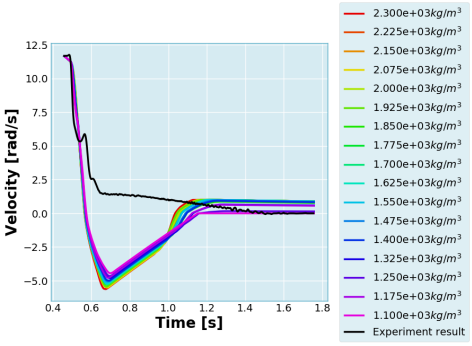

(a) Density

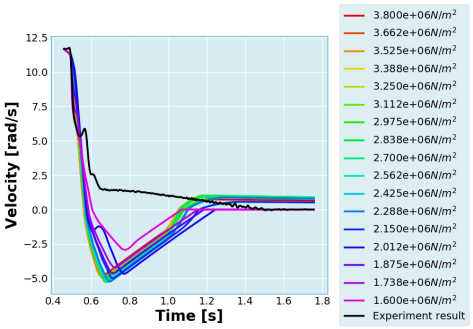

(b) Young's modulus

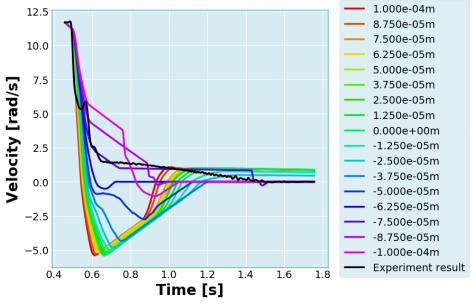

(c) Diameter

Figure G.5: *The results from the sensitivity analysis of three physical properties. Each subfigure shows the sensitivity to one property. The bristle diameter has highest influence on the outcome of the simulation. The experiment results are also shown in these figures*

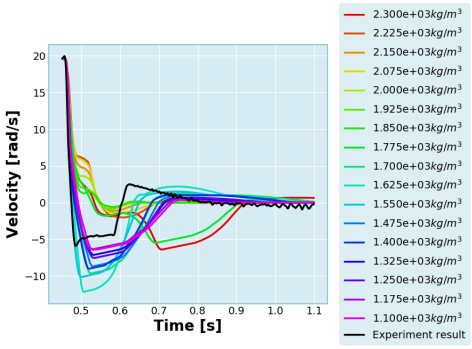

(a) Density

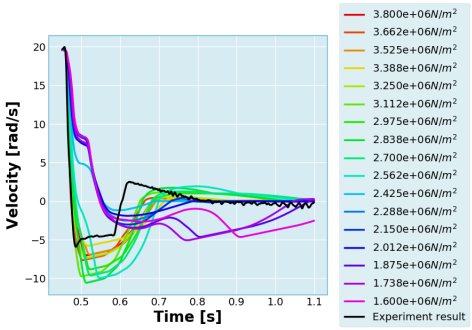

(b) Young's modulus

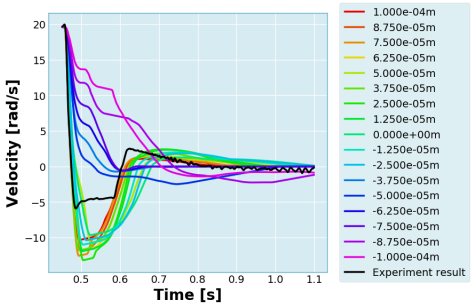

(c) Diameter

Figure G.6: *The results from the sensitivity analysis of three physical properties. Each subfigure shows the sensitivity to one property. The bristle diameter has highest influence on the outcome of the simulation. The experiment results are also shown in these figures*

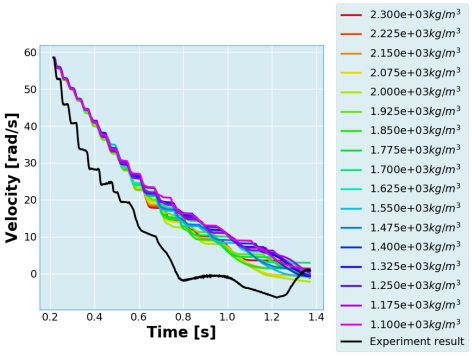

(a) Density

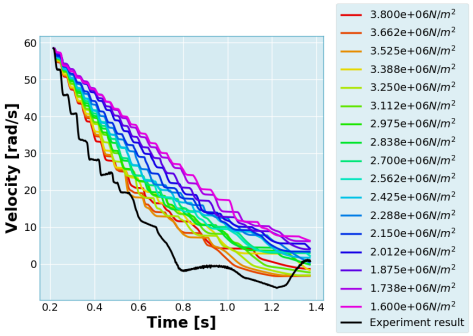

(b) Young's modulus

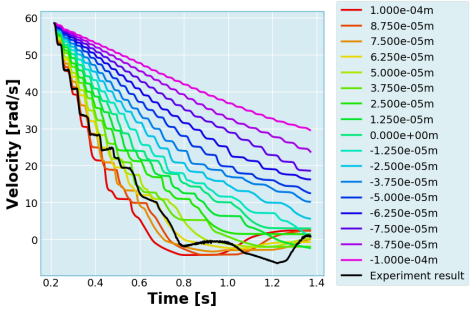

(c) Diameter

Figure G.7: *The results from the sensitivity analysis of three physical properties. Each subfigure shows the sensitivity to one property. The bristle diameter has highest influence on the outcome of the simulation. The experiment results are also shown in these figures*

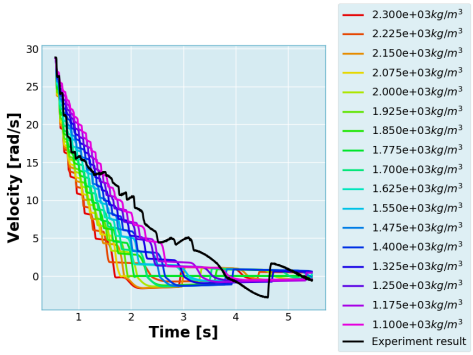

(a) Density

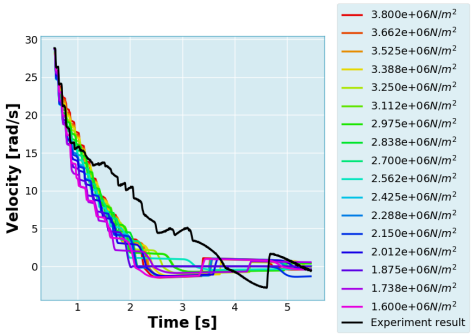

(b) Young's modulus

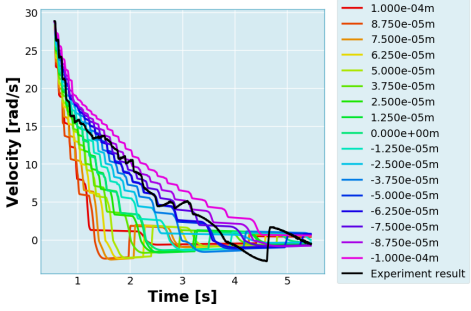

(c) Diameter

Figure G.8: *The results from the sensitivity analysis of three physical properties. Each subfigure shows the sensitivity to one property. The bristle diameter has highest influence on the outcome of the simulation. The experiment results are also shown in these figures*

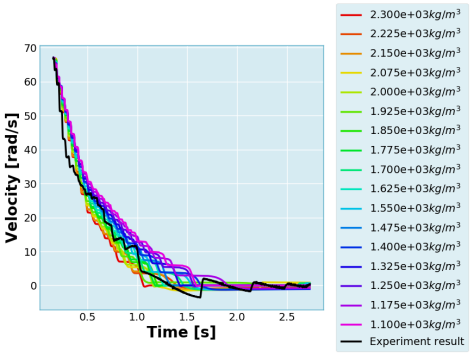

(a) Density

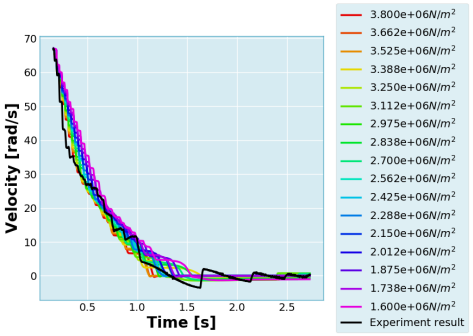

(b) Young's modulus

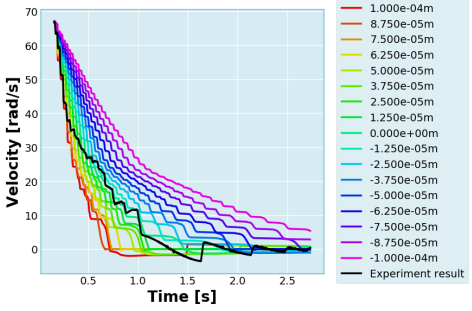

(c) Diameter

Figure G.9: *The results from the sensitivity analysis of three physical properties. Each subfigure shows the sensitivity to one property. The bristle diameter has highest influence on the outcome of the simulation. The experiment results are also shown in these figures*

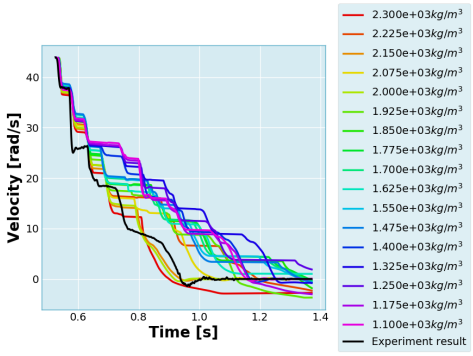

(a) Density

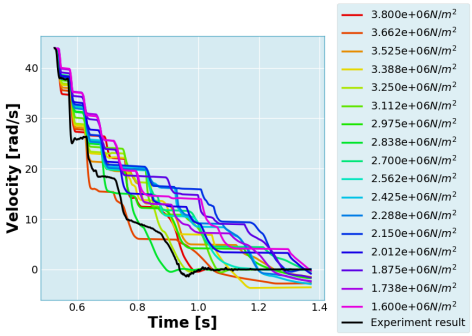

(b) Young's modulus

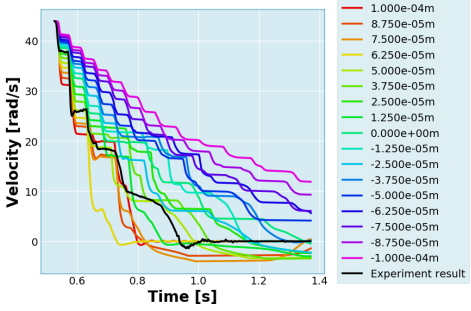

(c) Diameter

Figure G.10: *The results from the sensitivity analysis of three physical properties. Each subfigure shows the sensitivity to one property. The bristle diameter has highest influence on the outcome of the simulation. The experiment results are also shown in these figures*

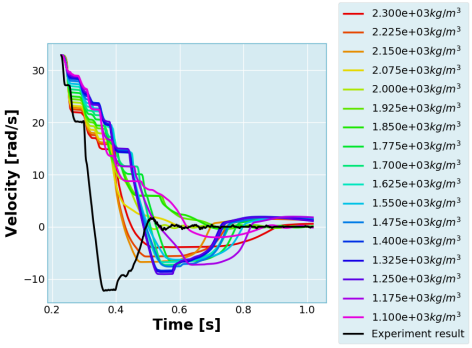

(a) Density

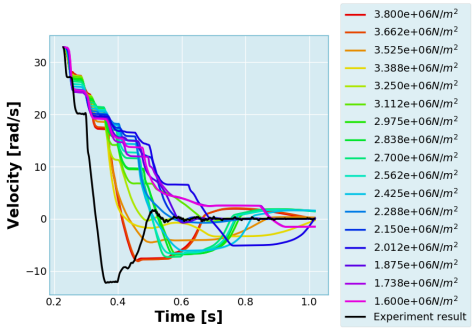

(b) Young's modulus

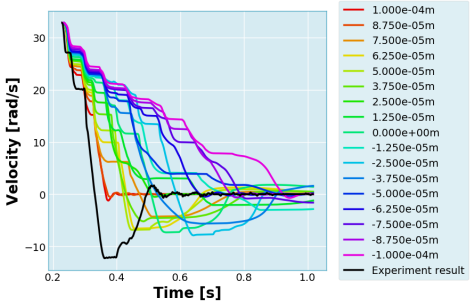

(c) Diameter

Figure G.11: *The results from the sensitivity analysis of three physical properties. Each subfigure shows the sensitivity to one property. The bristle diameter has highest influence on the outcome of the simulation. The experiment results are also shown in these figures*

H

YADE: ANGULAR MOMENTUM NOT CONSERVED FOR CLUMPS

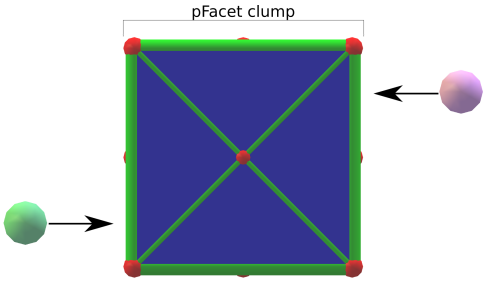

Figure H.1: *Scenario to test whether angular momentum is conserved*

Consider a scenario in which two spheres move antiparallel to each other but in offset paths. The two spheres collides with a stationary cube (see Figure H.1). Since there is no torque acting on this system about the centre of the cube, the angular momentum of this system must be conserved. However, a YADE simulation shows that the angular momentum before and after the collision is different. An error like this would suggest that the angular velocity integrator has an error. To further study this phenomenon, the mass of the spheres was kept constant while the cube's mass was changed. Plotting the per cent change in angular momentum after a collision resulted in Figure H.2. The results suggest that the error is maximum when the masses of the cube and the colliding body are the same. Since the brush has a lower mass than the bodies and the 20mm body is closer to the brush in mass, this could explain the discrepancy in the results. This was further tested with the following example (see appendix 4.39).

In this simulation, two brushes face each other, and the cube is placed between them. The roots of each brush are added to a clump; this acts as the brush fixture. The cube was given the initial angular velocity, and now the angular momentum of this system

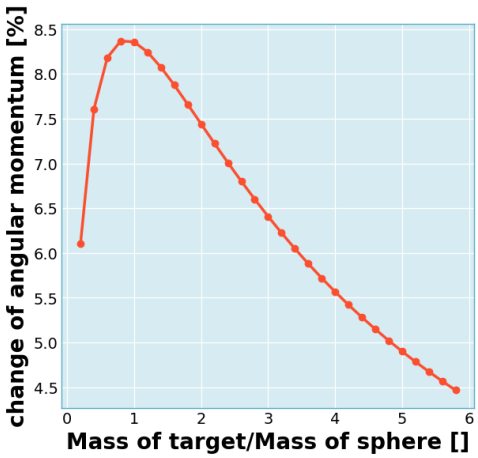

Figure H.2: *Comparing the change in angular velocity after collision of the spheres with the cube with the relative mass of the cube*

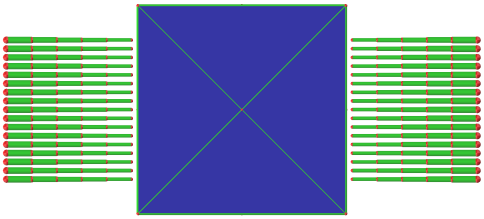

Figure H.3: *Scenario to test whether angular momentum is conserved with a brush*

was recorded. Now the per cent change in angular momentum was compared against the size of the cube. This is shown in Figure H.4. The results clearly show considerable change in the system's angular momentum with the 20mm cube after the collision. In the YADE simulation with the brush and the body, there are many such collisions with the brush. The error could accumulate and lead to the seen discrepancy.

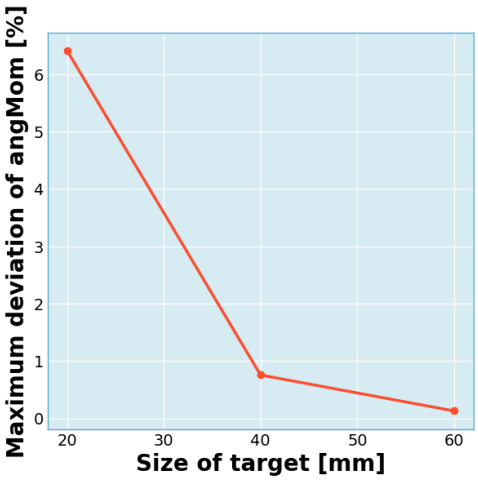

Figure H.4: textitGraph showing error in angular momentum conservation for the case with the brush. Notice that the error is small for bigger bodies